Geomatics
Engineering

UCGE Reports
Number 20108

Department of Geomatics Engineering

Augmentation of GPS with Pseudolites in a Marine Environment

By

Thomas G. Morley

May, 1997

Calgary, Alberta, Canada

THE UNIVERSITY OF CALGARY

Augmentation of GPS with Pseudolites in a Marine Environment

by

Thomas G. Morley

A THESIS

SUBMITTED TO THE FACULTY OF GRADUATE STUDIES

IN PARTIAL FULFILLMENT OF THE REQUIREMENTS FOR THE

DEGREE OF MASTER OF SCIENCE IN GEOMATICS ENGINEERING

DEPARTMENT OF GEOMATICS ENGINEERING

CALGARY, ALBERTA

MAY, 1997

PREFACE

This is an unaltered version of the author's M.Sc. thesis of the same title. This thesis was accepted by the Faculty of Graduate Studies in May, 1997.

The supervisor of this work was Dr. G. Lachapelle. Members of the examning committee were Dr. M. E. Cannon, Dr. E. J. Krakiwsky and Dr. B. Nowrouzian.

ABSTRACT

The augmentation of DGPS with ground-based GPS transmitters (pseudolites, or PLs) was investigated. A simulation analysis was conducted to determine the effects of PL augmentation on DGPS availability, accuracy and reliability measures, using various constant mask angles and a “real-world” horizon (measured at Lake Okanagan, British Columbia) plus a simulated obstruction. Field tests in the marine environment were conducted to validate the simulation and to assess the changes to PL augmented DGPS positioning using raw pseudoranges and carrier phase smoothed pseudoranges. Modelling of the multipath component between the PL and the reference GPS receiver was shown to improve PL augmented DGPS positioning. Beneficial effects of PL augmentation on a Fault Detection and Exclusion algorithm were illustrated. A field test in a mountainous marine environment (Lake Okanagan) was used to quantify improvements to OTF ambiguity resolution times and reliability due to PL augmentation.

ACKNOWLEDGMENTS

Firstly, I would like to thank my supervisor, Professor Gérard Lachapelle, for his academic and personal support and encouragement over the past twenty months, and for arranging financial support.

Secondly, this work was partly funded under contract from the Canadian Coast Guard. Thanks also to NovAtel for the use of their Stanford Telecom 7201 Wideband Signal Generator.

Thirdly, I would like to acknowledge the following graduate students for their help with the data collection for this thesis: Robert Harvey, Jamie Henriksen, Mike Szarmes, Chris Varner and Shawn Weisenburger. In addition, I would like to thank the following M.Sc. and Ph.D. students (both present and past) for their support: Geoffrey Cox, Richard Klukas, John Raquet (who always had an answer to every question I ever asked), Sam Ryan, Susan Skone and Huanqui Sun.

Fourthly, I wish to thank the academic and support staff of the Department of Geomatics Engineering. I would especially like to thank Anne Gehring for her efforts at getting my admission to the Department approved with great haste.

Fifthly, I would like to thank the Canadian Forces for rounding up all the experienced employees and paying them to retire (and to Scott Adams, creator of Dilbert, who helped me keep everything in perspective).

Lastly, and most of all, I would like to thank my wife Heather for believing in me, supporting me, and always being there.

TABLE OF CONTENTS

LIST OF TABLES

LIST OF FIGURES

CHAPTER 1

INTRODUCTION

To the marine community, the Global Positioning System (GPS) is an extremely valuable asset that can provide world-wide positioning and navigation information 24 hours a day, in any weather. Under most operational conditions, differential GPS (DGPS) solutions can be computed accurately and reliably. Under conditions of reduced satellite availability (due to local topography, obstructions or satellite unserviceability) or poor satellite geometry, the accuracy and particularly the reliability of the DGPS solution can be affected adversely. During a recent field trial of a Real-Time On-The-Fly (OTF) GPS Positioning System on board a United States Army Corps of Engineers dredge, kinematic OTF solutions for precise cm-level positioning were only available for 20 out of 24 hours due, in part, to a sparse GPS constellation [Frodge, *et al*., 1995]. An alternative to increasing the number of satellites available (which is a prohibitively expensive option), is to augment the space-borne GPS constellation with one or more ground-based transmitters, or pseudolites (for *pseudo*+satel*lites*). The pseudolite (PL) is then configured to broadcast GPS-like signals, providing an extra observation to the DGPS solution. This thesis will investigate the changes to DGPS availability, precision and reliability measures, and DGPS positioning (using code, and/or carrier phase information) due to the augmentation of GPS with pseudolites.

1.1 Marine Navigation and Position Requirements

The United States Federal Radionavigation Plan (FRP) recognizes the fact that the navigational requirements of a vessel will depend upon its type, its size, and its mission. In addition, the FRP identifies four distinct phases of marine navigation: inland waterway, harbour/harbour approach, coastal and ocean. Specific navigational performance requirements have been identified for each of these phases (with the exception of the inland waterway phase, which has waterway specific requirements), as summarized in Table 1.1. The navigational requirement which is most easily met is the oceanic phase, where positioning accuracies of 2 to 4 kilometres are acceptable. The most stringent navigational requirements are associated with the harbour/harbour approach phase, where repeatable accuracies of 8 m to 20 m (or better) are required. This phase is typically marked by a transition from the coastal phase into more restricted waters, where the pilot of a large marine vessel may be required to navigate well-defined channels from 180 m to 600 m in width, narrowing to as little as 120 m. For smaller vessels, the channel width may be as small as 30 m [FRP, 1994].

Table 1.1 Minimum Performance Criteria to Meet Safety of Navigation Requirements, US Federal Radionavigation Plan (1994)

Navigation Phase	Predictable Accuracy (metres, 2DRMS)	Coverage	Availability	Fix Interval
Ocean	1.8-3.7 km (desirable)	Worldwide	99% fix at least every 24 hours	15 minutes or less desired 2 hours max
Coastal	460 m	US Coastal Waters	99.7%	2 minutes
Harbour/Harbour Approach (Large Ships & Tows)	8-20 m	US Harbour & Harbour Approach	99.7%	6-10 seconds

In addition to the above Minimum Performance Criteria specified by the Federal Radionavigation Plan, certain marine tasks may have specific position and navigation requirements. Typical maritime missions and their associated positioning needs are summarized in Table 1.2 [Lachapelle, *et al*., 1991] . The positioning requirements span roughly four orders of magnitude, ranging from a general bathymetric survey (where the requirement is approximately 400 m, in the horizontal only) to navigation in constricted channels (which may require precise three dimensional positioning with an accuracy of less than 10 cm).

Table 1.2 Typical Marine Navigation and Positioning Requirements

Activity	Accuracy (2DRMS)
General Bathymetric Survey[1]	≥ 400 m
Oil & Gas	25 - 50 m
Site Surveys, Recovery & Reentry	10 - 20 m
Pipelines	2 - 20 m
Dredging	2 - 10 m
3-D Seismic	10 m
Navigational Aids in Constricted Waterways	3 m
Construction	2 m
Future 3-D Seismic	10 cm (Ranges ≤ 10 km)
Navigation in Constricted Channels	≤ 10 cm (3D)

1. Pathak, *et al*. [1990]

1.2 Expected GPS Performance

The GPS service available to a civilian user is termed the Standard Positioning Service (SPS). The expected horizontal accuracy for a SPS user, equipped with a stand-alone GPS receiver, is 100 metres (2DRMS, approximately 95%). Comparing this value to the requirements summarized in Tables 1.1 and 1.2, it can be seen that a stand-alone GPS receiver meets only the requirements for the Oceanic and Coastal phases of marine navigation, and the needs of a general bathymetric survey. Fortunately, differential GPS (DGPS), can improve significantly the performance of GPS. Achievable horizontal accuracies for various DGPS techniques are summarized in Table 1.3. The accuracy values presented in this table are estimates only. Many variables, such as the quality of the GPS user equipment, the processing techniques used, the separation distance between the reference GPS receiver and the remote GPS receiver, and atmospheric activity (to name just a few) will have an affect on the actual DGPS accuracy achievable. It is evident, however, that under appropriate conditions, DGPS techniques can be employed to meet some, if not all, of the navigation and positioning requirements outlined in Table 1.2.

Table 1.3 Approximate Horizontal Accuracies (2DRMS) of Various DGPS Techniques

DGPS Technique Employed	Approximate Horizontal Accuracy
None	100 m
Single Difference (Code Only)	1 to 10 m
Single Difference (Code and Carrier)	< 1 m to 5 m
OTF Ambiguity Resolution	< 10 cm to < 1 m

1.3 Augmentation of GPS With Pseudolites

While differential techniques can be used to improve the GPS solution, in applications where accuracy is essential, such as harbour navigation, a transit through a constricted waterway or hydrographic surveying, the surrounding topography or man-made structures may mask the line-of-sight GPS signals. This may result in reduced satellite availability, reduced reliability, degraded geometry and reduced horizontal DGPS accuracy. The use of one or more pseudolites (ground-based transmitters broadcasting GPS-like signals) can be used to augment the standard GPS constellation, and provide enhanced coverage during times of poor satellite geometry or during periods of reduced satellite availability due to unserviceability. In addition to enhancing coverage, a pseudolite (PL) can improve dramatically the integrity and reliability of the GPS solution.

1.4 Thesis Outline

The purpose of this thesis is to illustrate the use of a PL to augment the standard space-borne GPS satellite constellation, particularly for use in a challenging marine environment, such as a constricted waterway.

In Chapter 2 a review of GPS methodology is presented. This includes a review of the pseudorange and carrier phase GPS observables, and various error sources associated with GPS measurements. Two differential techniques are discussed, namely between-receiver single difference, and on-the-fly (OTF) ambiguity resolution. Methods by which to quantify GPS accuracy and reliability are introduced, and various techniques to detect and eliminate faulty observations are summarized.

In Chapter 3, PL technology is reviewed. Several technical and practical considerations of PL usage are discussed. Results of a field test at the University of Calgary are presented.

In Chapter 4, results from a simulation analysis are presented to assess the effect of up to three pseudolites on the DGPS availability, accuracy and reliability measures under the following two conditions: various constant mask angles, and a simulated obstructed horizon.

In Chapter 5, results from two field tests are presented. The first test was conducted at the Glenmore Reservoir in Calgary, and the second test was conducted at Lake Okanagan in British Columbia. The emphasis of this chapter is on the changes to the single difference DGPS performance due to PL augmentation.

In Chapter 6, the Lake Okanagan data were processed with and without the use of a shore-based PL to assess the changes to the OTF ambiguity resolution performance due to the use of a PL.

Recommendations and conclusions are presented in Chapter 7.

CHAPTER 2

GPS METHODOLOGY

The Global Positioning System was declared operational on December 8, 1993 with the announcement that GPS had reached Initial Operational Capability (IOC). This system, developed by the United States Department of Defense (DoD), is capable of providing position, velocity and timing information to an unlimited number of users. A space-borne constellation of 21 satellites and 3 active spares, orbiting in 6 planes, is configured to provide line-of-sight signal coverage from at least four satellites to a user located anywhere on the Earth. Each satellite transmits the GPS ranging signal on two frequencies: 1575.42 MHz (L1) and 1227.6 MHz (L2). The typical civilian user will use only the primary, or L1, frequency. A specific pseudorandom noise (PRN) code is assigned to each satellite, and is modulated onto the L1 frequency at a chipping rate of 1.023 MHz. This code is unencrypted, and it is also referred to as the C/A (Coarse/Acquisition) Code. The C/A code is replicated by the user's GPS receiver, and, by correlating the incoming C/A code with this replica, a range measurement can be made between the satellite and the receiver. Because the user's inexpensive crystal clock is not synchronized to GPS time, the range measurements to the various satellites include a receiver clock offset. Thus, the measured ranges are called pseudoranges. Four simultaneous pseudorange measurements are therefore required to solve for the four unknowns of latitude, longitude, altitude and receiver clock offset.

2.1 GPS Observables

The two most common GPS measurements are the pseudorange and the carrier phase observation. The pseudorange measurement is made by correlating a receiver generated replica of the transmitted C/A code against the received C/A code from a satellite. The amount of time that the replicated code is shifted (delayed) to produce a suitable degree of correlation to the received signal can be directly converted to a pseudorange by multiplying this time shift by the speed of light. The carrier phase measurement is the accumulated fractional phase offset between the receiver reference signal and the received satellite signal. Other inputs, such as the height of the GPS antenna on a marine vessel, can be used as a quasi-observation to help improve the GPS solution [Weisenburger and Cannon, 1997].

2.1.1 Pseudorange Observations

The pseudorange observation from a receiver (r) to a satellite (s) can be modelled as follows [Lachapelle, *et al*., 1992]:

$$p_r^s = \rho_r^s + d\rho^s + c(dt^s - dT_r) + d_{ion}^s + d_{trop}^s + \varepsilon(p_{rx}) + \varepsilon(p_{mult})_r^s \qquad 2.1$$

where p_r^s ... is the pseudorange measurement made by the receiver to the satellite at time t_k (m),

ρ_r^s ... is the geometric range at time t_k (m),

$d\rho^s$ ... is the orbital error term for the satellite which includes the nominal broadcast orbital error and the intentional error due to Selective Availability (SA) (m),

dt^s ... is the satellite clock error (m),

dT_r ... is the receiver clock error (m),

d_{ion}^s ... is the ionospheric delay of the satellite signal (m),

d_{trop}^s ... is the tropospheric delay of the satellite signal (m),

$\varepsilon(p_{rx})$ ... is the error in the pseudorange measurement due to receiver noise (m),

and $\varepsilon(p_{mult})_r^s$ ... is the error in the pseudorange measurement due to multipath (m).

Using World Geodetic System 1984 (WGS-84) coordinates, the geometric range from the receiver to the satellite at time t_k is shown graphically at Figure 2.1, and mathematically as follows:

$$\rho_r^s = \left|\mathbf{r}^s - \mathbf{r}_r\right| = \sqrt{\left(x^s - x_r\right)^2 + \left(y^s - y_r\right)^2 + \left(z^s - z_r\right)^2} \qquad 2.2$$

where ρ_r^s ... is the geometric range from the receiver to the satellite at time t_k (m),

$\mathbf{r}^s$ ... is the satellite position vector at time t_k, referenced to the WGS- 84 frame (m),

$\mathbf{r}_r$ ... is the receiver position vector at time t_k, referenced to the WGS- 84 frame (m),

x^s, y^s, z^s ... are the satellite WGS-84 coordinates at time t_k,

and x_r, y_r, z_r ... are the receiver WGS-84 coordinates at time t_k.

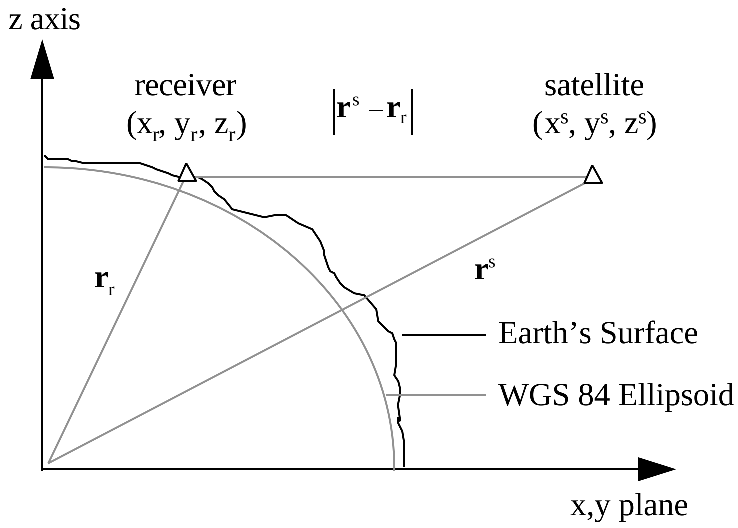

Figure 2.1 Geometric Range From a Receiver to a Satellite.

2.1.2 Carrier Phase Observations

In the same manner that the pseudorange measurement can be modelled by Equation 2.1, the carrier phase measurement can be modelled as follows:

$$\Phi_r^s = \rho_r^s + d\rho^s + c(dt^s - dT_r) + \lambda N_r^s - d_{ion}^s + d_{trop}^s + \varepsilon(\Phi_{rx}) + \varepsilon(\Phi_{mult})_r^s, \qquad 2.3$$

where Φ_r^s ... is the carrier phase measurement made by the receiver to the satellite at time t_k (m),

λN_r^s ... is the carrier phase ambiguity between the receiver and the satellite, multiplied by the wavelength of the carrier (m),

$\varepsilon(\Phi_{rx})$ ... is the error in the carrier phase measurement due to receiver noise (m),

and $\varepsilon(\Phi_{mult})_r^s$ ... is the error in the carrier phase measurement due to multipath (m).

2.1.3 Height as a Quasi-Observation

In a marine environment, the height of a vessel is generally known to within a few metres. This extra information increases the redundancy, and consequently, it improves the accuracy and reliability measures of the GPS solution. The design matrix is modified to incorporate the height constraint as a quasi-observation, and the *a priori* knowledge of the height parameter (i.e. the variance of the height constraint,

σ^2_{HC}) is incorporated into the least squares observation covariance matrix [Tang, 1996; Morley and Lachapelle, 1997].

2.2 GPS Error Sources

As shown in Equations 2.1 and 2.3, the GPS signals are subject to many errors that can affect adversely the ability to calculate the user's position, velocity and time. The SA errors ($d\rho^s$) are intentionally introduced by the DoD to reduce the achievable accuracy of a civilian receiver. The effect of some of these errors can be reduced through modelling, while others can be reduced significantly by employing various differential correction techniques. The GPS errors can be roughly divided into four distinct groups: errors that occur at the satellite (orbital and clock), errors that occur because of signal propagation through the atmosphere (ionospheric and tropospheric), errors that occur because of signal reflection (multipath) and errors that occur internal to the GPS receiver (receiver noise).

2.2.1 Satellite Errors ($d\rho^s$)

In order for a user to determine position, velocity and time based on the GPS pseudorange measurement, the satellite coordinates and the satellite clock error with respect to the master GPS time must be provided. As it is unfeasible to transmit the exact satellite coordinates and the clock corrections every epoch, parameters are included in the GPS navigation message which allow for each user to autonomously calculate this information as required. Satellite position and clock correction parameters are propagated into the future based on previous information using a Kalman filter. Thus, the expected accuracy of the predicted satellite coordinates and clock corrections will decrease over time until a new set of parameters is generated. Additionally there are errors intentionally induced by the DoD in the transmitted GPS signals to reduce the achievable accuracy of a civilian user. This intentional degradation of the L1 C/A signal is termed Selective Availability, or SA.

The Control Segment is responsible for the generation of the ephemeris and clock corrections contained in the GPS navigation message. These corrections are uploaded regularly to the GPS satellites, and they are, in turn, re-transmitted to the various GPS users in the 50 bit-per-second navigation message. These parameters can then be utilized by the users to compute estimates for satellite coordinates and satellite clock corrections on an as-required basis. Ephemeris errors occur when the parameters in the GPS navigation message do not yield the correct satellite location. Observed radial, cross-track and along-track errors are summarized at Table 2.1 [Zumberge and Bertiger, 1994]. Note that only the projection of the satellite position error along the line of sight between the user and the satellite is important for assessment of ranging accuracy.

Table 2.1 Observed Satellite Position Errors Between Ephemeris and Precise Orbits

Parameter	Observed Error (m)
Radial (σ_r)	1.2
Cross-track ($\sigma_\dagger$)	3.2
Along-track (σ_a)	4.5

For single receiver (i.e. non DGPS) positioning, the ability to predict the performance of the GPS satellite clocks is critical to the overall performance of the system. Because the GPS satellites use very high quality cesium atomic clocks, their predictable performance is quite good. Specified frequency stabilities over one day are $2x10^{-13}$, with observed values for broadcast ephemerides of $1.2x10^{-13}$ [Spilker, 1994]. For the GPS user, this equates to an error of about 10^{-8} seconds (or 3.5 m) over one day (~ 10^5 seconds).

The United States Department of Defense has the ability to intentionally degrade not only the information contained in the navigation message, but the transmitted GPS signal itself. The Selective Availability (SA) error is the sum of two components: a bias component (or epsilon error), and a rapidly varying error due to satellite clock dither. The epsilon error is the intentional manipulation of the GPS navigation message orbit data, causing errors in the calculation of satellite coordinates. These errors result in slowly varying user positions, with periods of several hours. The GPS satellite clock dither results in rapidly changing errors in the pseudorange measurements, with periods on the order of minutes. Without SA, GPS is capable of providing horizontal accuracies of approximately 20 m (95%). With SA, however, the achievable accuracy for a stand-alone receiver is specified at 100 m (95%) in the horizontal, and 140 m (95%) in the vertical.

2.2.2 Ionospheric (d^s_{ion}) and Tropospheric (d^s_{trop}) Errors

Before the transmitted GPS signal is received by a user, it must travel from the satellite, through the Earth's atmosphere, to the GPS antenna. Propagation through the atmosphere can have a significant effect on the nature of the received signal. Two distinct atmospheric regions have been identified, namely the ionosphere and the troposphere, each with its own influence on the GPS signal.

The ionosphere is a region of weakly ionized plasma, extending from approximately 50 km to 1000 km above the Earth's surface. The ionospheric effects vary depending on the frequency used and the electron content along the signal propagation path (which is a function of solar activity levels and geographic location). Range errors at GPS frequencies can vary from less than 1 m to greater than 100 m. It is important to note that the code and phase range measurement errors due to the ionosphere are divergent. That is, the code is delayed and the phase is advanced.

For GPS purposes, the troposphere can be defined as the portion of the Earth's atmosphere extending from the Earth's surface to a height of approximately 50 km. The wet and the dry components of the troposphere have different effects on the propagation of the GPS signal. The dry component accounts for approximately 90% of the total tropospheric affect, and can be modelled to a large degree. The wet component, however, varies considerably with time and location, and is notoriously difficult to model effectively. As most of the water vapour in the atmosphere occurs at heights less than 4 km, signals from low elevation satellites, which have a long propagation path length through the troposphere, are most affected. For a satellite signal, the total tropospheric delay is on the order of 2 - 25 m [Spilker, 1994]. Tropospheric models can be used to correct for a large portion of the total tropospheric delay [Hopfield, 1969] .

For differential GPS applications, the satellite signals received at the reference and remote stations have travelled along essentially the same propagation path (assuming that the stations are relatively close to one another), thus the ionospheric and tropospheric delay experienced by each receiver will be highly correlated and it will be reduced significantly through the application of the differential corrections.

2.2.3 Code and Phase Multipath [$\varepsilon(p_{mult})_r^s$ and $\varepsilon(\Phi_{mult})_r^s$]

The reflection and diffraction of a transmitted GPS signal can result in multiple signals being received by a user. This phenomenon, termed multipath, is a major error source in precise GPS applications. Multipath can distort the signal modulation, resulting in measurement errors of the pseudorandom code. Multipath can also degrade the phase of the carrier, resulting in measurement errors of the L1 phase. Unlike many of the other error sources, it tends to be an uncorrelated error that will not difference out using DGPS techniques.

For the code measurement, the multipath signals will always arrive at the user antenna by a longer path than the direct signal. The ideal and reflected signals will superimpose to produce the net received signal, shown in Figure 2.2. A GPS receiver will correlate its copy of the PRN code against the net received signal, not the actual signal. The time delay (ΔT) between the actual signal and the received signal multiplied by the speed of light yields the net pseudorange error due to multipath. The magnitude of this error is site, geometry and equipment dependent, but it is typically less than 3 metres. In extreme cases, the value of the code error can exceed 100 m [Braasch, 1995].

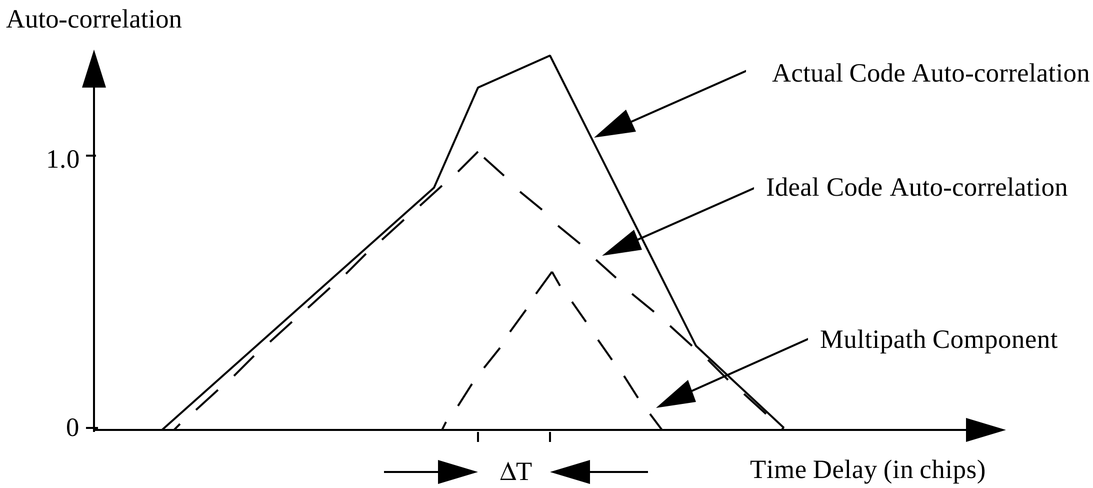

Figure 2.2 Effect of Multipath on Code Auto-correlation.

A mathematical representation of the carrier phase observable for a two-path signal can be expressed as

$$S_o = V\cos(\phi_d) + \alpha V\cos[\phi_d + \theta] \qquad 2.4$$

where S_o ... is the observed (received) signal,

V ... is the voltage of the ideal signal,

ϕ_d ... is the phase of the ideal (direct) signal,

α ... is a reflectivity coefficient that relates the relative strength of the reflected signal to the actual signal (typically less than 1),

δ ... is the relative time delay of the reflected signal with respect to the actual signal,

and θ ... is the phase shift caused by the reflected signal.

The carrier phase multipath delay (ψ), as a function of the reflectivity coefficient (α) and the phase distortion due to multipath (θ) can be written as

$$\psi = \tan^{-1}\left(\frac{\alpha\sin\theta}{1+\alpha\cos\theta}\right). \qquad 2.5$$

The case of maximum path delay must fulfill the condition $\partial\psi / \partial\theta = 0$, which occurs at $\theta_{max} = \pm\cos^{-1}(-\alpha)$. Thus, the maximum carrier phase multipath error induced by a single reflected signal is a function of only the reflected signal strength ratio (α). The maximum theoretical error therefore occurs for an α of 1, which corresponds to $\pm 90°$. As $90°$ is equivalent to one quarter of a cycle, the maximum theoretical carrier phase error due to multipath is $\lambda_{L1}/4$, or approximately 4.8 cm [Leick, 1995]. Typical carrier phase multipath is on the order of 1 to 2 cm.

2.2.4 Receiver Noise Errors [$\varepsilon(p_{rx})$ and $\varepsilon(\Phi_{rx})$]

With the measurement of pseudoranges and phases comes a noise component associated with the receiver itself. Fortunately, this receiver noise tends to be small in magnitude, uncorrelated between measurements, and it can be well modelled by a Gaussian distribution. Code tracking errors vary considerably between GPS receiver models, but are generally in the range of 0.03 to 1.0 % of the C/A code chip length, or 0.1 m to 3 m. The L1 carrier phase noise is generally less than 0.3 cm.

2.3 Differential GPS Techniques

The fundamental goal of DGPS is to improve the position solution of the GPS user. The standard approach is to use a stationary GPS receiver (termed the reference station) at known coordinates to observe all satellites in view and calculate the difference between the calculated distance to the satellites and the measured pseudoranges to the satellites. These differences, or differential corrections, are then broadcast to the GPS users, who can then apply these corrections to their measurements of the same satellites. In this way, correlated errors (such as satellite orbital errors, satellite clock errors, ionospheric errors and tropospheric errors) can be reduced significantly. Using differential techniques, the horizontal positioning accuracy can be improved from 100 m (95th percentile) to better than 1 m (1σ), providing that the user is within approximately 50 km of the reference station, and the differential corrections are applied within ten seconds [Parkinson and Enge, 1995]. The restrictions on remote/reference separation and correction age are due to the spatial and temporal decorrelation of the GPS error sources. The following two sections describe two different DGPS techniques: between-receiver single difference and on-the-fly (OTF) ambiguity resolution.

2.3.1 Between-Receiver Single Difference

The University of Calgary software package C^3NAV™ (Combined Code and Carrier for Navigation), which was used as a starting point for some of the investigations presented in this thesis, is based on the between-receiver single difference concept [Cannon & Lachapelle, 1992]. As shown in Figure 2.3, a GPS reference receiver observes all satellites in view, and calculates differential corrections to all satellites at each epoch. A user (remote station) then applies these corrections. For a real-time system, the corrections are broadcast to the user via a separate data link. For post-processing, the corrections are saved to a data file and applied to the remote observations as required.

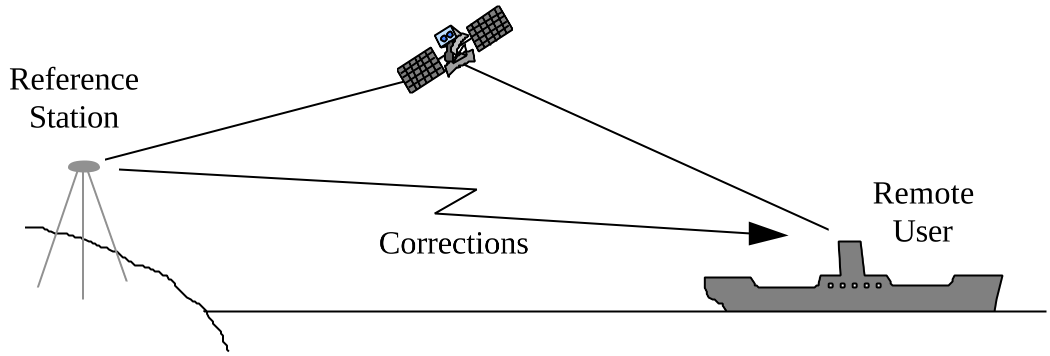

Figure 2.3 Between-Receiver Single Difference Technique.

The between-receiver single difference equation for the pseudorange measurement is

$$\Delta p_r^s = \Delta\rho_r^s + \Delta d\rho^s + c\Delta dT_r + \Delta d_{ion}^s + \Delta d_{trop}^s + \Delta\varepsilon(p_{rx}) + \Delta\varepsilon(p_{mult})_r^s \qquad 2.6$$

where Δ ... represents the difference in the specified quantity after the two observations are subtracted (e.g. $\Delta p_r^s = \Delta p_{r1}^s - \Delta p_{r2}^s$).

Note that in the above equation the satellite clock error (dt^s) is eliminated, and the orbital and atmospheric errors are greatly reduced (due to their spatial correlation over short baselines). Because of the differencing, the magnitude of the receiver noise term is increased. The multipath component may increase or decrease, depending on the degree of correlation of the observed multipath signal at each receiver. As stated previously, the expected positioning accuracy of this technique is 0.5 m to 5 m, again, depending on the timely application of the differential corrections, the quality of the GPS equipment, and the separation of the reference and remote stations.

Carrier phase smoothing of the pseudoranges can be used to further improve the accuracy of DGPS techniques. By exploiting the inherently accurate (but ambiguous) carrier phase measurements with the noisier (but unambiguous) pseudorange measurements, a much improved DGPS position solution can be computed. Carrier phase smoothing of the pseudoranges can reduce significantly the deleterious effects of multipath. The technique described here is the method implemented in C^3NAV™. The basic carrier phase smoothed pseudorange equation is

$$\left(\tilde{p}_r^s\right)_k = W_k^p\left(p_r^s\right)_k + W_k^{\Phi}\left\{\left(\tilde{p}_r^s\right)_{k-1} + \left(\Phi_k - \Phi_{k-1}\right)\right\} \qquad 2.7$$

where $\left(\tilde{p}_r^s\right)_k$ ... is the computed smoothed pseudorange at time k (m),

$\left(p_r^s\right)_k$ ... is the measured smoothed pseudorange at time k (m),

$\left(\tilde{p}_r^s\right)_{k-1}$ ... is the computed smoothed pseudorange at time k-1 (m),

$\left(\Phi_k - \Phi_{k-1}\right)$ ... is the range difference computed from the measured carrier phases at times k and k-1 (m),

W_k^p ... is the weight assigned to the pseudorange measurement,

and W_k^Φ ... is the weight assigned to the carrier phase measurement.

The relatively noisy code pseudorange measurement is used to guide the ambiguous carrier phase measurement to approximately the correct cycle (within typically three to five cycles, or 1 m [Seeber, 1993]) by progressively increasing the relative weight of the phase measurement. For the first epoch, the weight for the code measurement is set to 1.00, whereas the weight for the carrier phase measurement is set to 0.00. At the second epoch, the code weight is reduced to 0.99, while the phase weight is increased to 0.01. This process continues until the code weight equals 0.01 and the carrier phase weight equals 0.99, at which time the weights have reached a steady state value.

Two smoothing ramps, running in parallel, are used in C^{3}NAV. This is required because of code and carrier divergence, caused by signal propagation through the ionosphere. The dual ramp methodology is shown in Figure 2.4. Both ramps initialize at the same time, and the pseudorange and carrier phase weights are adjusted at the same rate. Either ramp can be used to generate the smoothed pseudorange. After a certain number of epochs, typically 400 to 1000, the weights on ramp 1 are reset, and ramp 2 is used to generate the smoothed pseudoranges. After the next number of epochs, ramp 2 is reset, and ramp 1 is used to generate the smoothed pseudoranges, and the cycle continues. If a loss of lock on the carrier phase is detected, both ramps are reset for that satellite, and the process begins again.

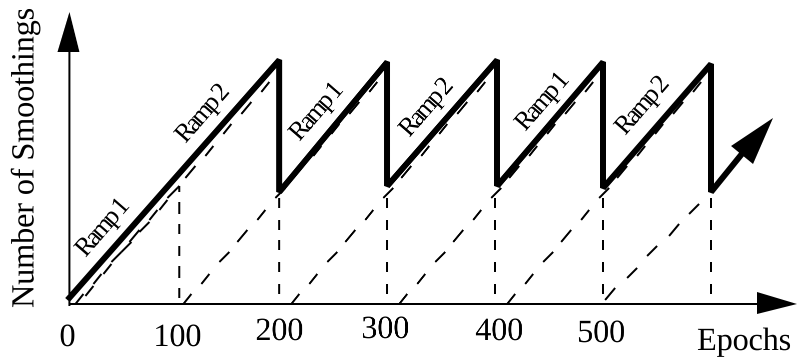

Figure 2.4 C^{3}NAV Dual Ramps for Carrier Phase Smoothing of the Pseudorange Measurements.

2.3.2 On-The-Fly Ambiguity Resolution

For certain applications, a very precise three dimensional GPS position solution must be obtained. To accomplish this, the exact number of L1 (19 cm) cycles between the satellite and the reference and remote receivers, (the integer ambiguities) must be determined. This will allow full use of the fractional carrier phase measurement, resulting in a position solution with an expected 3D accuracy of 3 to 10 cm for a 10 kilometre station separation [Hoffmann-Wellenhof, *et al.*, 1994]. The determination of the integer ambiguities is not a trivial matter. The basic approach is to use the noisy pseudorange measurements to define a volume which is assumed to contain the correct set of integer ambiguities. All possible integer ambiguity combinations within this volume are then tested to determine a set that is "best" in some sense. The integer ambiguity set that minimizes the sum of squared carrier phase residuals is an often used test criterion. A ratio test is often performed between the sum of squared carrier phase residuals of the "best" and "second best" integer ambiguity sets. If this ratio exceeds a certain threshold, say 3:1, then the "best" set is considered to be the correct ambiguity combination, and the carrier phase ambiguities are "fixed".

As the number of integer cycles between a receiver and a satellite is always changing, a technique known as double differencing is used to create a "double difference ambiguity" ($\Delta\nabla N$) that is constant with respect to time (assuming no cycle slips occur). The basic methodology is shown graphically in Figure 2.5. A high elevation satellite, observed by both GPS users is chosen as the "base satellite". At each GPS station the observations from the base satellite are subtracted from the observations to all other satellites observed at each epoch. The differences for the reference station are then subtracted from the differences at the remote station to create the "double difference".

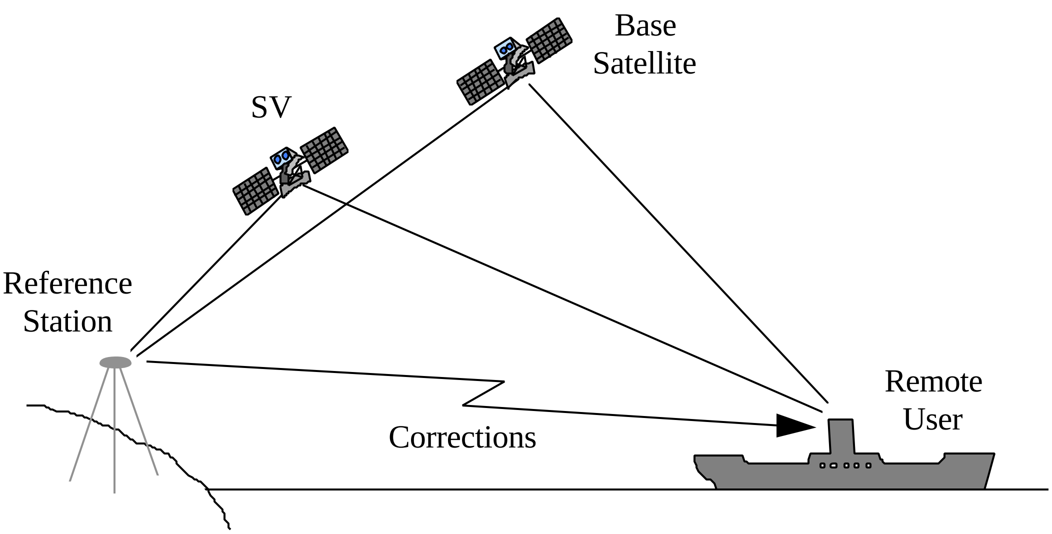

Figure 2.5 Satellite-Receiver Double Difference (DÑ) Technique.

The general form of the satellite-receiver double difference is

$$\Delta\nabla = \left\{(\mathrm{data})^{\mathrm{sat}} - (\mathrm{data})^{\mathrm{base}}\right\}_{\mathrm{rem}} - \left\{(\mathrm{data})^{\mathrm{sat}} - (\mathrm{data})^{\mathrm{base}}\right\}_{\mathrm{ref}} \qquad 2.8$$

where $\Delta\nabla$ ... is the satellite-receiver double difference,

$(\mathrm{data})^{\mathrm{sat}}$ ... is the data from any satellite (other than the base satellite),

$(\mathrm{data})^{\mathrm{base}}$ ... is the data from the base satellite

$\{\ \}_{\mathrm{rem}}$ ... is the differenced data calculated by the remote station,

and $\{\ \}_{\mathrm{ref}}$ ... is the differenced data calculated by the reference station.

The satellite-receiver double difference equation for the carrier phase measurement is then

$$\Delta\nabla\Phi = \Delta\nabla\rho + \Delta\nabla d\rho + \lambda\Delta\nabla N - \Delta\nabla d_{\mathrm{ion}} + \Delta\nabla d_{\mathrm{trop}} + \varepsilon\Delta\nabla\left(\Phi_{\mathrm{rx}}\right) + \varepsilon\Delta\nabla\left(\Phi_{\mathrm{mult}}\right). \qquad 2.9$$

Note that the above equation assumes that all observations are taken at the same time and that both the reference and remote stations observe the same base satellite. The satellite and receiver clock terms are eliminated, and the effects of orbital and atmospheric errors are reduced greatly. This method increases the contributions of receiver noise or multipath due to quadratic error propagation.

The University of Calgary software package FLYKIN™ uses the Fast Ambiguity Search Filter (FASF) to solve for the integer ambiguities [Chen, 1994]. A modified version of FLYKIN™, named SEAFLY, was recently completed which incorporates, in addition to the FASF, a Kalman filter that allows for an optimal floating ambiguity solution [Weisenburger & Cannon, 1997]. Further modifications were made to SEAFLY (termed SFLYPL) to post-process information from the standard space borne GPS constellation and one PL.

2.4 GPS Accuracy and Reliability Measures

Three important concepts are frequently used in the design and analysis of a GPS configuration: precision, accuracy, and reliability. Precision refers to the distribution of repeated observations relative to the sample mean. Accuracy refers to the distribution of repeated observation relative to the true value. Reliability measures can be divided into internal and external reliability. Internal reliability reflects the ability of a system to detect and localize blunders, whereas external reliability quantifies the effect of an undetected blunder on the estimated parameters. Ultimately, the goal is to produce a system that is both precise and accurate, with a strong capability to detect, localize and remove blunders.

The Dilution of Precision (DOP) is a measure of the geometrical strength of a satellite constellation. As DOP values are calculated from the unit vectors to each satellite, as observed by the user, they are location and time specific. To obtain DOP values associated with the user's local horizontal and vertical directions, it is necessary to express the geometry in terms of curvilinear coordinates rather than in Cartesian coordinates. The elements of the design matrix (**A**) are then the partial derivatives with respect to the curvilinear coordinates (Φ, λ, h) and the time bias (t). The DOP calculation is shown as follows:

$$\left[\mathbf{A}^T\mathbf{A}\right]^{-1} = \begin{bmatrix} \sigma^2_{\Phi} & \sigma^2_{\Phi\lambda} & \sigma^2_{\Phi h} & \sigma^2_{\Phi t} \\ \sigma^2_{\lambda\Phi} & \sigma^2_{\lambda} & \sigma^2_{\lambda h} & \sigma^2_{\lambda t} \\ \sigma^2_{h\Phi} & \sigma^2_{h\lambda} & \sigma^2_{h} & \sigma^2_{ht} \\ \sigma^2_{t\Phi} & \sigma^2_{t\lambda} & \sigma^2_{th} & \sigma^2_{t} \end{bmatrix}. \qquad 2.10$$

The DOP values of interest lie along the main diagonal. The Dilution Of Precision in the user's horizontal plane, or HDOP, can then be calculated as follows:

$$\mathrm{HDOP} = \sqrt{\sigma^2_{\Phi} + \sigma^2_{\lambda}}\ . \qquad 2.11$$

As mentioned previously, accuracy refers to the distribution of the repeated observations relative to the true value. An accuracy measure can be derived from a precision measure if and only if any errors included in the measurements are truly random with a mean error of zero. If correlated errors or blunders occur, then the accuracy measure is no longer valid, as the sample mean will no longer coincide with the true value. As shown in Figure 1, the variables α and β can be chosen by the system designer to yield the non-centrality parameter, δ_o. The parameter α represents the probability of rejecting a good observation (Type I Error), while the parameter β represents the probability of accepting an incorrect observation (Type II Error). The parameter δ_o represents the magnitude of the bias between the true value and the calculated value (biased due to possible systematic errors or blunders). Typical values used in practice for α, β and δ_o are summarized at Table 2.2 [Leick, 1995].

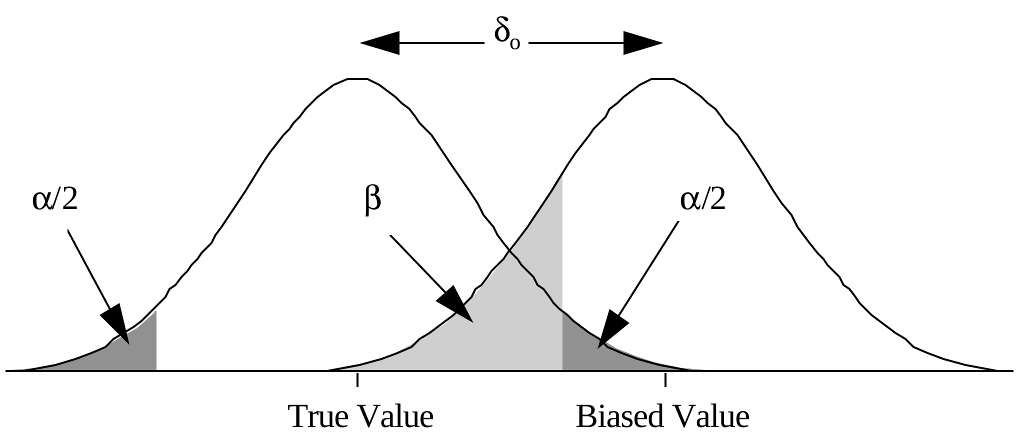

Figure 2.6 Representation of a Biased Measurement.

Table 2.2 Typical Values for a **,** b **and** d_o

a (**Type I Error**)	b (**Type II Error**)	d_o
0.050	0.20	2.80
0.025	0.20	3.10
0.001	0.20	4.12
0.050	0.10	3.24
0.025	0.10	3.52
0.001	0.10	4.57

Internal reliability is a measure of the capability of the system to detect and localize a blunder. The Marginally Detectable Blunder (MDB) is the smallest magnitude blunder that can be detected. For the case of only one blunder in a typical GPS epoch (with uncorrelated observations), the MDB of the i^{th} observation in the system can be computed. First, the covariance matrix for the residuals is calculated using the covariance matrix of the observations and the design matrix, as follows:

$$\mathbf{C}_{\hat{r}} = \mathbf{C}_{l} - \mathbf{A}\left[\mathbf{A}^{T}\mathbf{C}_{l}^{-1}\mathbf{A}\right]^{-1}\mathbf{A}^{T} \tag{2.12}$$

where $\mathbf{C}_{\hat{r}}$ ... is the covariance matrix of the residuals,

$\mathbf{C}_{l}$ ... is the covariance matrix of the observations,

and $\mathbf{A}$ ... is the design matrix.

Next, the covariance matrix of the residuals is combined with the weight matrix of the observations. The elements of the main diagonal are extracted to produce a vector, **r**, which represents the redundancy contribution for each observation:

$$\mathbf{r} = \left(\mathbf{C}_{\hat{r}}\mathbf{C}_{l}^{-1}\right)_{ii} \quad . \tag{2.13}$$

Finally, the marginally detectable blunder associated with the i^{th} observation (∇l_i^o) is calculated using the non-centrality parameter (d_o) described previously, and the standard deviation of the i^{th} observation (σ_{ii}):

$$\nabla l_i^o = \sigma_{ii}\frac{\delta_o}{\sqrt{r_i}} \tag{2.14}$$

where ∇l_i^o ... is the i^{th} element of the ∇l^{o} vector, corresponding to the marginally detectable blunder of the i^{th} observation,

σ_{ii} ... is the standard deviation of the i^{th} observation,

δ_o ... is the non-centrality parameter,

and r_i ... is the ith element of the **r** vector, representing the redundancy contribution of the i^{th} observation.

Thus, at a given epoch, there exists an MDB associated with each observed satellite. If a blunder occurs in an observation to a satellite, and if it is smaller than the MDB for that satellite, the error will not be detected by statistical testing of the residuals, and the erroneous observation will be accepted as valid. It is therefore desirable to have MDBs as small as possible.

As mentioned previously, external reliability is defined as the effect on the unknown parameters of a systematic error or blunder. Thus, the effect of an MDB on the estimated parameters can be calculated as follows:

$$\nabla \mathbf{X}_i^o = \left(\mathbf{A}^T \mathbf{C}_l^{-1} \mathbf{A}\right)^{-1} \mathbf{A}^T \mathbf{C}_l^{-1} \nabla \mathsf{l}^o \ . \qquad 2.15$$

The effect of a blunder on the horizontal position can then be determined by calculating the effect of the i^{th} element of the MDB vector ($\nabla \mathsf{l}^o$) on the estimated parameters. It is assumed that only one error in an observation to a satellite occurs in a given epoch, and that the magnitude of this error is equal to the MDB for that satellite. Thus, all elements of the $\nabla \mathsf{l}^o$ vector are equal to zero except for the i^{th} element, as shown below:

$$\nabla \mathsf{l}^o = \begin{bmatrix} 0 \\ 0 \\ 0 \\ \nabla \mathsf{l}_i^o \\ 0 \\ 0 \end{bmatrix} \ . \qquad 2.16$$

This results in a worst-case error in latitude ($\nabla\phi_i$), longitude ($\nabla\lambda_i$) and height (∇h_i) (all expressed in metres) associated with the i^{th} observation. The error in latitude and longitude will then yield the horizontal error ($\nabla \mathbf{h}_i$), due to the i^{th} element of $\nabla \mathsf{l}^o$, as follows:

$$\nabla \mathbf{h} = \sqrt{\nabla \Phi_i^2 + \nabla \lambda_i^2} \ . \qquad 2.17$$

Finally, the largest horizontal error that theoretically could occur at a specific epoch due to an undetected blunder on any of the observations, is defined as the largest magnitude element of the $\nabla \mathbf{h}$ vector, or:

$$\mathrm{MHE} = (\nabla \mathbf{h})_{max} \ . \qquad 2.18$$

This value is termed the Maximum Horizontal Error, or MHE. The MHE is thus a function of satellite geometry at a given epoch, the redundancy that exists at that epoch, the standard deviations of the observations, and the non-centrality parameter. A plot of the MHE with respect to time will create a worst-case "envelope", where all possible horizontal errors due to an undetected blunder at a particular epoch will be guaranteed to be less than or equal to the value of the MHE envelope. It is important to note that the MHE envelope is evaluated assuming that each epoch is treated independently, a worst-case blunder (with respect to horizontal positioning) occurs at each epoch, and that no filtering of the position solution occurs.

2.5 GPS Integrity, Fault Detection and Exclusion

Integrity is defined as the ability of a system to provide timely warnings to the user when the system should not be used for navigation [van Graas, 1996]. For differential GPS operations, the concept of integrity monitoring is sub-divided into issues concerned with the reference station (and the generation of valid differential corrections), and the remote station (which must apply the differential corrections then autonomously perform some form of Fault Detection and Exclusion [FDE]). Much work has been completed on the concept of integrity monitoring at the reference station [Shively and Faunce, 1996; Skidmore et. al, 1996], and the reader is referred to these selected papers for a detailed explanation.

For this thesis, it is assumed that the differential corrections have passed all integrity checks, and are assumed blunder free. What is of utmost importance is the ability of the remote station to successfully apply the corrections, assess the quality of its position solution, and, if required, detect and (if necessary) exclude one or more observations from the GPS solution. This process is termed Fault Detection and Exclusion (FDE). When the position solution generated cannot be guaranteed to lie within a certain region, an alert must be presented to the user.

Two fault detection techniques are briefly described. The first fault detection method, as described by Leick and summarized above, performs statistical testing on the least squares residuals. The second method, as described by van Graas, makes the integrity assessment in position space, quantifying the degree of "scattering" of the position solutions that occurs in the event of a blunder. The two methods share one main attribute: a measurement of the system (whether this is residuals, or position "scattering") is compared against some form of a test statistic, and a decision is made as to whether a particular observation contains a blunder.

The first fault detection technique has been described previously in section 2.4. The magnitude of the residual for the i^{th} satellite is tested against the i^{th} MDB (marginally detectable blunder) at a given epoch. If the residual is smaller than the MDB, the observation is considered to be blunder free. If, on the other hand, the i^{th} residual is larger than the i^{th} MDB, it is concluded that the observation contains a blunder.

The second fault detection method quantifies the degree of scattering of subsets of the all-in-view position solution. If, at a certain epoch, there are five satellites in view, and if a blunder occurs on the measurement to one of these satellites, the position solution (using all five satellites) will be affected by this blunder. If subsets of four satellites are formed, and position solutions computed for each subset, every subset that contains the erroneous observation will be affected by the error. The degree of scattering of the subsets, as compared to the all-in-view position solution, can potentially be used to identify (and possibly remove) the erroneous measurement [van Graas, 1996]. Figure 2.7 shows this concept of fault detection. Specific positioning and navigation requirements determine the Horizontal Alert Limit (HAL). For the harbour/harbour approach navigation phase, the HAL is defined as 8 to 20 metres. The Horizontal Protection Level (HPL) is a calculated value which is geometry dependent. It is guaranteed the all-in-view position will lie within the HPL, according to the specified levels of false and missed alerts. The HPL must be smaller than the HAL, or a warning must be issued before the position output can be used. For DGPS applications, the HPL is given by:

$$\mathrm{HPL} = R_{bias} = \left(\sqrt{\bar{x}_i^2 + \bar{y}_i^2}\right)_{max} \qquad 2.19$$

where HPL ... is the Horizontal Protection Level at a particular epoch,

R_{bias} ... is the maximum horizontal radial position error,

and $\bar{x}_i$, $\bar{y}_i$ ... are the horizontal components associated with the biased errors of the i^{th} satellite.

This method is very similar to the procedure described previously, except that the statistical testing of the DGPS solution occurs in position space rather than residual space.

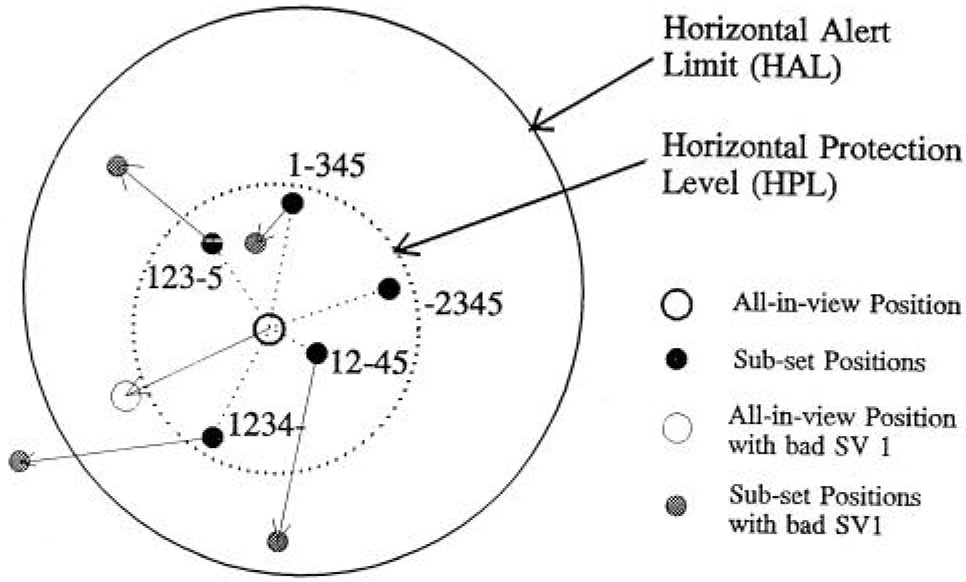

Figure 2.7 Illustration of Fault Detection in Position Space.

CHAPTER 3

PSEUDOLITES

As mentioned previously, a pseudolite (or pseudo-satellite) is a ground-based transmitter that broadcasts GPS like signals. While this may seem to be a new and revolutionary technology, the concept of a terrestrial GPS transmitter is actually quite mature. In fact, the Inverted Range, a GPS user equipment test facility located at the Yuma Proving Ground, used four ground transmitters (GTs) to augment the limited number of space-borne GPS satellites during initial GPS trials as early as 1977 [Denaro, *et al*., 1980]. Since then, interest in augmenting GPS with pseudolites (PLs) has grown steadily. One of the first papers to suggest the use of PLs for civilian aviation and maritime users was presented in 1986 [Klein and Parkinson, 1984].

This chapter reviews the potential benefits that can be achieved through the use of pseudolite technology, summarizes some of the technical considerations that must be addressed before PL augmentation can be implemented, and describes some of the many practical considerations with respect to PL augmentation of GPS. Finally, results will be presented of a proof-of-concept static field test conducted at the University of Calgary on September 28, 1996.

3.1 Potential Benefits of PL Augmentation of GPS

There are many potential benefits that can be realized by augmenting GPS with PLs. Some of these benefits include: greater positioning accuracy, improved reliability, availability, continuity, and integrity monitoring, and a reduction in integer ambiguity resolution time [Ndili, 1994]. By using the PL signal's integral data link capability, DGPS operations can be supported, resulting in accuracy and integrity enhancement, through the timely transmittal of DGPS corrections and integrity warning information. This list of potential benefits, while impressive, is not achievable without due consideration of several technical issues related to the design of the PL system, and several operational issues related to the deployment and expectations of the PL system.

3.2 Technical Considerations

There are many technical issues that must be addressed before GPS can be successfully augmented with a PL. One of the major obstacles is termed the 'near-far' problem, described below. Other technical issues include the PL signal design, the PL data message, and the ability to synchronize the PL clock to GPS time.

3.2.1 The 'Near/Far' Problem

As a GPS satellite is at a relatively large distance from the GPS user, the average power received by the user remains relatively constant. A typical GPS receiver is designed for a received power level of approximately -130 dBm (or -160 dB) [Van Dierendonck, 1990]. For the case of a PL however, the assumption of relatively constant received power may not always be valid. As the received power is inversely proportional to the square of the PL/user distance, a GPS receiver can be subjected to vastly different received power levels. At one extreme, the PL signal may be below the detection threshold of the GPS receiver (the 'far' limit), whereas at the other extreme, the GPS receiver may be overwhelmed by the strength of the PL transmission, effectively jamming out other GPS satellites (the 'near' limit).

A graphical representation of the 'near/far' problem is shown in Figure 3.1. If a user is outside of the 'far' bubble, they will not receive the PL signal, but they will be able to track GPS signals. If a user is inside the 'near' bubble, the PL will jam the GPS receiver and they will be unable to track GPS satellites. Within these two limits, the user will be able to track successfully both the PL and the GPS satellite constellation.

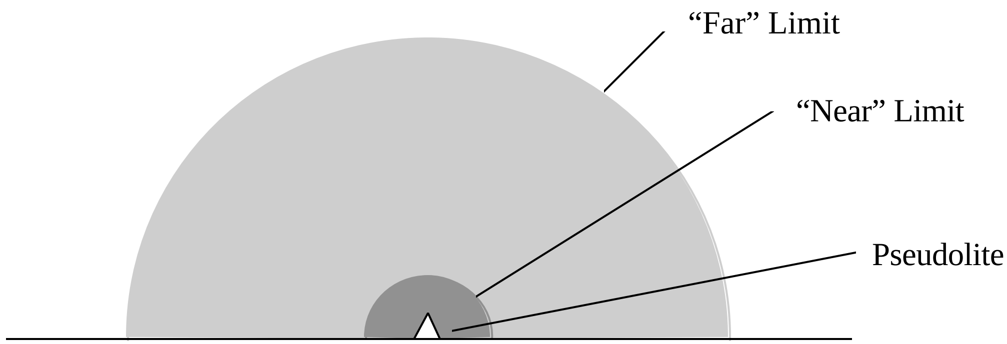

Figure 3.1 The 'Near/Far' Problem.

A rough estimate of the ratio between the near and far limits can be determined by considering the worst-case cross correlation between two C/A code signals, which is given as -21.6 dB [Spilker, 1980]. Thus, if a GPS receiver is designed to receive signals at -160 dB, and the received PL signal is at -138.4 dB (21.6 dB stronger), one can expect cross-correlations to begin to occur between the C/A codes of the GPS satellites and the C/A code of the PL. These values can then be substituted into the following equation:

$$P_{rec} = P_{des} + 20\log\left(\frac{d_o}{d}\right) \qquad 3.1$$

where P_{rec} ... is the power received at a GPS receiver (dB),

P_{des} ... is the power level for which the GPS receiver was designed, typically -160 dB,

and $\frac{d_o}{d}$ ... is the ratio between the distance at which the transmitted signal is received at the P_{des} power level (d_o), and a variable distance corresponding to the actual transmitter distance (d).

The ratio between the near and the far radii is found to be approximately 12:1. Thus, both GPS signals and the PL signal would be useable only within this limited distance ratio. Due to limitations of the signal processing techniques this ratio is actually on the order of only 10:1. This is a very restrictive property, and much work has been conducted on solving, or at least reducing, the 'near/far' problem. Most of this effort has been concentrated on the design and nature of the PL signal design.

3.2.2 PL Signal Design

There are essentially three signal processing techniques by which to mitigate the effects of the C/A code cross-correlation, or 'near/far' problem [Elrod and Van Dierendonck, 1995]. These techniques include: use of alternative codes (a variation of Code Division Multiple Access, or CDMA); use of a frequency offset (a variation of Frequency Division Multiple Access, or FDMA); or the use of a pulsed signal (a variation of Time Division Multiple Access, or TDMA). Of the three methods, the TDMA techniques is favoured. A brief overview of the three signal diversity techniques follows.

The GPS already uses CDMA techniques by assigning different pseudo-random noise “Gold Code” to each satellite. As mentioned above, the worst-case cross correlation that exists between these codes is approximately 21.6 dB. By using a more powerful C/A code for a PL, it is possible to reduce this cross correlation by 21 dB. This can be accomplished by using 17 stage code registers instead of the 10 stage registers normally used with GPS satellites. The chipping rate of the code is not changed so as to not affect adversely the requirements on the receiver bandwidth [Van Dierendonck, 1990]. Unfortunately, CDMA techniques such as this add complexity (and cost) to a GPS receiver.

Another promising technique, while not FDMA in the strict sense, is to simply offset the transmitted PL signal from the L1 frequency of 1575.42 MHz. By transmitting at an offset of 1.023 MHz, the PL carrier can be placed in the first null of the C/A code spectrum of the GPS satellite signals. Figure 3.2 shows the typical spectrum of the GPS C/A code for PRN 2. This FDMA technique is quite effective in that it virtually eliminates the cross-correlation between the PL signal and the GPS satellite signals. At the 1.023 MHz offset, the spectral lines for PRN 2 are below -80 dB, and they are also approximately 60 dB below the spectral lines at a 0 dB offset [Elrod and Van Dierendonck, 1995]. The Global Orbiting Navigation Satellite System (GLONASS) uses this technique to enable multiple codes to be assigned to multiple satellites.

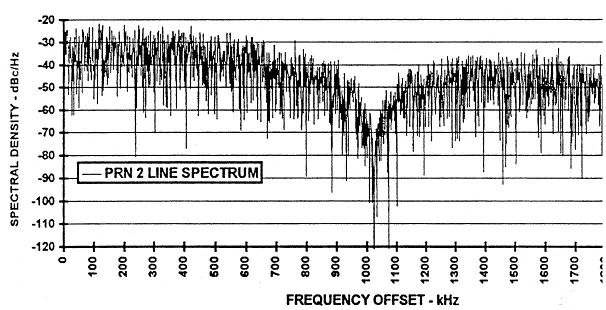

Figure 3.2 PRN 2 GPS C/A Code Spectrum.

The final, and most favoured signal diversity technique, is TDMA, using a pulsed signal. With a well designed pulsing scheme, the effect of the PL signal on GPS signal reception can be reduced significantly. Most modern GPS receivers will treat the pulsed PL signal as a continuous signal, allowing continuous tracking of the PL carrier signal. A typical pulsing scheme is shown by the Xs in Figure 3.3. The pulsing cycle repeats every 11 ms, so it would never be synchronous with bit patterns received from GPS. Each code cycle of 1 ms is further divided into 11 slots. As only one slot out of every 11 contains a pulse, the effective duty cycle is 1/11. A GPS receiver would then integrate the received energy from the PL over the entire time period. The resulting loss in signal to noise ratio for a GPS signal is typically less than 1.5 dB, even when close to a pulsed PL [Elrod and Van Dierendonck, 1995].

C/A Code Cycles	Slot No.										
	1	2	3	4	5	6	7	8	9	10	11
1	X							Y			
2		X							Y		
3			X							Y	
4				X							Y
5	Y				X						
6		Y				X					
7			Y				X				
8				Y				X			
9					Y				X		
10						Y				X	
11							Y				X
12	X							Y			
13		X							Y		
14			X							Y	
15				X							Y
16	Y				X						
17		Y				X					
18			Y				X				
19				Y				X			
20					Y				X		
21						Y				X	
22							Y				X
23								Y			
⋮											

X = PL_1 Pulses, Y = PL_2 Pulses, etc.

Figure 3.3 PL Pulsing Pattern.

Field test results for the FDMA and TDMA signal diversity techniques show impressive improvements with respect to the jamming of GPS signals by the PL [Elrod and Van Dierendonck, 1995]. Figure 3.4 shows, for one model of GPS receiver, the resulting changes to the received GPS satellite signals under the PL signal conditions of: no pulsing and no frequency offset, no pulsing but with a 1.023 MHz frequency offset, pulsing with no frequency offset, and pulsing and a 1.023 MHz frequency offset. As can be seen, the FDMA and TDMA techniques, when applied independently, show a marked improvement in the net effects on the received GPS signals. When applied in combination, the frequency offset and pulsing scheme result in a degradation of only approximately 2 dB over a PL signal variation of 60 dB. This means that a user at a 'far' limit of 20 nautical miles (37 km) would also be able to receive and track both the PL and GPS satellites at a ‘near’ limit of only 0.02 nautical miles (37 m) [Elrod, *et al*., 1994]. This is a vast improvement over the 10:1 (12:1 theoretically) distance ratio that could be expected with a continuous PL signal at the L1 frequency.

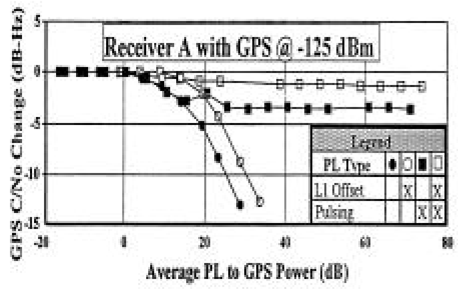

Figure 3.4 GPS Signal Degradation Versus PL Signal Power. With and Without Pulsing and 1.023 MHz Frequency Offset.

3.2.3 PL Signal Data Message

As mentioned previously, the PL signal can act as an integral data link to pass differential corrections and integrity information to the GPS user. Presently, the GPS navigation data message is transmitted by the GPS satellites at a rate of 50 bits per second (bps). A PL data rate of up to 1000 bps can be supported with a firmware change in most GPS receivers [Elrod and Van Dierendonck, 1995]. Field tests with data rates of 250 bps have been successfully conducted, as have laboratory tests at 500 bps. Initial tests at 1000 bps have also been conducted, but the available test data is not yet sufficient to characterize signal acquisition and tracking performance [Barltrop, *et al*., 1996].

Many groups, such as the Local Area Augmentation System (LAAS) Architecture Review Committee (LARC) and the RTCA SC-159 Working Group 4A, are working on establishing the message formats, data rate requirements and frequency bands for the LAAS data link concept. The basic PL message format proposed is based on the Wide Area Augmentation System (WAAS) specification. Typical message formats include: Carrier Measurement Message (Type 41/42), Code Range Measurement Message (Type 43/44), PL Almanac Message (Type 45) which contains the precise WGS84 coordinates of the PL transmit antenna, and Integrity Interrupt Message (Type 50) which, with a 1000 bps data rate and a 250 bit frame length, will provide a user with an integrity alert within 0.75 seconds of the ground segment measurement epoch upon which the alert is based.

3.2.4 PL Time Synchronization

A final PL system design consideration is the issue of time synchronization. The synchronization of a PL oscillator to GPS time is not overly important in post-processing applications using differential techniques as the PL clock offset is common to both reference and remote receivers and it will therefore cancel through single or double differencing. For real time or single point positioning applications, synchronization of the PL clock to GPS time can prove quite advantageous. There are basically two methods

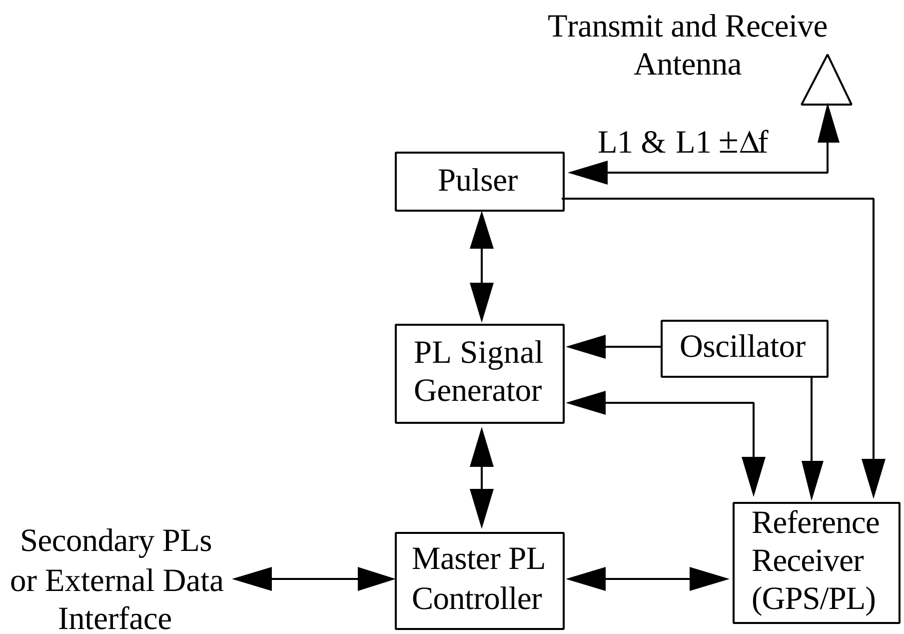

Figure 3.5 Collocated PL and Reference GPS Receiver Architecture.

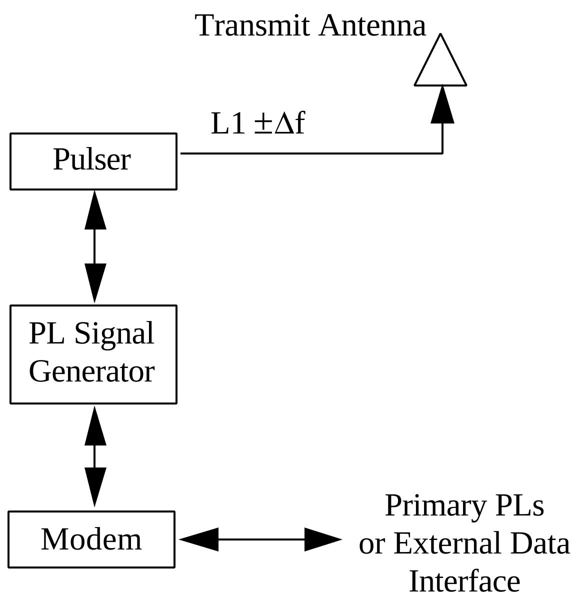

Figure 3.6 Non-Collocated PL Architecture.

by which to time synchronize the PL clock: collocate the PL with a local differential GPS (LDGPS) reference receiver, or send clock correction information from the reference receiver to a non-collocated PL. The two configurations are shown in Figures 3.5 and 3.6. If only one PL is to be used, the collocated approach is more desirable, whereas if two or more PLs are to be used, the remote PL technique with a common GPS reference receiver for synchronization is preferred.

3.3 Practical Considerations

In addition to the technical considerations (which are more concerned with the design of the pseudolite system), there are also many practical considerations that must be addressed before GPS can be augmented successfully with a PL. First, due to the low elevation angle, multipath is of much more concern with a PL signal than with a GPS satellite signal. Second, the received PL signal enters the reference and/or remote GPS antenna through a low gain portion of the antenna. This may result in a low signal to noise ratio for the received PL transmission, yielding noisier code and carrier phase measurements. Third, the modelling of the troposphere can be extremely important when one is attempting to fix integer ambiguities for precise positioning. Lastly, errors that are usually reduced significantly or eliminated entirely through differential techniques, such as satellite orbital errors (analagous to coordinate errors in the case of a PL), may not necessarily be reduced or eliminated with a PL.

Multipath is a consideration with all GPS applications, but it particularly important in PL augmented systems. For GPS satellites, the amount of transmitted multipath (i.e. originating at the satellite) is generally small, and since the unit vectors from both the GPS reference and remote receivers to a particular satellite are essentially identical, this multipath will tend to difference out using differential techniques.

This is not necessarily true for PL applications, as the unit vectors from the PL to the reference and the remote receivers can be significantly different. Thus, each GPS user could observe different transmitted multipath from the PL which would not generally cancel in the differencing procedure. The same situation exists for propagation multipath along the transmission path(s) from the PL to the GPS receivers. With a stationary reference receiver and a stationary transmitter (unlike GPS where the transmitter is orbiting the Earth), there is a constant transmission path. This could result in a bias in the measured range to the PL, which would ultimately result in biased differential corrections being computed for the PL. The bias could affect adversely the volume to be searched for integer ambiguity resolution [Ford, *et al*., 1996].

Most GPS antennas are designed to have lower gain at lower elevations to help reduce the deleterious effects of multipath. Unfortunately, for most PL applications, the transmitter will be located at a very low elevation angle with respect to the GPS receivers. Typically, a PL will be below 15°, an area sometimes considered marginal for GPS antennas. This can result in noisier measurements of the PL code and carrier.

Because a PL will be ground-based, the transmitted signal will not have to propagate through the ionosphere. The PL signal, however, propagates through the lower troposphere, a region notoriously difficult to model, due mainly to spatial variations in atmospheric pressure, temperature and humidity. Unmodelled tropospheric delays up to 6 m could be experienced by users separated by 10 km. With adaptive tropospheric delay estimation techniques which rely on local weather data, a tropospheric delay correction can be applied to the PL (and GPS) observations, reducing the differential tropospheric errors to less than 10 cm over the same 10 km separation [Barltrop, *et al*., 1996].

For each of the field tests the dry temperature, total atmospheric pressure and the partial pressure of water vapour are considered constant. Thus, a constant value for tropospheric refractivity is used for corrections to the PL measurements. The value for the tropospheric refractivity is given by the Smith-Weintraub equation [Lachapelle, 1995]:

$$N = (77.6 / T)\left\{P + 4.81\mathrm{x}10^3\left(e / T^2\right)\right\} \qquad 3.2$$

where N ... is the tropospheric refractivity (parts per million),

T ... is the dry temperature (degrees K),

P ... is the total atmospheric pressure (millibars),

and e ... is the partial pressure of water vapour (millibars).

The last practical consideration concerns what are normally assumed to be correlated errors, such as satellite orbital errors. For conventional GPS observations, a 5 m error in the broadcast satellite position will have little effect on the DGPS position solution, as both GPS users will be affected by the error. An analogous scenario is shown in Figure 3.7. There is a 5 m discrepancy between the actual and calculated

PL coordinates (relative to the reference coordinates), so that the differential corrections generated by the reference receiver are always 5 m in error. An observer located at 'Remote A' will observe the same 5 m error, and therefore this error will difference out with the application of the differential correction. An observer located at 'Remote B', however, does not observe any range error from the PL, thus when the differential correction from the reference receiver is applied, a 5 m error will be induced in the PL measurement. This systematic observation error will then propagate into the least squares adjustment of the DGPS position solution.

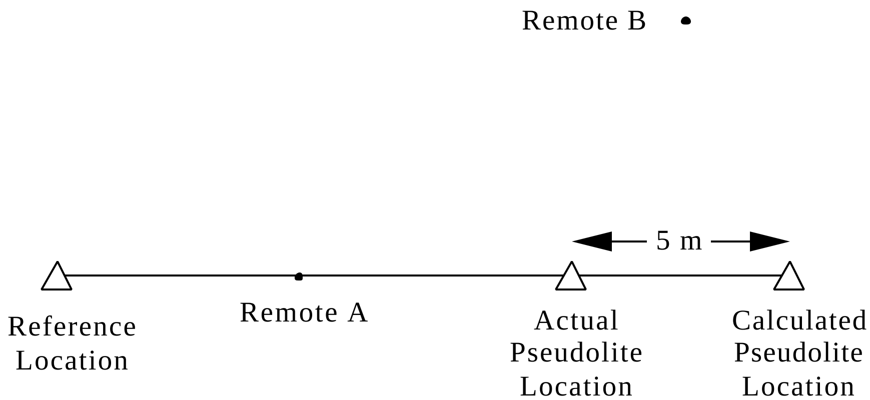

Figure 3.7 Effect of PL Coordinate Error

3.4 Static Field Test - September 28, 1996

A field test was conducted on September 28, 1996 to confirm that the PL signal could be successfully received at a relatively long range (in excess of 5 km) and to assess the modifications to C^3NAV (termed C^3NAVPL) which would enable the post-processing of PL and GPS satellite data. The GPS equipment used for this test were NovAtel OEM-2 (with RT-20 software) 12-channel single frequency receivers which incorporate Narrow Correlator technology, and each receiver used a 503 antenna with chokering. The reference antenna was on Pillar N2, on the lower roof of the Engineering Building at the University of Calgary. The remote antenna was on a tripod, placed over a metal roof drain, located on the upper roof of the Engineering Building. The PL antenna was located on a tripod placed over a metal spike on Nose Hill which is north of the University, beside Shaganappi Trail. The coordinates of the metal roof drain and the metal spike were determined relative to Pillar N2 by SEMIKIN™ double-difference fixed integer ambiguity solution. The distance between the reference and remote antennas was 27.38 m, and the distance between the reference and the PL was 5.24 km. The PL antenna was at an elevation of 1.15°, relative to the reference antenna. A plan view of the Shaganappi test configuration is shown at Figure 3.8.

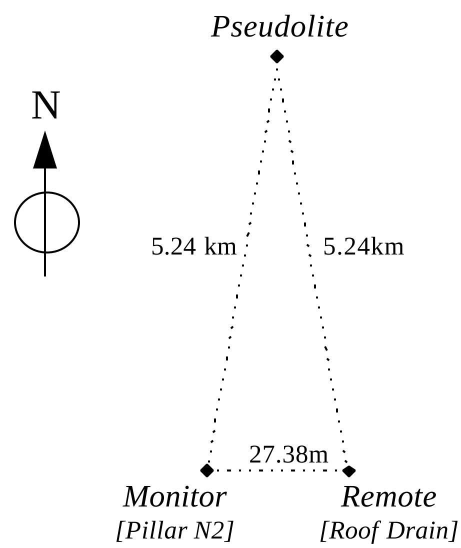

Figure 3.8 Plan View of Shaganappi Field Test.

No special hardware modifications were made to the NovAtel GPS receivers to track and record the PL signal. The only required operator input was to manually assign the PL PRN to one of the twelve receiver channels. This step was required as the PL was configured to broadcast as PRN 07, which was an active satellite (below the horizon during all tests), and the receivers would not normally look for the signal until the almanac information predicted that the satellite should be visible. As no ephemeris information was included with the PL signal, the receivers would flag the PL data as being recorded with “Old Ephemeris” and not use the PL information for any receiver generated positioning. The information would, however, be recorded to the data files for use in post processing.

3.4.1 Pseudolite Description

The PL used for this test was a Stanford Telecom (STel) NAVSTAR GPS Programmable Wideband Signal Generator (Model 7201) configured to broadcast a continuous signal (non-pulsed) at the L1 frequency. Frequency aiding was provided using an external 5 MHz OCXO reference oscillator. A 30 dB low noise amplifier was attached near the L1 antenna. A laptop computer was used to interface with the PL. The PL configuration is shown in Figure 3.9. The ‘near/far’ problem was not an issue during this field test as the PL and the GPS receivers were static throughout the data collection period, and both the reference and remote receivers were at approximately the same distance from the PL.

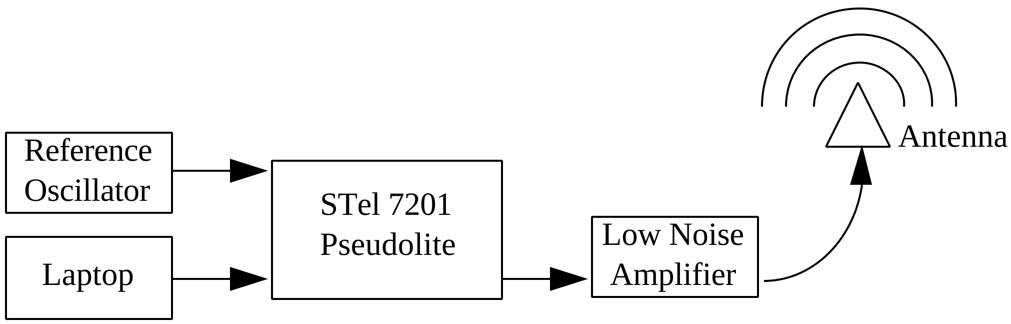

Figure 3.9 Schematic of PL Configuration.

3.4.2 Shaganappi Test Results

Both the reference and remote receivers maintained lock on the PL transmission for approximately 40 minutes. The PL was configured (via software) to transmit at full power (0 dB attenuation), with the signal then amplified by the 30 dB low noise amplifier. The signal to noise ratios (C/N_o) for the PL, as measured by the reference and remote receivers is shown in Figure 3.10. For comparison, the C/N_o measurements for satellite 23 (elevation angle decreasing from 34° to 21°) are included in Figure 3.11. Note that for the PL, the signal is very weak, due to a combination of inadequate transmission power (only one 30 dB low noise amplifier was available) and signal reception through a low gain portion of the GPS antennas (the PL was barely above 1° elevation). A gain pattern for a typical NovAtel antenna (503 or 501) is shown in Figure 3.12 [Fenton, *et al*., 1991]. As this was a fully static test, the variations in received PL signal strength (which follow the same trend for each receiver) are most likely attributable to variations in the transmitted power and/or variations in the propagation. Note also that the reference antenna seems to be more sensitive than the remote antenna, as the average measured signal strength is 1 to 1.5 dB higher for both the PL and the satellite signal.

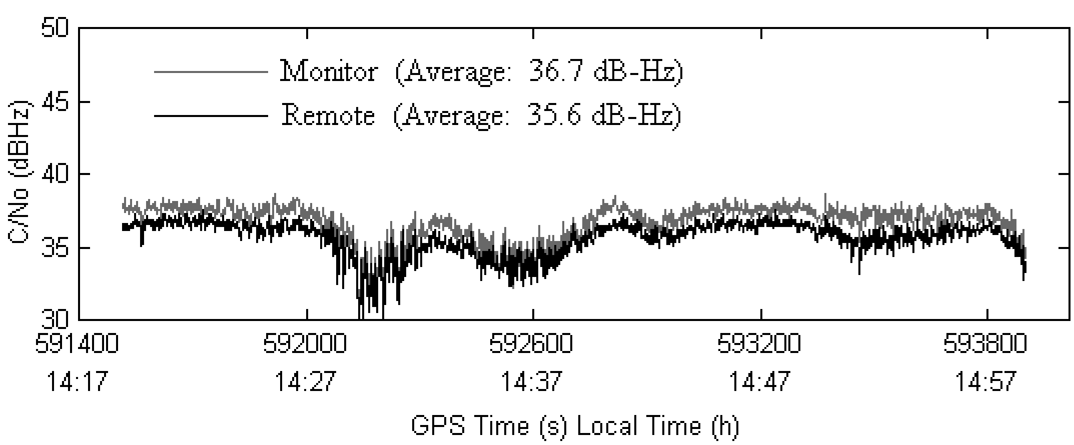

Figure 3.10 Shaganappi. PL C/N_o As Measured By The Reference and Remote Receivers. PL Elevation 1.15°.

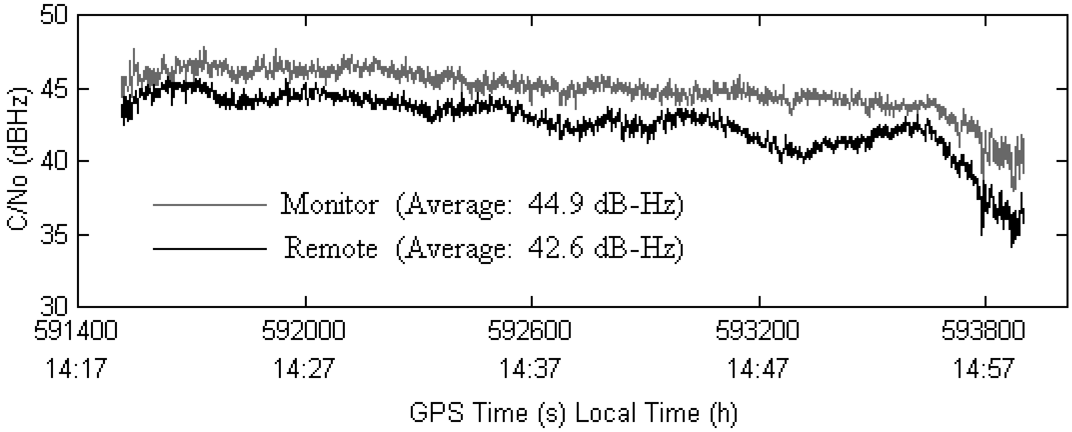

Figure 3.11 Shaganappi. PRN 23 C/N_0 As Measured By The Reference and Remote Receivers. Satellite Elevation 34° to 21°.

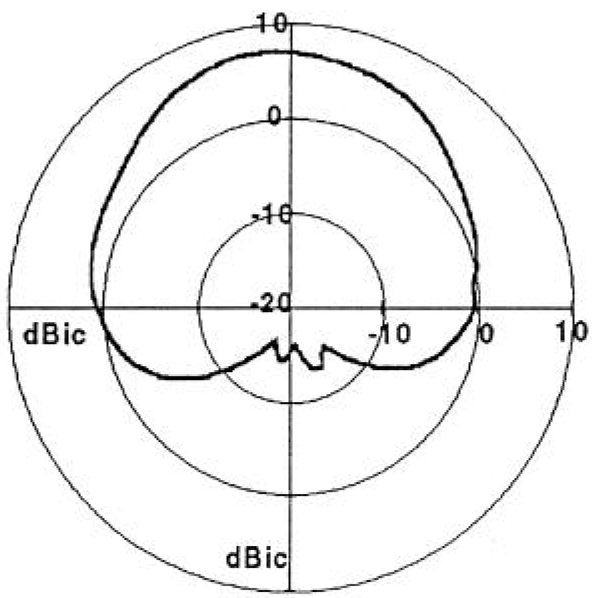

Figure 3.12 Typical NovAtel Antenna Gain Pattern for L1.

Plots of the HDOP and number of satellites tracked (including PL) for a mask angle of 10° are shown in Figure 3.13. The average number of satellites tracked over the forty minute data collection window was 7.04, resulting in an average HDOP of 1.08 for the unaugmented constellation. With a PL included, these numbers changed to 8.04 and 0.98, respectively.

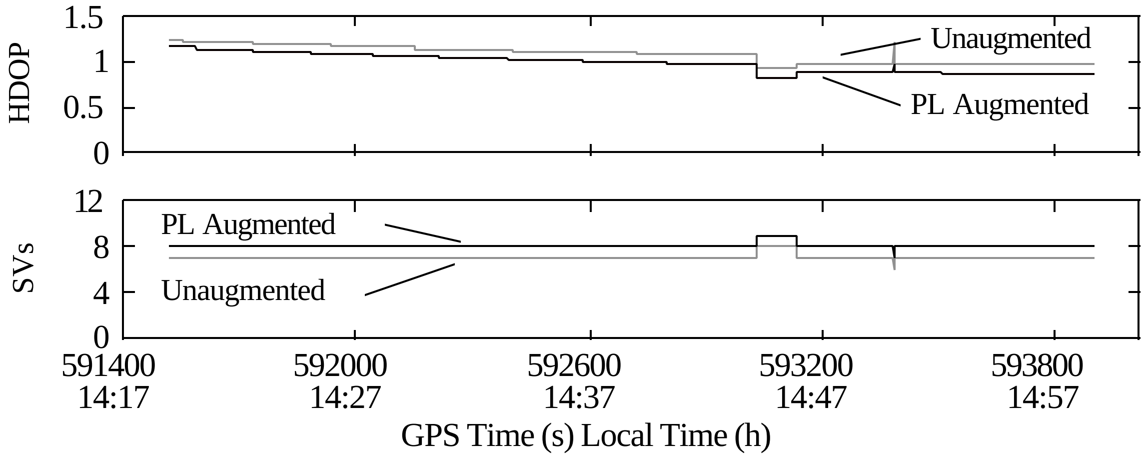

Figure 3.13 Shaganappi. HDOP and Number of Observations. Mask Angle 10°.

To assess the DGPS position accuracy, the C^{3}NAVPL post-processed position solution for the remote receiver was compared against the known coordinates of the remote antenna, located on the upper roof of the Engineering Building. The resulting C^{3}NAVPL raw code latitude, longitude and height errors for the unaugmented and PL augmented tests are shown at Figure 3.14. Summary statistics for the latitude, longitude and height errors are presented in Table 3.1. The addition of the PL information has biased slightly the latitude and height errors. This is due to time-invariant multipath component between the PL and reference antennas causing an error in the calculation of the differential corrections for the PL signal. When applied by the remote receiver, these biased corrections will propagate into the least squares adjustment and result in biased parameters. A further analysis of this observation is included in Chapter 5, Section 5.2.3. A plot of the cumulative frequency distribution for the horizontal errors for the unaugmented and PL augmented configurations is shown in Figure 3.15, along with statistics for the 50th and 95th percentile horizontal errors, summarized in Table 3.1. Finally, plots of the C^{3}NAVPL raw code residuals for two satellites and the pseudolite are presented in Figure 3.16 and Table 3.3. For the unaugmented case, the raw code residuals for the two satellites considered (PRN 01 and 09) are essentially unbiased. For the PL augmented case, however, the residuals are biased by 27 and 49 cm. The average PL residual is biased by 56 cm.

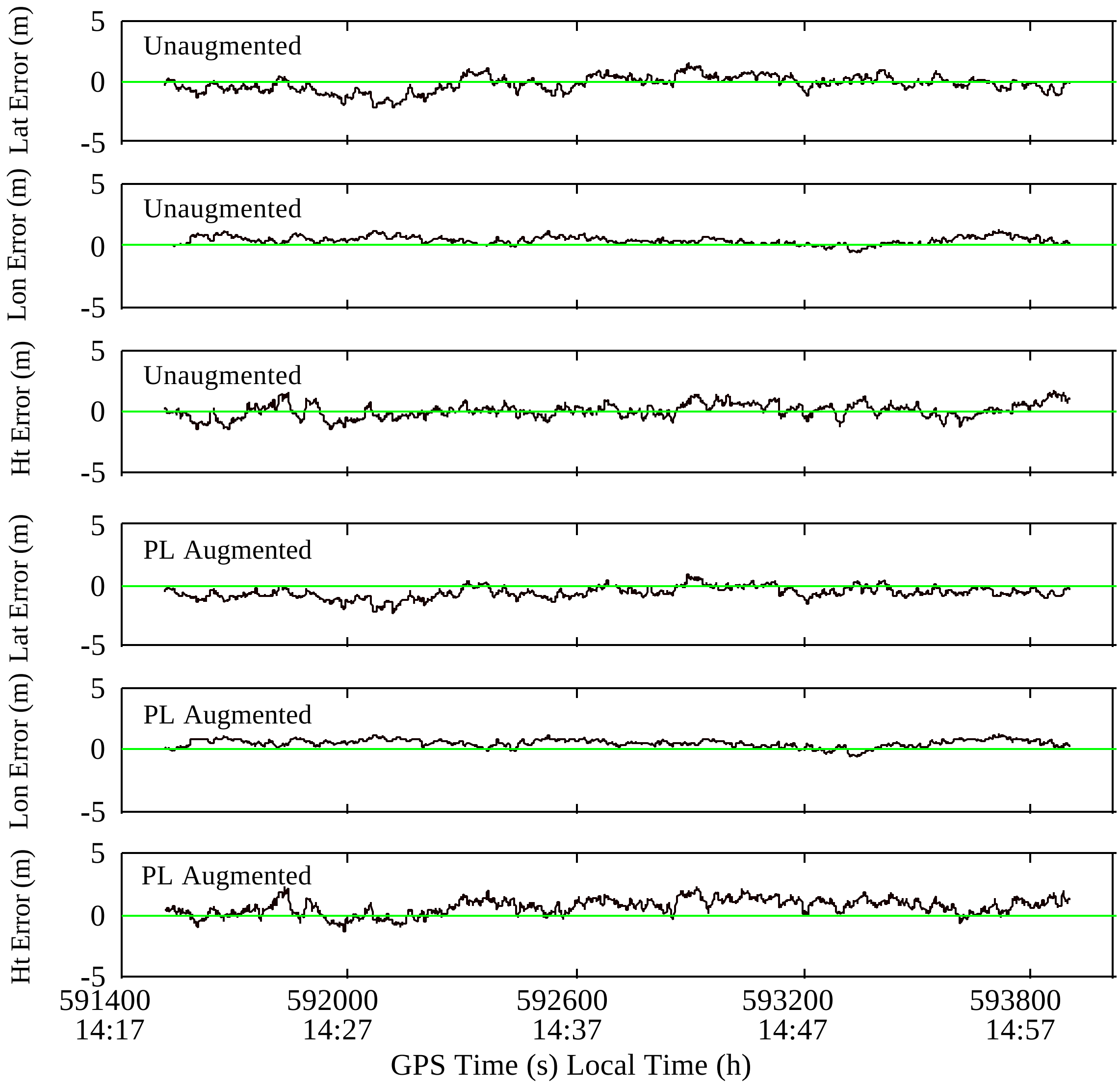

Figure 3.14 Shaganappi. C[3]NAVPL Raw Code Error Comparison Between Unaugmented and PL Augmented GPS Constellations. Mask Angle 10°. Unconstrained Height. No Satellites Rejected.

Table 3.1 Shaganappi. C[3]NAVPL Raw Code Errors. Unaugmented and PL Augmented GPS Constellations. Mask Angle 10°. No Satellites Rejected.

PL Used	Latitude		Longitude		Height	
	mean	**95 %**	**mean**	**95 %**	**mean**	**95 %**
No	-0.251	1.356	0.471	1.150	0.056	1.142
Yes	-0.631	1.620	0.473	1.148	0.691	1.872

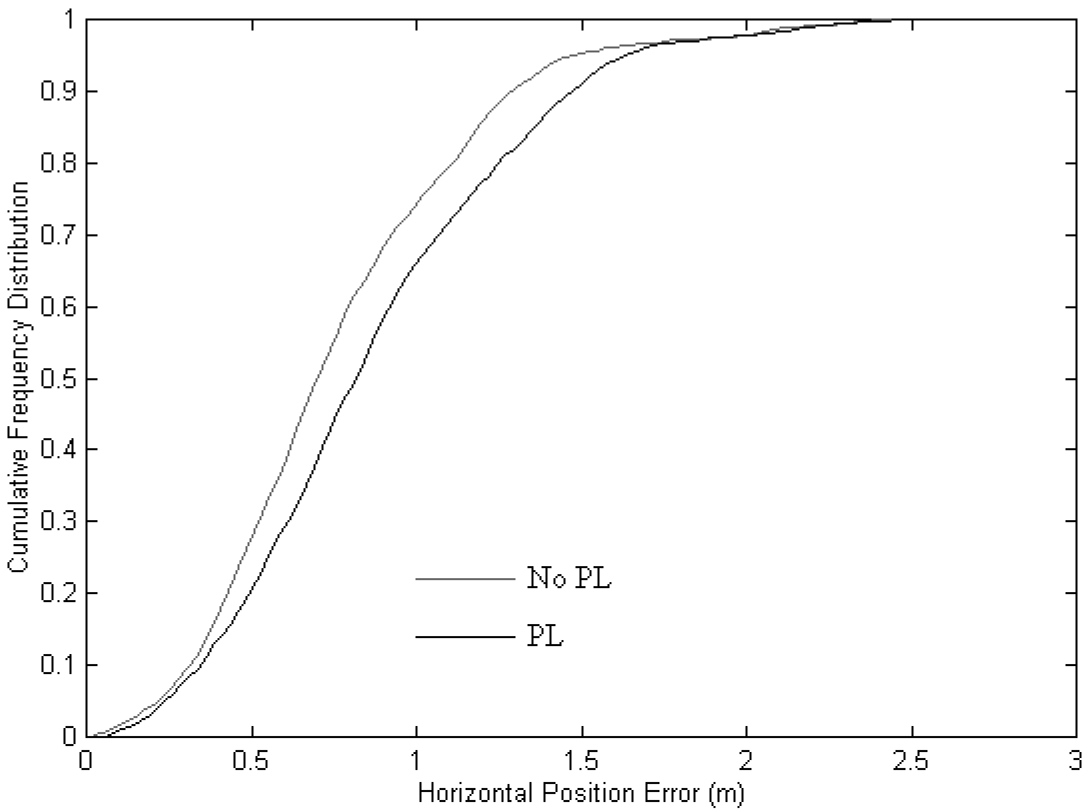

Figure 3.15 Shaganappi. C[3]NAVPL Raw Code Cumulative Frequency Distribution of Horizontal Position Error. Unaugmented and PL Augmented GPS Constellations. Mask Angle 10°. No Satellites Rejected.

Table 3.2 Shaganappi. C^{3}NAVPL 50th and 95th Percentile Horizontal Position Error and 2DRMS Horizontal Accuracy. Mask Angle 10°. No Satellites Rejected.

Configuration	50th percentile	95th percentile	2DRMS (m)
Unaugmented	0.700	1.480	1.423
PL Augmented	0.818	1.636	1.207

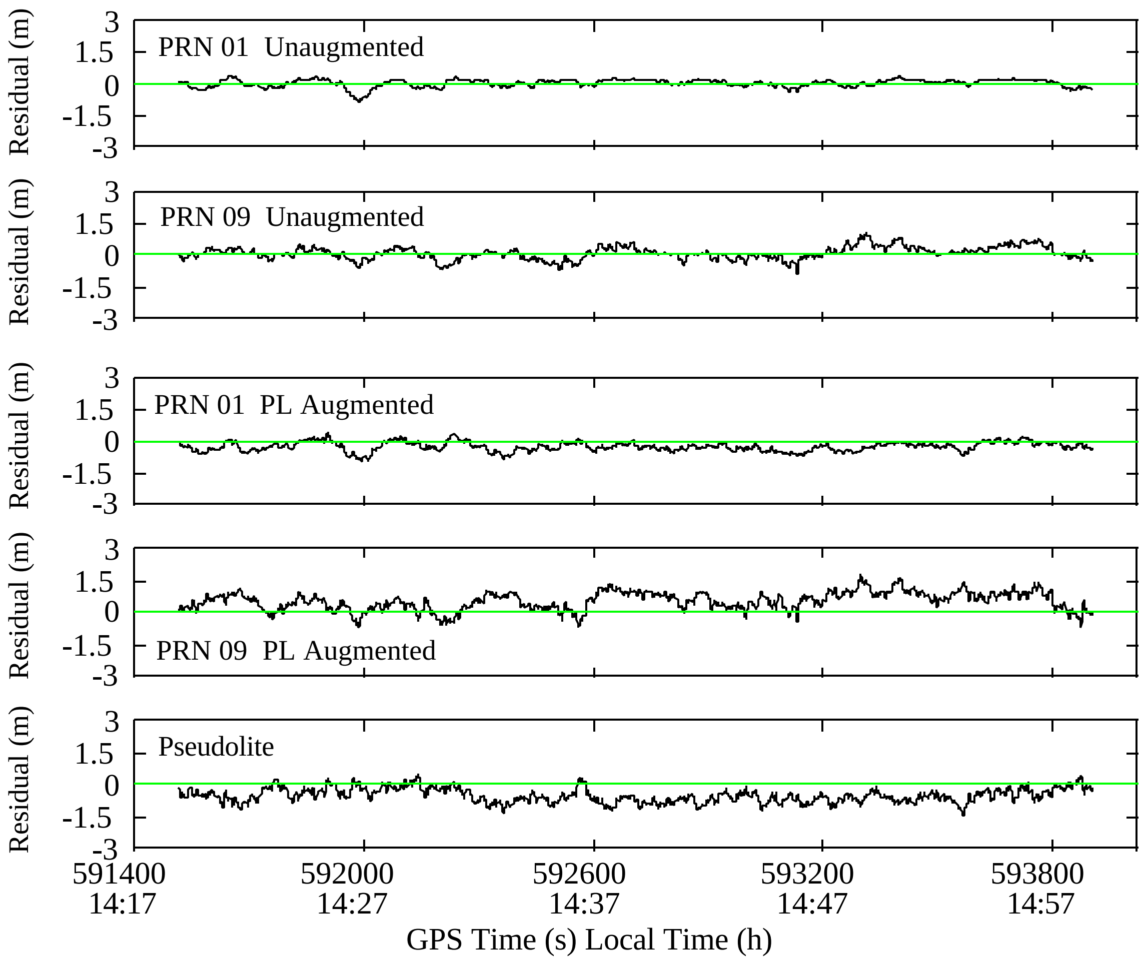

Figure 3.16 Shaganappi. C^{3}NAVPL Raw Code Residuals for Unaugmented and PL Augmented GPS Constellations. Mask Angle 10°. No Satellites Rejected.

Table 3.3 Shaganappi. C^3NAVPL Raw Code Residual Statistics.

PRN (elev)	Unaugmented		PL Augmented	
	Mean (m)	RMS (m)	Mean (m)	RMS (m)
01	0.001	0.200	-0.274	0.350
09	0.076	0.335	0.491	0.661
PL	N/A	N/A	-0.556	0.328

CHAPTER 4

SIMULATION ANALYSIS

GPS simulations can be a valuable tool when pre-planning a mission, or when attempting to assess the affect of different parameters on the GPS measures. The availability, accuracy and reliability measures discussed in Chapter 2 are functions of satellite geometry and user defined parameters such as remote receiver location, elevation mask angle, code variance and non-centrality parameter. By varying these (and other) parameters, it is possible to evaluate the changes to the GPS measures, and determine when a potential problem (with respect to these measures) is likely to occur. As mentioned previously, a PL can be used to increase the number of available ranging sources and to improve the accuracy and reliability measures. Since these values are a function of geometry, the placement of the PL with respect to the remote receiver location may be critical, and a simulation analysis that quantifies the level of improvement with respect to GPS satellite/PL/remote receiver geometry can prove extremely beneficial. Additionally, the effect of signal masking due to the local horizon or man-made structures can have a significant affect on the placement of the PL(s).

This chapter includes a description of the simulation software program, as well as a comprehensive availability, accuracy and reliability analysis for the standard GPS satellite constellation, and a PL augmented constellation. In addition, the improvements in the accuracy and reliability measures due to the use of a height constraint are included. The simulation analysis is conducted to investigate the following two scenarios: a) the effect of increasing constant mask angles; and b) the effect of a "real world" horizon, as measured in a mountainous area, with a simulated obstruction.

4.1 PLPLAN Simulation Software Description

A software package, called PLPLAN (*P*seudo*L*ite *PLAN*ning), was written to allow a user to assess the effect of using up to three pseudolites at various geometries on the between-receiver-single-difference GPS availability, accuracy and reliability measures. The following are input parameters to PLPLAN: remote coordinates, simulation start and stop times, data interval, constant mask angle, variable horizon mask angle data (if required), number, elevation and spacing of pseudolites, rejected satellites, code variance, non-centrality parameter, height constraint (if required) and input/output file information. It is assumed that the between-receiver single difference receivers observed the same satellites at each epoch, which is a reasonable assumption for a local area augmentation.

A simplified PLPLAN flowchart is shown in Figure 4.1. Once the input parameters have been read, the various PL coordinates must be calculated. This is accomplished by 'placing' the PL to the north of the remote location. As the simulation is concerned with the relative geometry of the PL with respect to the remote location, the unit vector to the PL is required, rather than the actual distance to the PL. The height of the PL is then adjusted until the desired elevation angle relative to the remote location is achieved. These coordinates then correspond to a PL at 0° azimuth relative to the remote location. The PL is then 'moved' by adjusting the PL longitude until the PL reaches 10° azimuth relative to the remote location. The PL height is then adjusted until the desired elevation angle is reached. These coordinates then correspond to a PL at 10°. This continues until 45°, where the longitude is held constant and the latitude is adjusted. This process of adjusting longitude, latitude and height continues until the PL has made a 'box' around the remote location, and all PL coordinates corresponding to azimuth increments of ten degrees have been determined. This process is shown graphically in Figure 4.2.

Once all PL coordinates have been determined, the simulation is initiated using an initial PL azimuth of 0°. At the user-defined simulation start time, the WGS-84 coordinates for all satellites are computed from the ephemeris (or almanac) file. Satellites can then be rejected at this for one of two reasons: the user has requested that a particular satellite not be used (to simulate a failure) or the satellite is not above the specified horizon. This horizon can either be a constant mask angle, or it can vary from sector to sector to simulate a "real world" horizon. The accuracy and reliability measures are then calculated for this epoch The simulation time is incremented by the data interval, and the simulation is conducted for the next epoch, until the user-defined simulation stop time is reached. At this point, the PL is "moved" to the coordinates corresponding to 10°, and the simulation is repeated from start time to stop time. This continues until the PL has made on complete revolution around the remote location.

If two PLs are used, the simulation is completed as above, except that the coordinates of the second PL are chosen to correspond to the user-defined spacing of the PLs. Thus, if two PLs are used, and the spacing is set at 70°, during the first run of the simulation the PL azimuths will be 0° and 70°. For the second run, the PL pair will have "moved" to 10° and 80°. The last run will end with the first PL at 350° and the second PL at 60°. The same logic applies when three PLs are used.

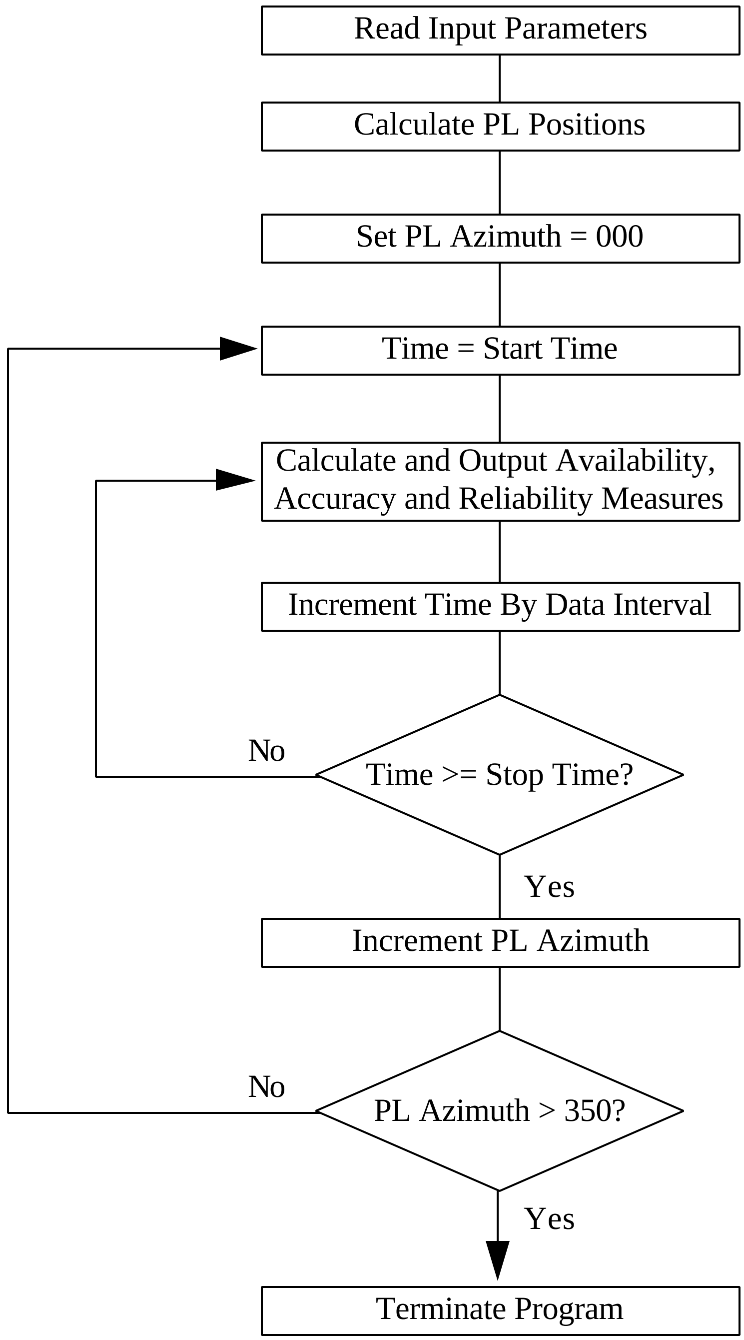

Figure 4.1 PLPLAN Flowchart Overview.

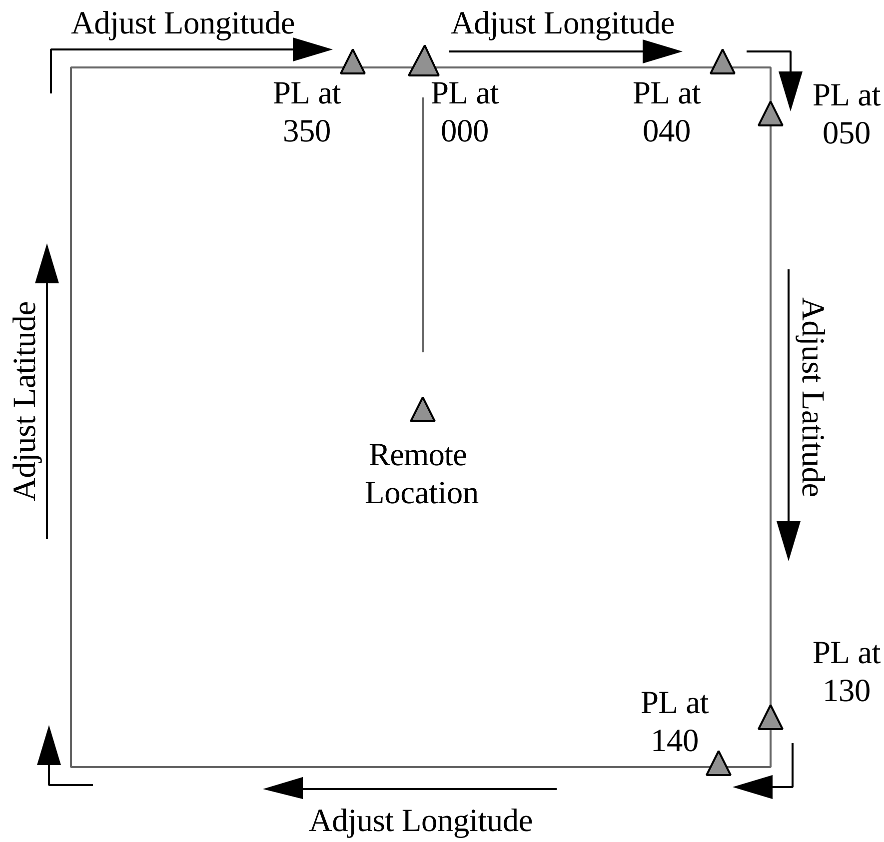

Figure 4.2 Determination of the PL Coordinates.

4.2 Effect of Increasing Mask Angles on GPS Availability, Accuracy and Reliability Measures

As the elevation mask angle increases, the number of satellites above this mask angle will decrease. Fewer satellites lead to poorer geometry and an increase in the magnitude of the Maximum Horizontal Error (MHE) envelope (refer to section 2.4). Mask angles of 10° and 20° were used as input parameters to PLPLAN to illustrate the deleterious effects of increasing mask angles on GPS availability, accuracy and reliability. Ephemeris information was collected for a period of 24 hours on May 8 and 9, 1996, on the roof of the Engineering Building at the University of Calgary. Simulation of a 24-hour period is sufficient since the GPS constellation repeats itself every 24 hours. Input parameters used in the simulations are summarized in Table 4.1.

Table 4.1 PLPLAN Input Parameters.

Parameter Description	**Parameter Value**
Start Time (GPS Time)	315000
Stop Time (GPS Time)	401400
Data Interval (s)	180
Pseudolite Spacing	70° (Two PLs), 70° and 200° (Three PLs)
Pseudolite Elevation	10°
Code Variance (m^2)	1
Non-Centrality Parameter	4.57
Height Constraint Variance (m^2)	5.0 (when used)

Figures 4.3 and 4.4 were produced with no PL augmentation, and with no height constraint, using constant mask angles of 10° and 20°, respectively. For the 10° scenario (Figure 4.3), between four and nine satellites are available for the entire 24-hour period. The HDOP is quite acceptable for the entire simulation, even when the number of satellites in view drops to only four. Unfortunately, a good HDOP does not guarantee a good MHE. The MHE envelope for the 10° case indicates several periods where the magnitude of the worst-case maximum horizontal position error due to an undetectable blunder exceeds 100 m. At time 358200, the HDOP is approximately 2 and the number of satellites above 10° varies between 6 and 7. The MHE, however, exceeds 100 m. Compare this to time 316000 where, again, the HDOP is approximately 2 and the number of satellites drops from 7 to 5. Based on the previous observation, one would expect a dramatic increase in the MHE. In fact, the MHE increases to only 20 m. During the period where the number of satellites drops to four, no redundancy exists, and no reliability assessment is available (i.e. the MHE is infinite).

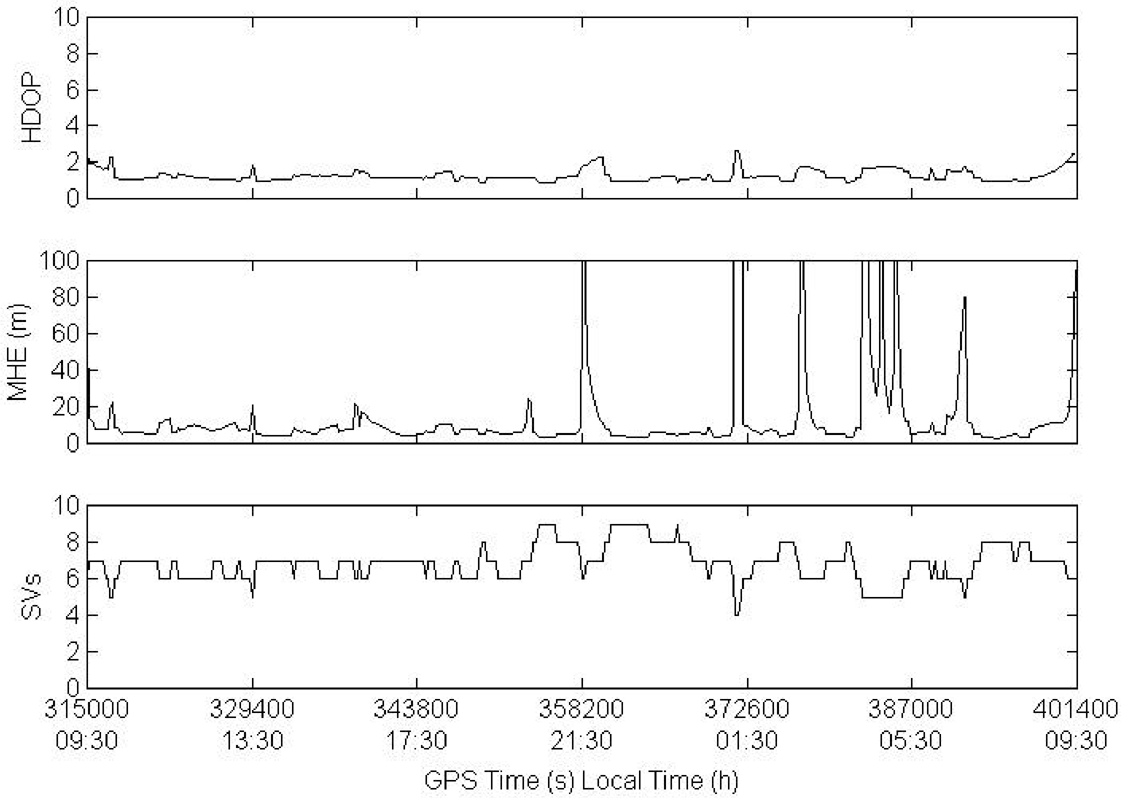

Figure 4.3 24-Hour HDOP, MHE and Satellites Visible at Calgary, May 8/9 1996. Mask Angle 10°. No PL. No Height Constraint.

Figure 4.4 shows the degradation in HDOP and MHE and number of satellites visible for a 20° mask angle. Such a large mask angle will be unlikely to occur unless the navigation channel is very near the shore in a mountainous area, or if the vessel is conducting docking maneouvres in an obstructed harbour. For the 20° mask angle case, there are periods where the unaugmented GPS constellation is quite strong with respect to precision and reliability, and there are other periods where it is quite weak, especially with respect to reliability. The average HDOP is 2.55 (with 6.5 % of the epochs exceeding an HDOP of 10), and the average MHE is 110.1 m (with 34.0 % of epochs exceeding an MHE of 100 m).

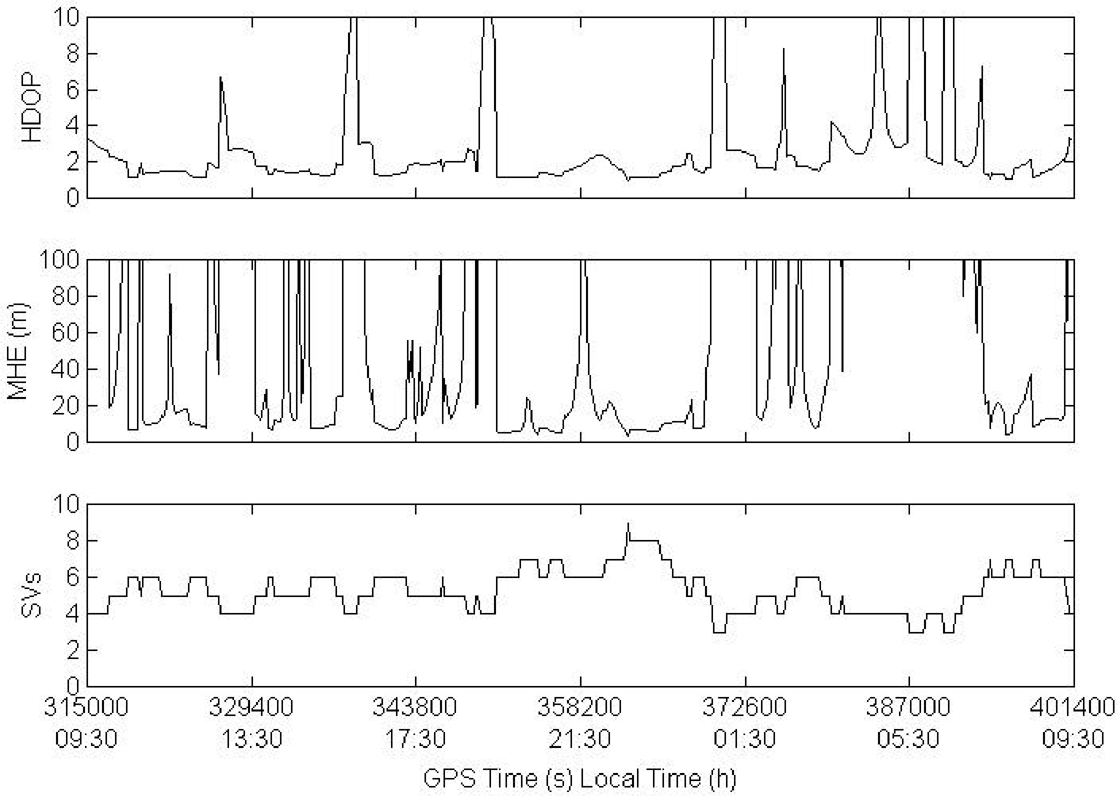

Figure 4.4 24-Hour HDOP, MHE and Satellites Visible at Calgary, May 8/9 1996. Mask Angle 20°. No PL. No Height Constraint.

Figures 4.5 illustrates the HDOP and MHE plots for an unaugmented constellation using a height constraint of $5m^2$ and a constant mask angle of 20°. As no PL is used, the two surfaces are independent of the PL axis. The incorporation of the height information has improved dramatically the HDOP and MHE, as compared to the unconstrained height configuration shown at Figure 4.4. The average HDOP has been reduced from 2.55 to 1.71 (with no periods where the HDOP exceeds 10), and the average MHE has been reduced from 110.1 m to 37.8 m (with only 9.2 % of epochs exceeding an MHE of 100 m).

Figure 4.6 shows the HDOP and MHE surfaces for a constellation augmented with one PL at successive azimuths relative to the reference location. Again, a constant mask angle of 20° and a height constraint of $5m^2$ were used. In this figure, the relative orientation of the PL with respect to the remote location has a significant influence on the improvements to the HDOP and MHE measures. Certain PL sectors, such as 090° - 110° and 290° - 310° have a lesser effect on the HDOP and MHE plots. Other PL sectors, such as 190° - 240° and 320° - 350° have a significant effect. The average HDOP is now reduced to 1.39, and the MHE has been reduced to 12.6 m (with only 1.3 % of epochs exceeding an MHE of 100 m).

Two PLs, spaced at 70° relative to each other, were used to produce the plots in Figure 4.7. There has been a significant improvement to the HDOP surface, and the periods where the HDOP was weak (shown in

Figures 4.5 and 4.6) have been completely eliminated. In fact, the HDOP for the entire 24-hour period never exceeds 2, with the HDOP averaging 1.12. The MHE surface also shows a significant improvement, with only a few, brief periods where the magnitude of the MHE exceeds 20m. The average MHE is now only 5.9 m, with no periods where the MHE exceeds 100 m, and only 0.6 % of epochs even exceed 20 m. The positions for the PLs have very little effect on the HDOP, and the geometrical influence on the MHE envelope is reduced greatly.

Finally, Figure 4.8 shows the effect of three PLs, spaced at 70° and 200° relative to the primary PL. The HDOP surface is essentially constant with respect to both time and PL geometry. The average HDOP for the three PL case is 0.96. The MHE surface is also quite regular. The average MHE is 4.4 m, with only 0.1 % of epochs exceeding 20 m. Summary statistics for Figures 4.3 through 4.4.8 are included in Table 4.2.

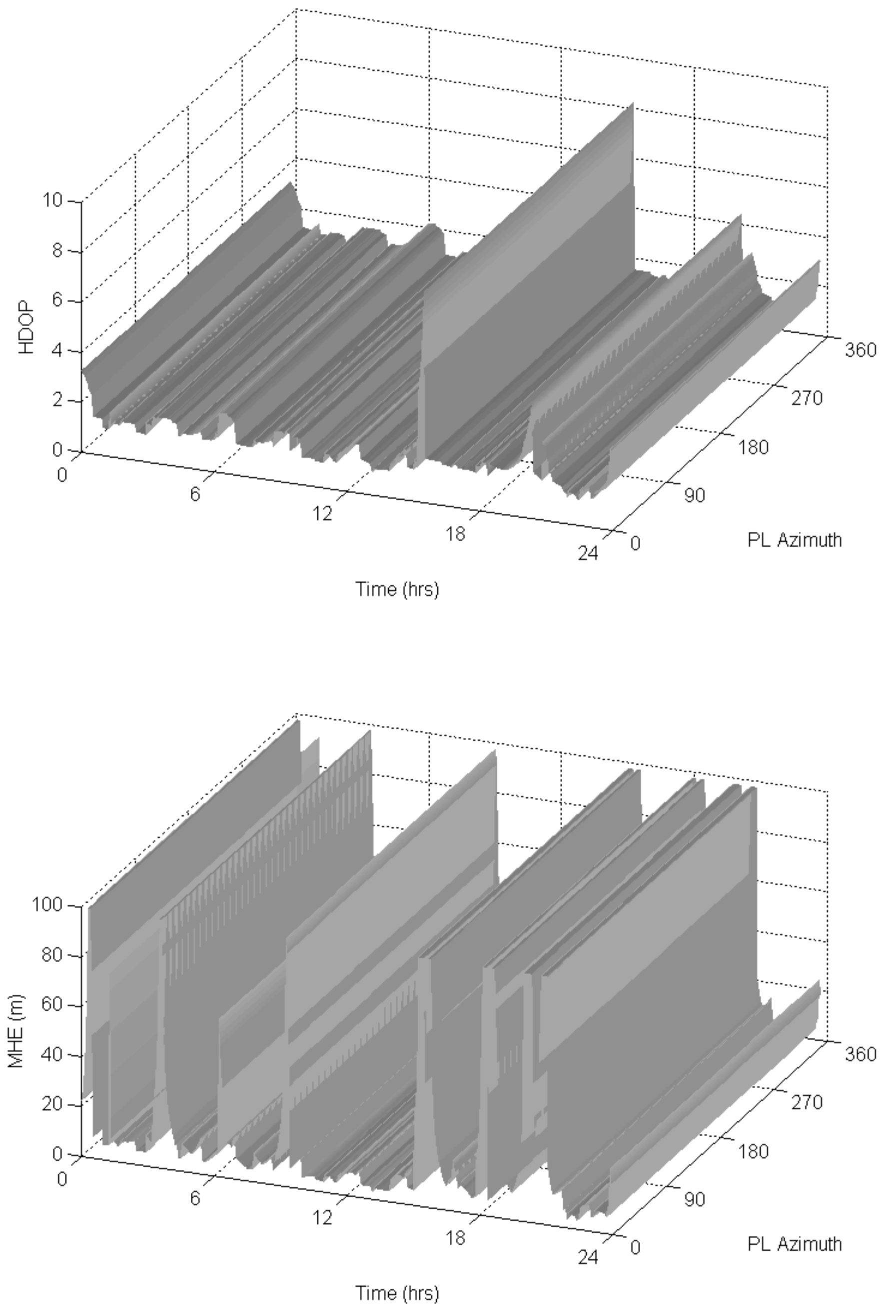

Figure 4.5 24-Hour HDOP and MHE at Calgary, May 8/9 1996.
Mask Angle 20°. No PL. 5 m² Height Constraint.

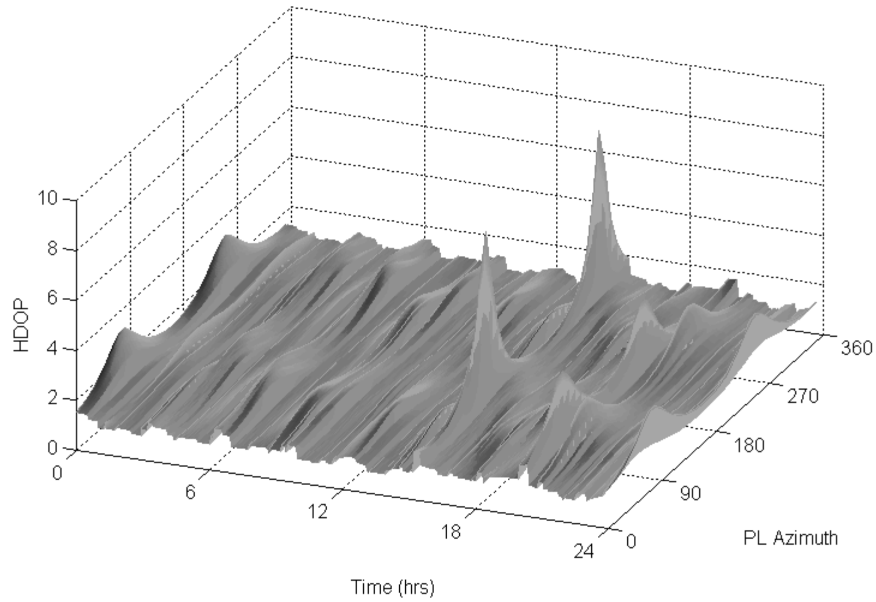

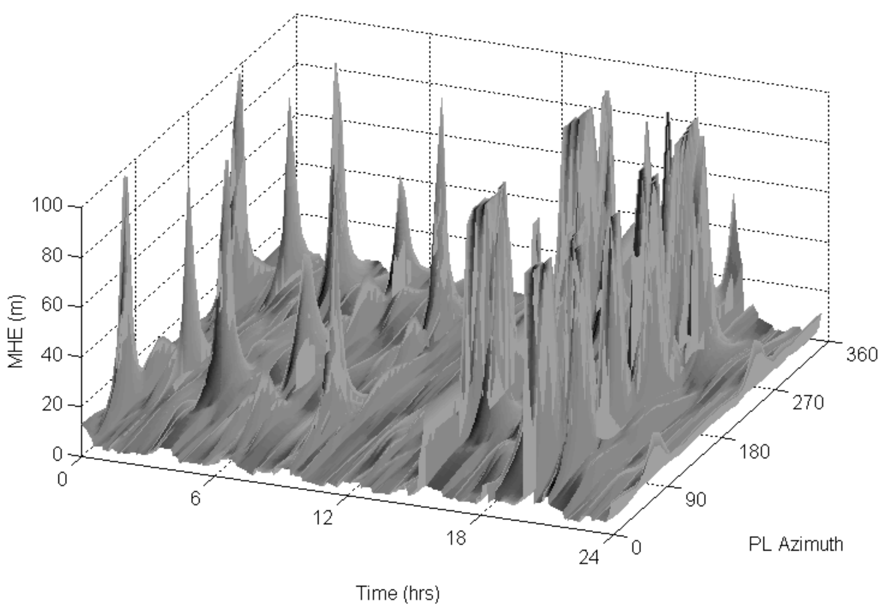

Figure 4.6 24-Hour HDOP and MHE at Calgary, May 8/9 1996. Mask Angle 20°. One PL. 5 m^2 Height Constraint.

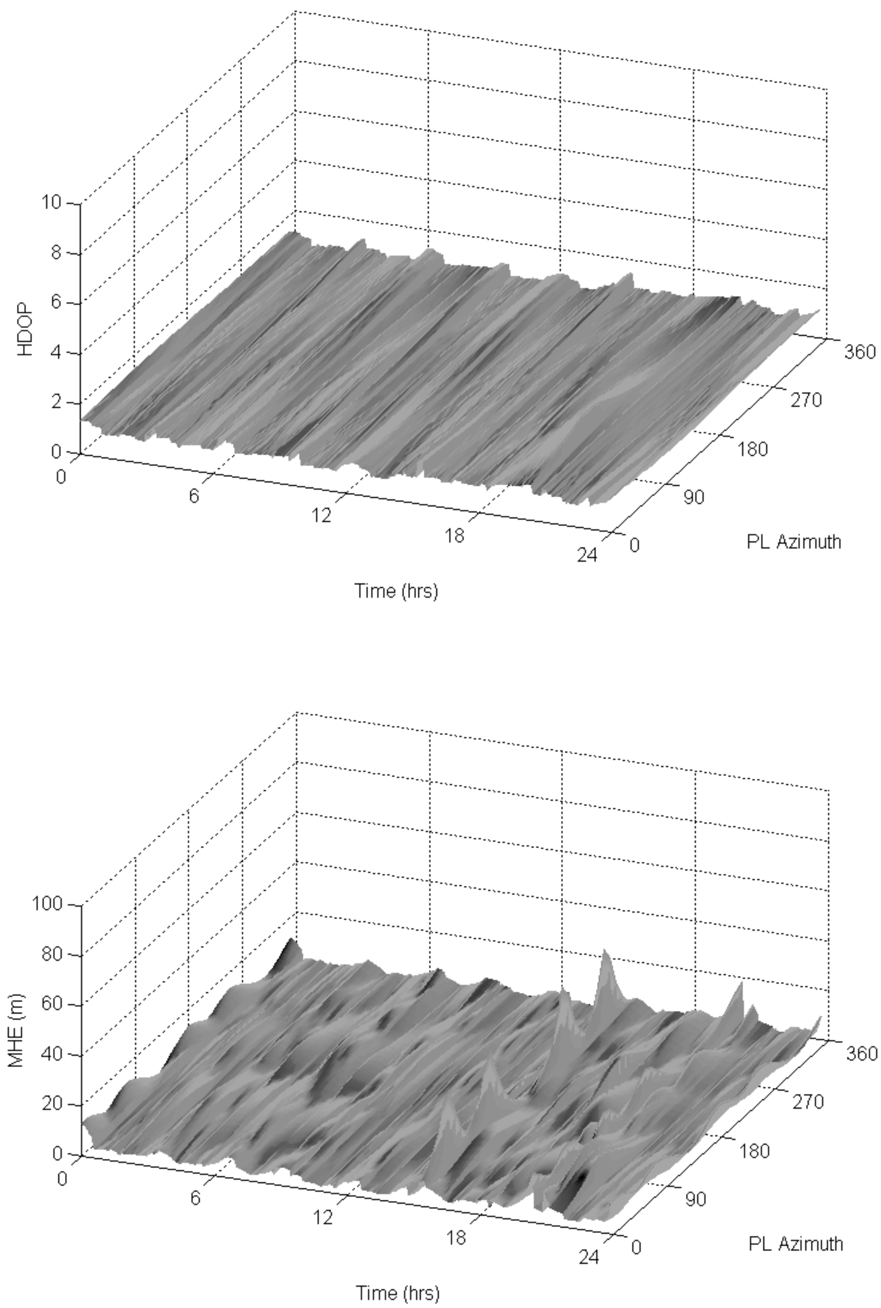

Figure 4.7 24-Hour HDOP and MHE at Calgary, May 8/9 1996.
Mask Angle 20°. Two PLs (70° spacing). 5 m^2 Height Constraint.

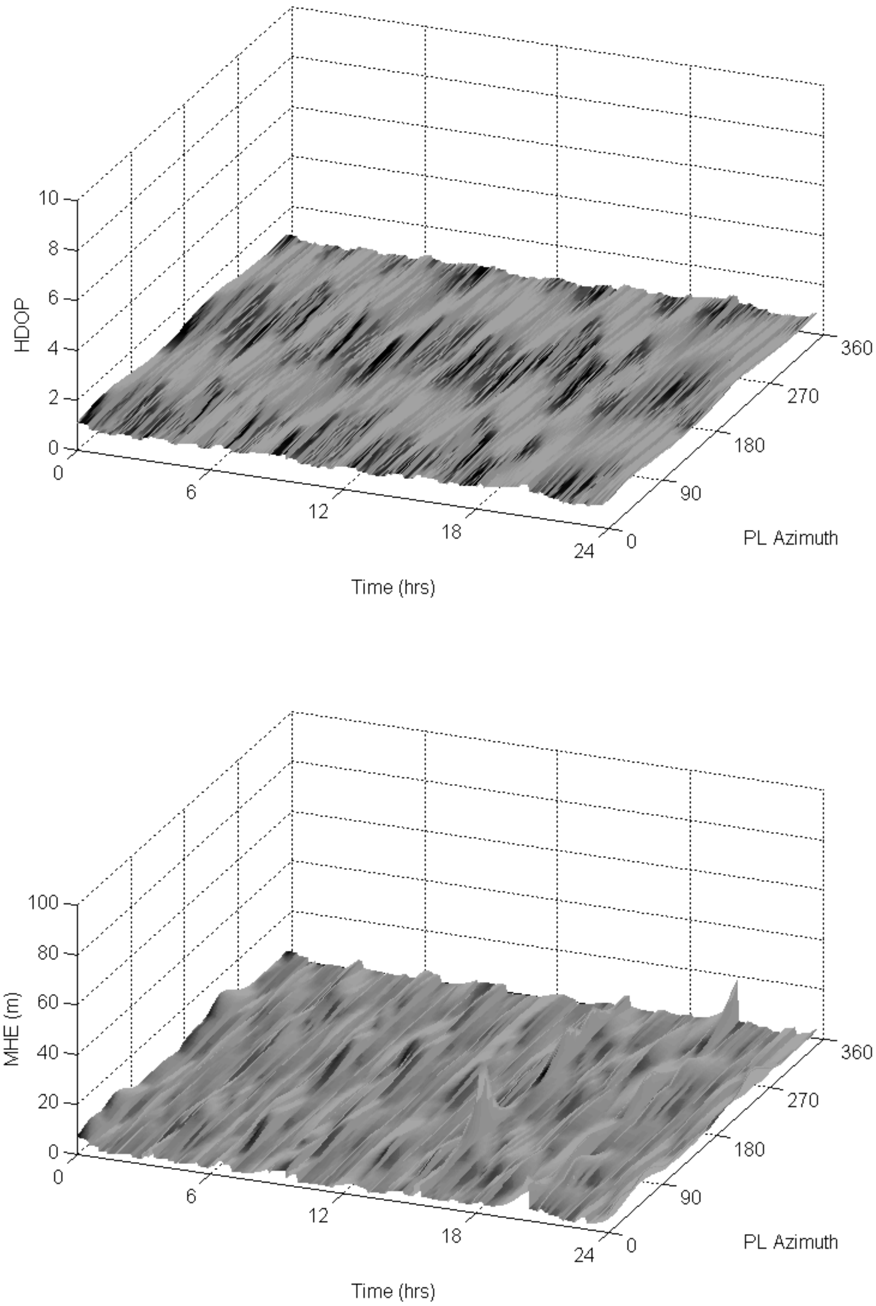

Figure 4.8 24-Hour HDOP and MHE at Calgary, May 8/9 1996.
Mask Angle 20°. Three PLs (70° and 200° spacing). 5 m^2 Height Constraint.

For the calculation of average values, the maximum HDOP was 10 and the maximum MHE was 100 m. If, at a particular epoch, the calculated HDOP or MHE exceeded the maximum value (or, in the case of the MHE, if no reliability assessment was available due to the number of satellites visible being less than 5), the HDOP or MHE was set equal to the maximum allowable value.

Table 4.2 Summary Statistics for Average HDOP and Average MHE for Unaugmented and PL Augmented GPS Constellations. Various Mask Angles. Various Configurations. With and Without 5 m^2 HC.

Mask Angle	5 m^2 HC?	# of PLs	HDOP Average	HDOP % > 10	MHE Average	MHE % > 20 m	MHE % > 100 m
10°	No	0	1.26	0	15.12	10.4	2.5
20°	No	0	2.55	6.5	110.11	55.2	34.0
10°	Yes	0	1.15	0	7.54	0.8	0.6
		1	1.03	0	4.88	0.2	0
		2	0.92	0	3.70	0	0
		3	0.82	0	2.74	0	0
20°	Yes	0	1.71	0	37.84	27.5	9.2
		1	1.39	0	12.64	9.4	1.3
		2	1.12	0	5.89	0.6	0
		3	0.96	0	4.37	0.1	0

4.3 Effect of Mountainous Topography and a Simulated Obstruction on GPS Availability, Accuracy and Reliability Measures

During docking, significant portions of the sky may be obscured by buildings and/or local topography. To assess the changes to the DGPS availability, accuracy and reliability measures, a simulated horizon was used as an input parameter to PLPLAN. The simulated horizon, shown in Figure 4.9 is based on measurements of the actual horizon at Lake Okanagan, British Columbia. In addition to the local topography, a simulated obstruction was added to the simulation. A constant mask angle of 10° was also used.

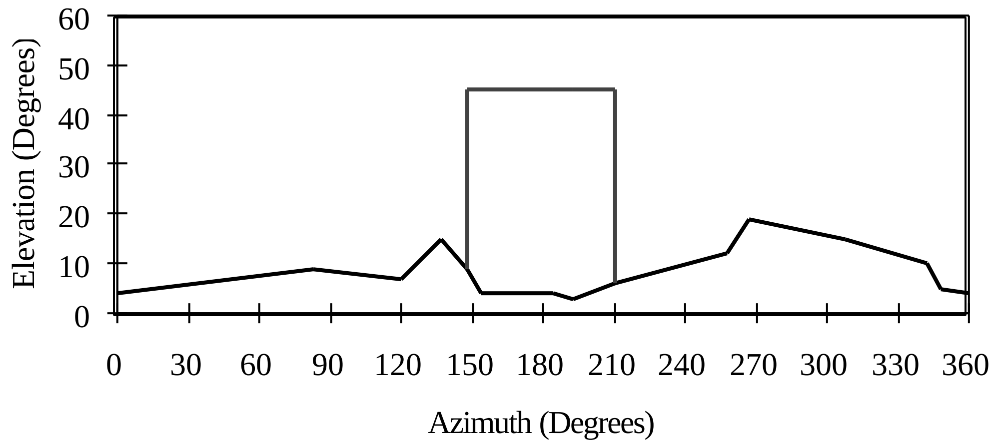

Figure 4.9 Okanagan Horizon Plus Simulated Obstruction Profile.

A plot of the HDOP, MHE and SVs with an unconstrained height is shown in Figure 4.10. The number of satellites above the simulated horizon and obstruction varies between 3 and 8. As in Figure 4.4 (mask angle 20°), there are several periods where the HDOP becomes excessive. With the Okanagan/obstruction horizon, however, the average HDOP is lower than the 20° case (1.83 versus 2.55), and the percentage of epochs which have an HDOP in excess of 10 is significantly less (1.9 % versus 6.5 %). There are also many epochs where the magnitude of the MHE exceeds 100 m. The average MHE is approximately half of the 20° case (57.9 m versus 110.1 m) as is the percentage of epochs which have an MHE in excess of 100 m (15.8 % versus 34.0 %).

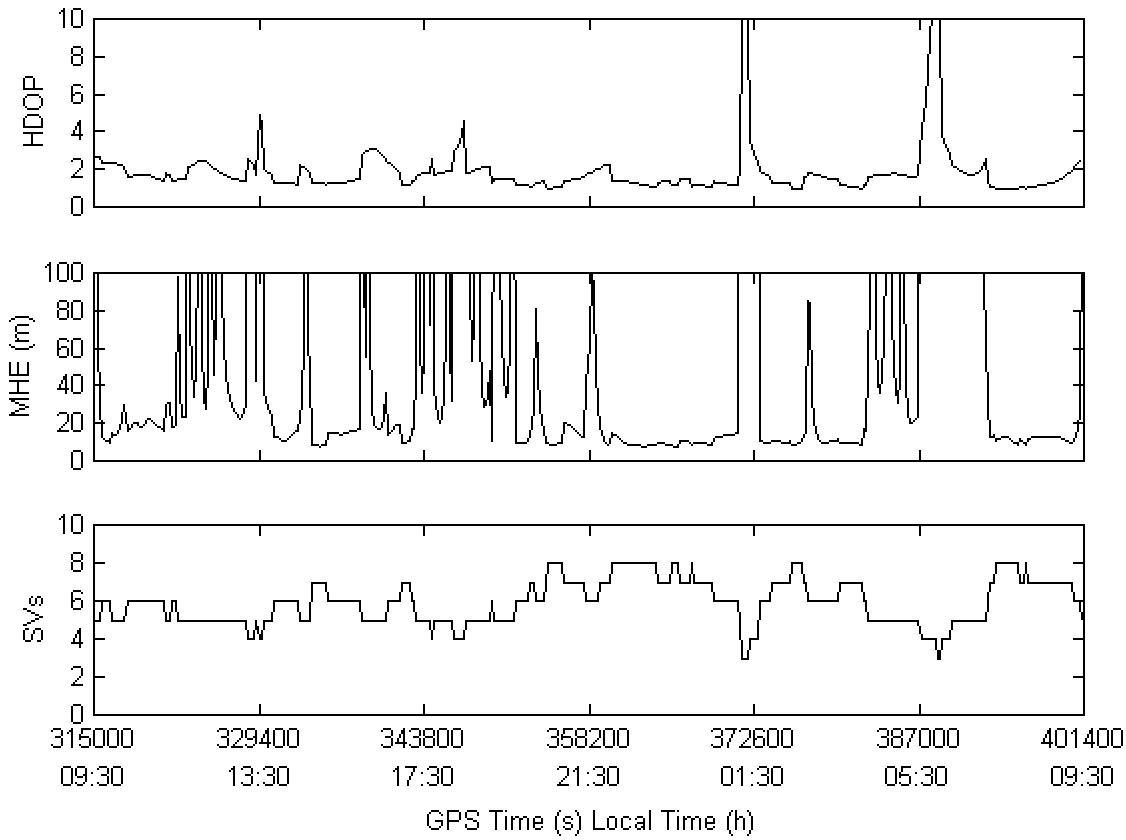

Figure 4.10 24-Hour HDOP and MHE at Calgary, May 8/9 1996. Okanagan Horizon Plus Obstruction. No Pseudolite. 5 m^2 Height Constraint.

Figures 4.11 illustrates the HDOP and MHE plots for an unaugmented constellation using a height constraint of 5m^2 and the Okanagan/obstruction horizon. The average HDOP has been reduced from 1.83 to 1.64 (with no periods where the HDOP exceeds 10), and the average MHE has been reduced from 57.9 m to 20.7 m (with only 3.8 % of epochs exceeding an MHE of 100 m).

Figure 4.12 shows the HDOP and MHE surfaces for a constellation augmented with one pseudolite at successive azimuths relative to the reference location. Again, a constant a height constraint of 5m^2 was used. The average HDOP is now reduced to 1.27, and the MHE has been reduced to 9.8 m (with less than 1 % of epochs exceeding an MHE of 100 m).

Two pseudolites, spaced at 70° relative to each other, were used to produce the plots in Figure 4.13. The HDOP for the entire 24-hour period never exceeds 2, with the HDOP averaging 1.04. The MHE surface also shows a significant improvement, yet there are noticeable periods where the MHE exceeds 50 m, but these periods can be effectively eliminated through appropriate positioning of the pseudolite relative to the remote location. The average MHE is now only 5.4 m, with almost no periods where the MHE exceeds 100 m (0.06 % of epochs), and only 1.1 % of epochs exceed 20 m.

Finally, Figure 4.14 shows the effect of three pseudolites, spaced at 70° and 200° relative to the primary pseudolite. The HDOP surface is essentially constant with respect to both time and pseudolite geometry. The average HDOP for the three pseudolite case is 0.89. The MHE surface still shows periods where the augmented constellation is weak with respect to reliability, but for the vast majority of time the MHE surface is below 10 m. The average MHE has been reduced to 3.9 m, with only 0.25 % of epochs exceeding 20 m. Summary statistics for Figures 4.10 through 4.14 are included in Table 4.3.

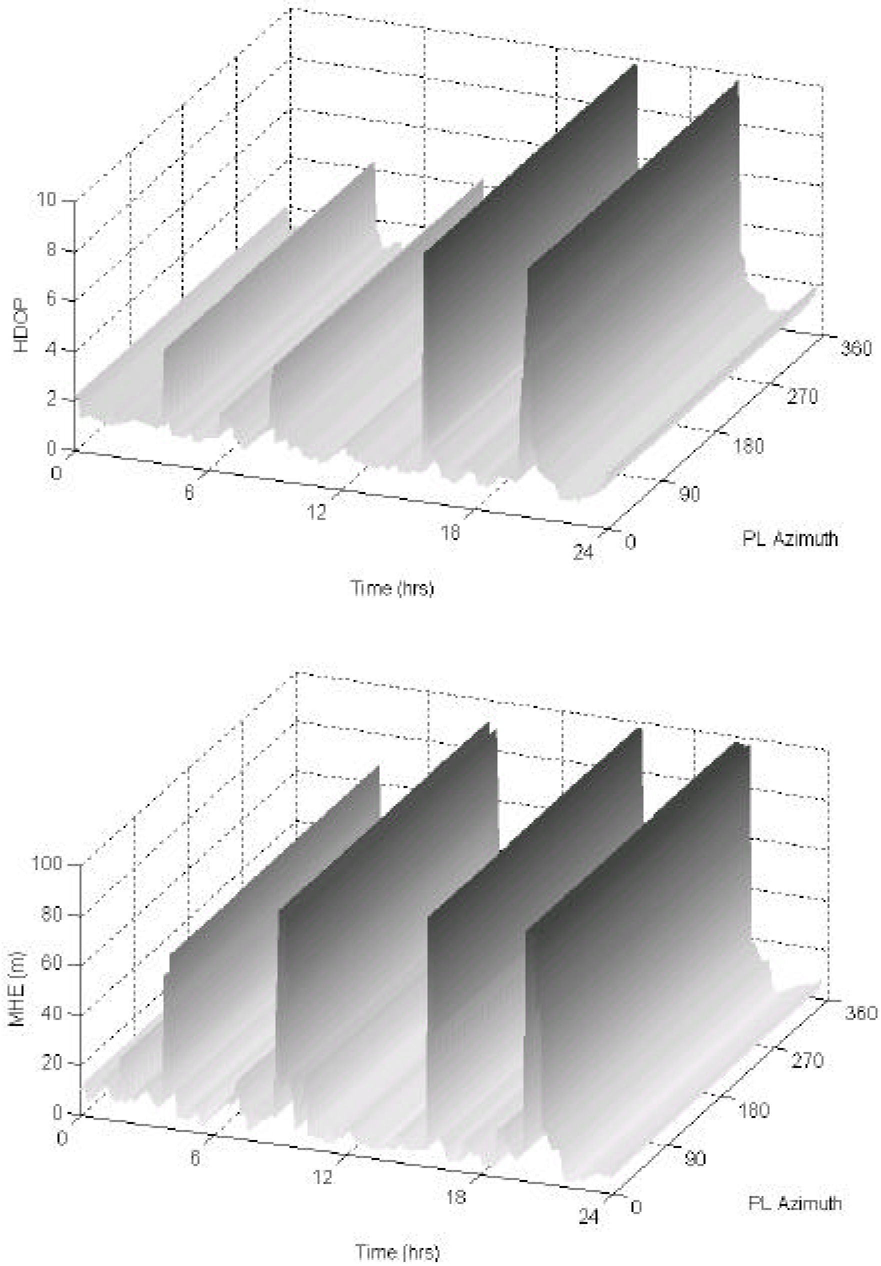

Figure 4.11 24-Hour HDOP and MHE at Calgary, May 8/9 1996.
Okanagan Horizon Plus Obstruction. No PL. 5 m² Height Constraint.

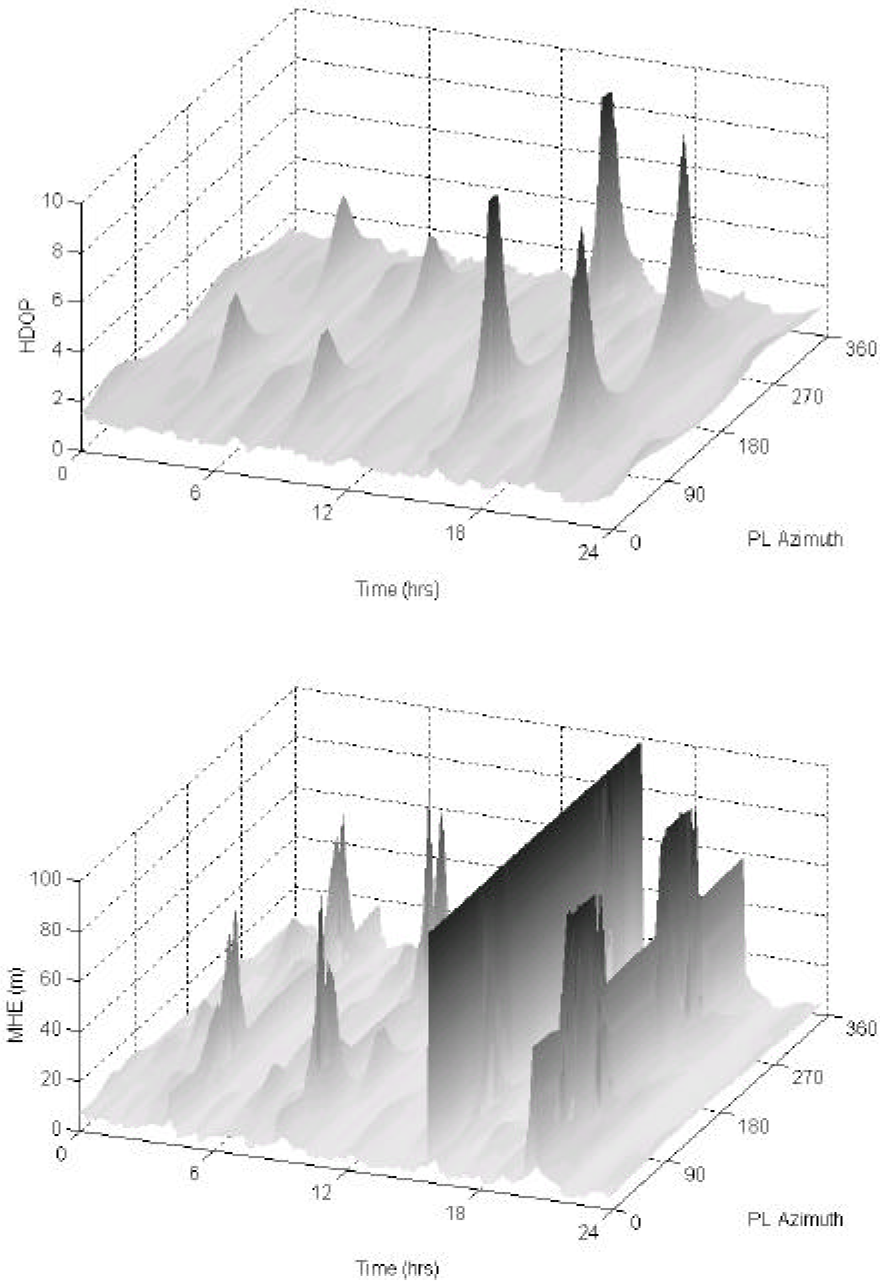

Figure 4.12 24-Hour HDOP and MHE at Calgary, May 8/9 1996. Okanagan Horizon Plus Obstruction. One PL. 5 m^2 Height Constraint.

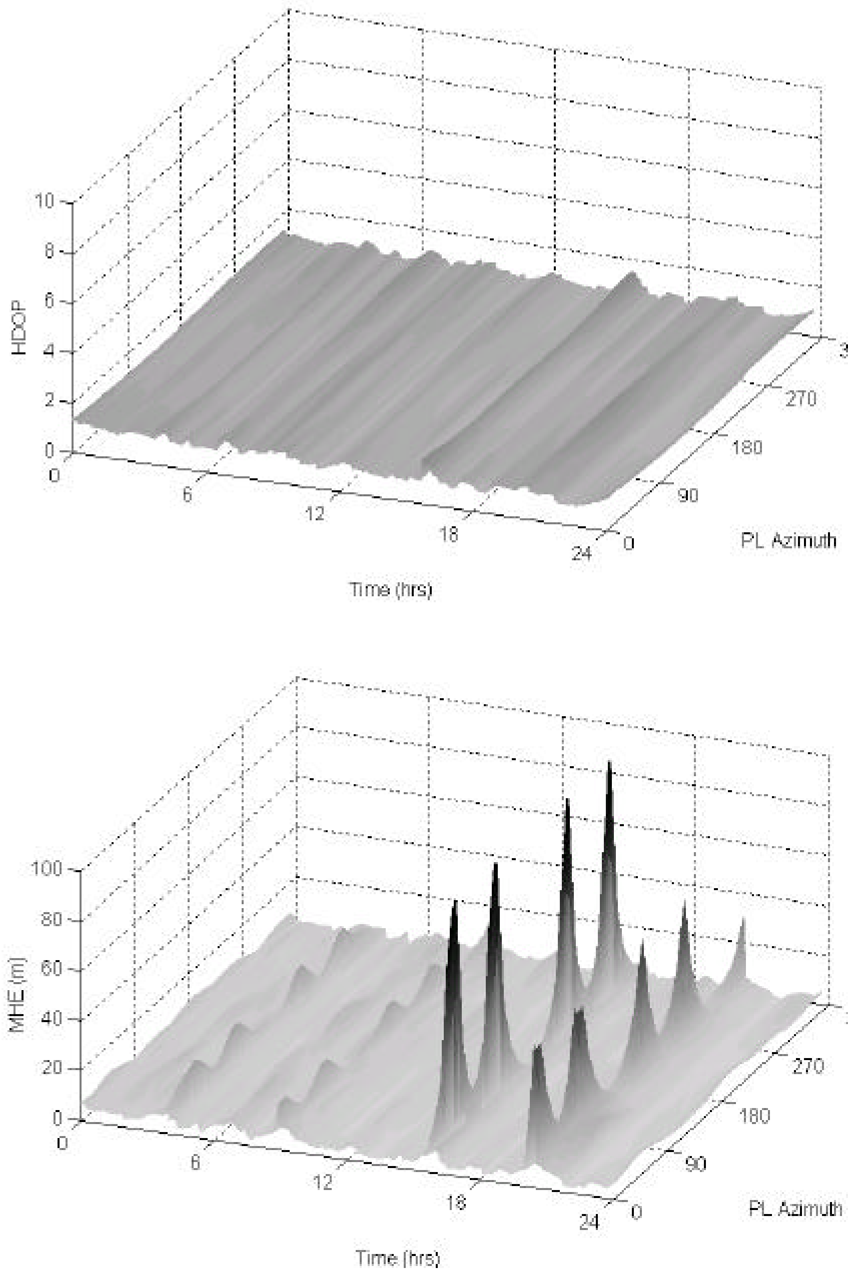

Figure 4.13 24-Hour HDOP and MHE at Calgary, May 8/9 1996. Okanagan Horizon Plus Obstruction. Two PLs (70° spacing). 5 m^2 Height Constraint.

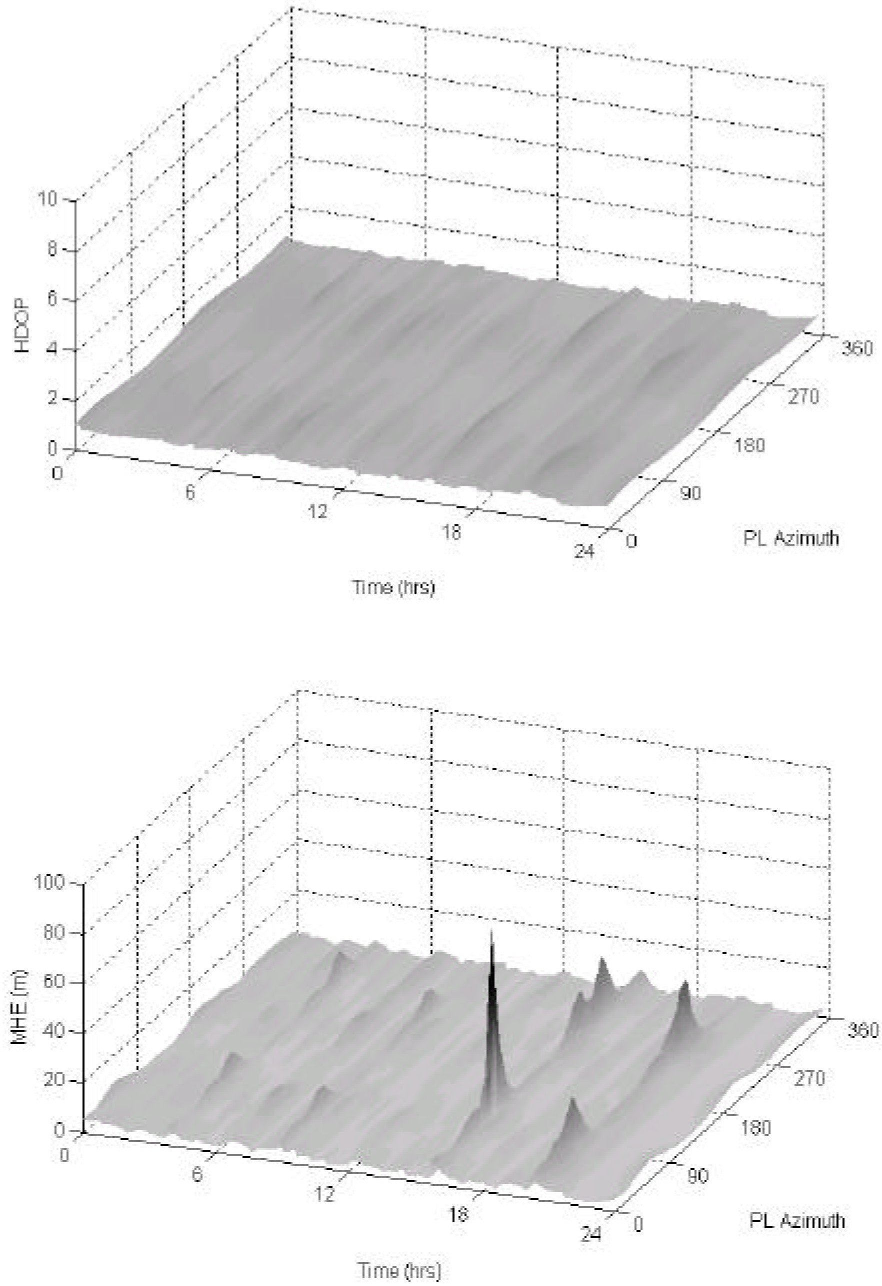

Figure 4.14 24-Hour HDOP and MHE at Calgary, May 8/9 1996. Okanagan Horizon Plus Obstruction. Three PLs (70° and 200° spacing). 5 m^2 Height Constraint.

As before, for the calculation of average values, the maximum HDOP was 10 and the maximum MHE was 100 m. If, at a particular epoch, the calculated HDOP or MHE exceeded the maximum value (or, in the case of the MHE, if no reliability assessment was available due to the number of satellites visible being less than 5), the HDOP or MHE was set equal to the maximum allowable value.

Table 4.3 Summary Statistics for Average HDOP and Average MHE for Unaugmented and PL Augmented GPS Constellations. Okanagan Horizon Plus Obstruction. Various Configurations. With and Without 5 m^2 Height Constraint.

5 m^2 HC?	# of PLs	HDOP Average	HDOP % > 10	MHE Average	MHE % > 20 m	MHE % > 100 m
No	0	1.83	1.88	57.87	41.46	15.83
Yes	0	1.64	1.04	20.71	13.75	3.75
	1	1.27	0.10	9.82	4.75	0.82
	2	1.04	0	5.42	1.13	0.06
	3	0.89	0	3.92	0.25	0

CHAPTER 5

EFFECT OF PSEUDOLITE AUGMENTATION ON BETWEEN-RECEIVER SINGLE DIFFERENCE DGPS

Two field tests were conducted to assess the effect of PL augmentation on GPS availability, accuracy and reliability measures, and the resulting effects on the DGPS position solution. C^3NAVPL was used to post-process the data. The first field test was conducted on October 20, 1996 at the Glenmore Reservoir in Calgary. The goals of this test were to gain field experience with the PL, and validate the C^3NAVPL software modifications. The remote GPS receiver was located in an aluminum canoe which was maneouvered within approximately 500 m of the shore stations. One hour of continuous PL data was collected. The second field test was conducted on November 7, 1996 at Lake Okanagan, British Columbia. The purpose of this test was to collect PL data in a marine environment in a mountainous area. The remote GPS receiver was located on a 44 foot boat which operated at distances between approximately 600 m and 3500 m of the shore stations. Two hours and twenty minutes of continuous PL data was collected by both the reference and remote GPS receivers during the morning session, and approximately one hour of non-continuous PL data was collected during the afternoon session.

This chapter summarizes the results of the Glenmore and Okanagan field tests. Each field test is sub-divided into two main sections: 1) changes to the GPS availability, accuracy and reliability measures under the following conditions: a) an unaugmented GPS satellite constellation with no height constraint, b) a PL augmented constellation with no height constraint, and c) a PL augmented constellation with a 1 m^2 height constraint; and 2) changes to the position solution using the above three conditions. For the Glenmore field test analysis, a greater emphasis will be placed on the changes to the GPS availability, accuracy and reliability measures. The Okanagan field test analysis will have a greater emphasis on the changes to the DGPS position solution as determined by C^3NAVPL.

PL augmentation results in an improvement to the accuracy and reliability measures for both field tests. Biases are evident in the latitude, longitude and height solution for the PL augmented constellation for both field tests, due to multipath between the PL and reference receiver antennas. A further analysis is conducted on the Lake Okanagan data set to illustrate how the multipath component between the PL and reference receiver antenna can be estimated. With the use of an appropriate multipath correction term, the PL augmentation results in more accurate DGPS positioning. The ability of a PL to improve fault detection and exclusion is illustrated by intentionally inducing a pseudorange error (as measured by the remote receiver) on one satellite.

5.1 Glenmore Reservoir Field Test - Overview

A small scale field test was conducted at the Glenmore Reservoir in Calgary on October 20, 1996. Two NovAtel OEM-2 (RT-20) GPS receivers were used for the reference and remote stations. Chokerings and 501 L1 antennas were used with each receiver. The reference antenna was located over a spike driven into the ground beside a bicycle path on the east shore of the reservoir. The coordinates of the reference station were determined with respect to pillar N2 on the roof of the Engineering Building at the University of Calgary by SEMIKIN™ double-difference fixed integer ambiguity solution. The distance between pillar N2 and the reference location was determined to be 11.215 km. The remote antenna and receiver were located in an aluminum canoe. The remote antenna was securely fastened to the centre seat of the canoe, as shown in Figure 5.1. The antenna was approximately 60 cm above the waterline.

Figure 5.1 Glenmore Reservoir. Photograph of Remote Platform.

The PL antenna was placed on a tripod which was located over an iron spike at the top of a small hill, overlooking the reservoir and the reference station. The coordinates of the PL with respect to the reference coordinates were determined the day after the field test, again using SEMIKIN™. The baseline between the reference and the PL was calculated to be 248.94 m.

The locations of the PL, the reference station, the approximate shore line, and the reference trajectory of the remote antenna on the canoe are shown in Figures 5.2 and 5.3. The reference trajectory for the remote antenna was determined using a FLYKIN™ fixed integer on-the-fly solution, with an expected 3D accuracy of better than 10 cm [Lachapelle, 1995]. The GPS times are annotated on the reference trajectories every 180 seconds, from the beginning of the data set (64905 seconds) to the end of the data set (68950 seconds). The elevation of the PL antenna with respect to the reference antenna was only 0.95°, but this was the best that could be accomplished given the location of the test. It was anticipated that such a low elevation angle could result in a large amount of undesired multipath from the PL due to the close proximity of the ground.

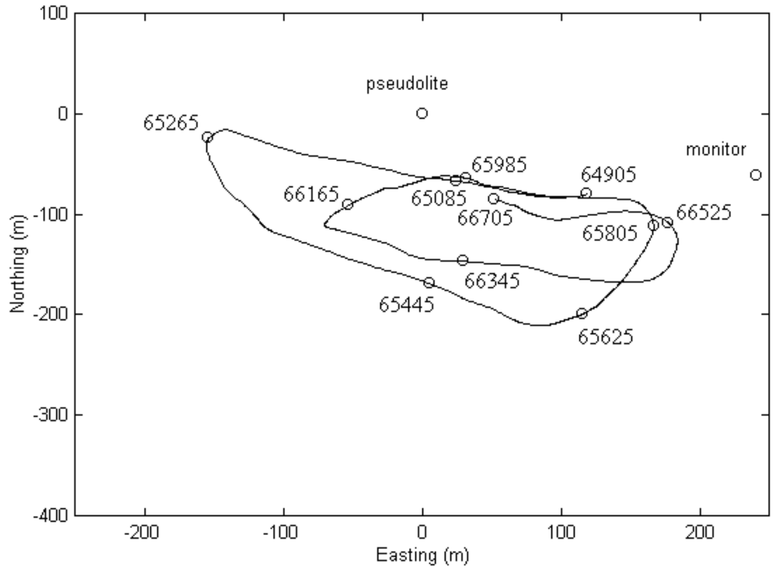

Figure 5.2 Glenmore Reservoir. Reference Trajectory (GPS Time 64905 to 66705)

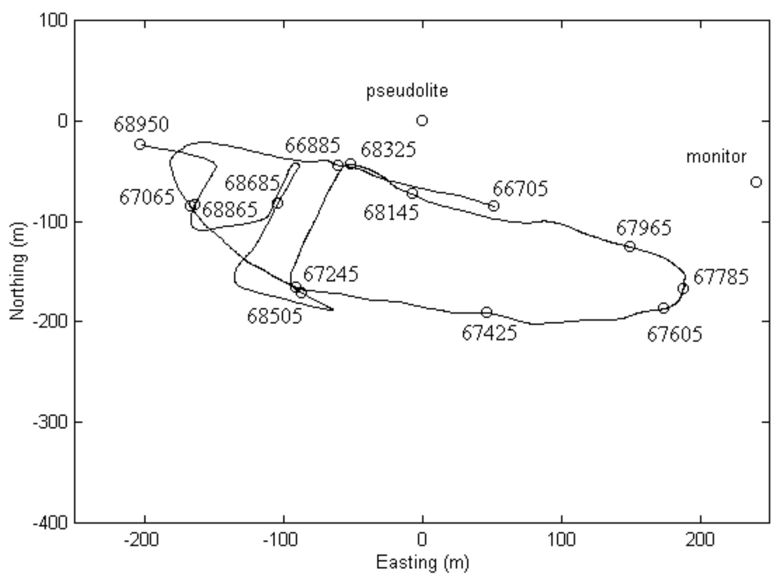

Figure 5.3 Glenmore Reservoir. Reference Trajectory (GPS Time 66705 to 68950)

A plot of the fixed ambiguity (GPS satellites only) height solution is included in Figure 5.4. As can be seen, the reservoir was particularly smooth, and there was very little vertical motion induced to the antenna due both to the central location of the antenna, and the paddling expertise of the canoe crew. The mean height of the remote antenna for the test was determined to be 1059.76 m, with a standard deviation of one centimetre. To give a complete picture of the movement of the remote platform, the fixed ambiguity horizontal velocity solution is presented in Figure 5.5. The horizontal velocity of the canoe varied between almost zero to just under two metres per second. The mean horizontal velocity for the Glenmore Reservoir test was 0.76 m/s. The vertical velocity was essentially zero for the duration of the Glenmore field test.

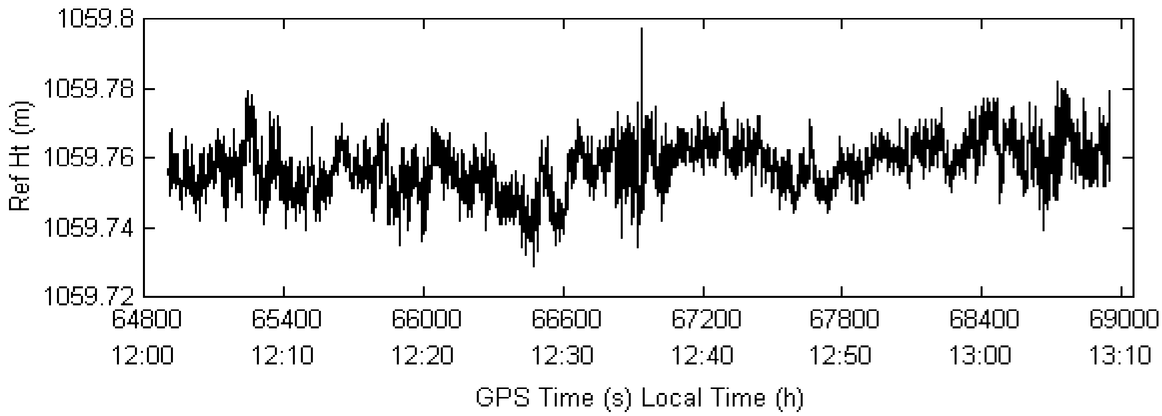

Figure 5.4 Glenmore Reservoir. Fixed Ambiguity Height Solution.

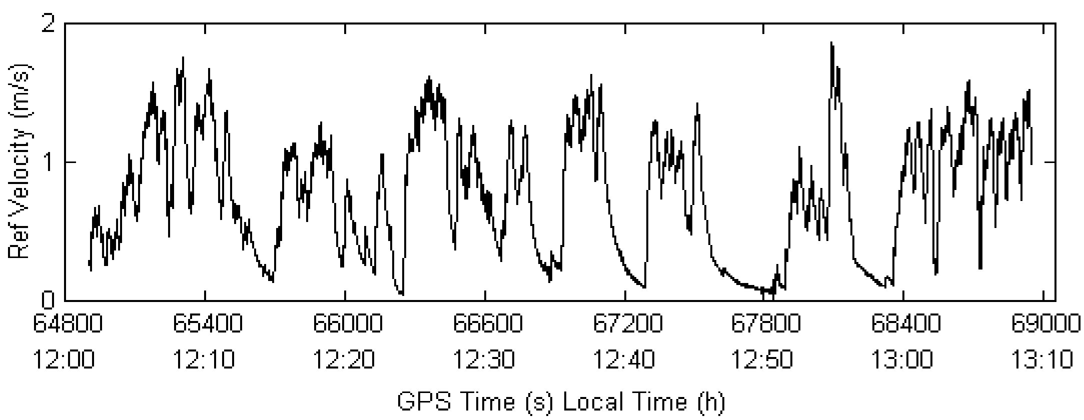

Figure 5.5 Glenmore Reservoir. Fixed Ambiguity Horizontal Velocity.

The calculated slant ranges from the remote antenna to both the reference station and the PL are presented in Figures 5.6 and 5.7. Both plots show a slowly changing slant range between the remote and the two shore stations, with a maximum separation between the reference and the remote of just over 400 m. The remote platform varied between approximately 50 m and 275 m from the PL. At no time during this data set did either of the GPS receivers lose lock on the PL signal.

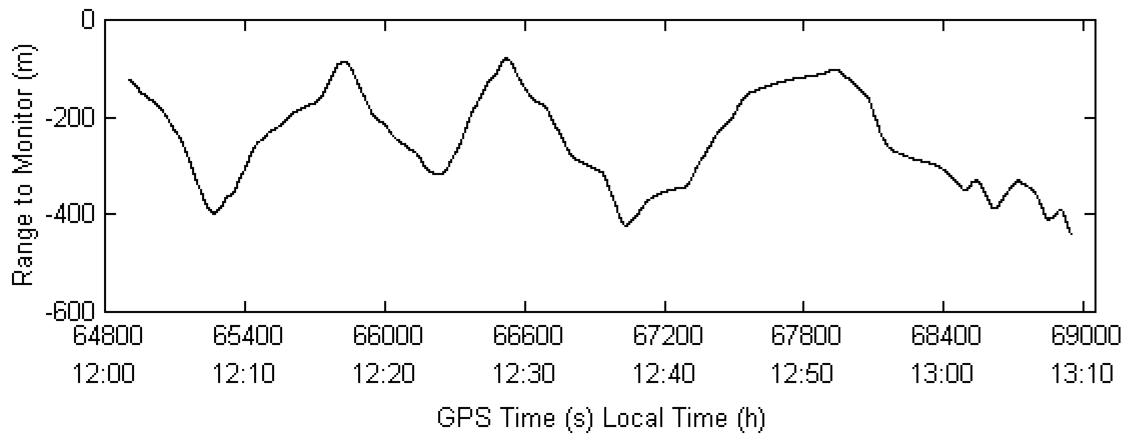

Figure 5.6 Glenmore Reservoir. Slant Range Between Reference and Remote.

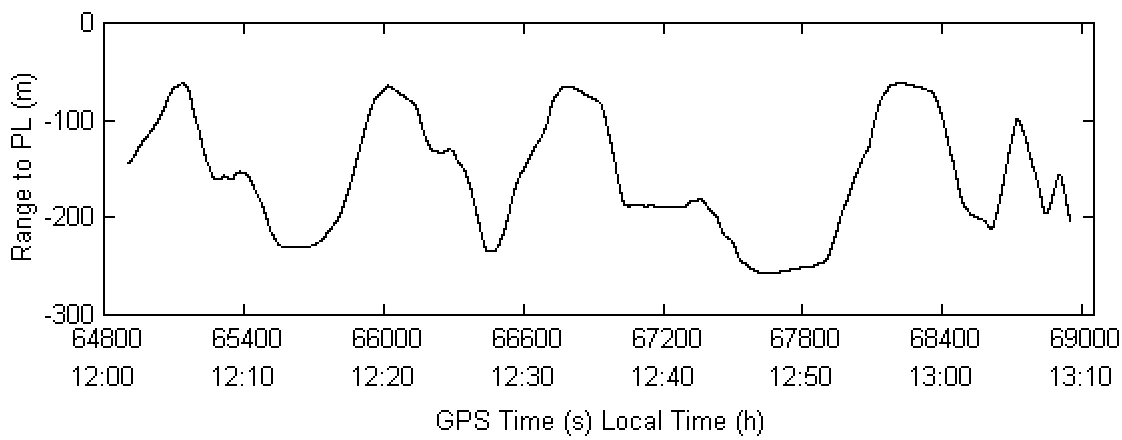

Figure 5.7 Glenmore Reservoir. Slant Range Between PL and Remote.

The pseudolite elevation, as observed by the remote platform, is shown in Figure 5.8. The observed pseudolite elevation varied between 3° and 13°. The signal to noise ratios (C/N_0), as measured by both the remote receiver and the reference receiver, are plotted in Figure 4.24. The pseudolite transmission, as measured by the reference receiver, shows some slight variation in the received signal, but overall, the signal is reasonably constant. The same is not true, however, for the signal strength at the remote, due to the large relative changes in distance between the pseudolite and the remote (approximately 50 m to 275 m) and multipath interference.

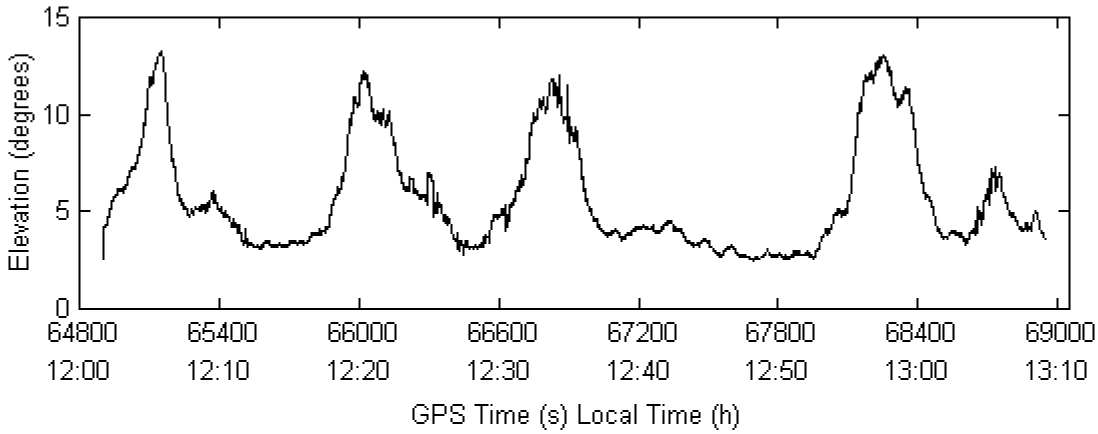

Figure 5.8 Glenmore Reservoir. Elevation of PL as Observed by Remote.

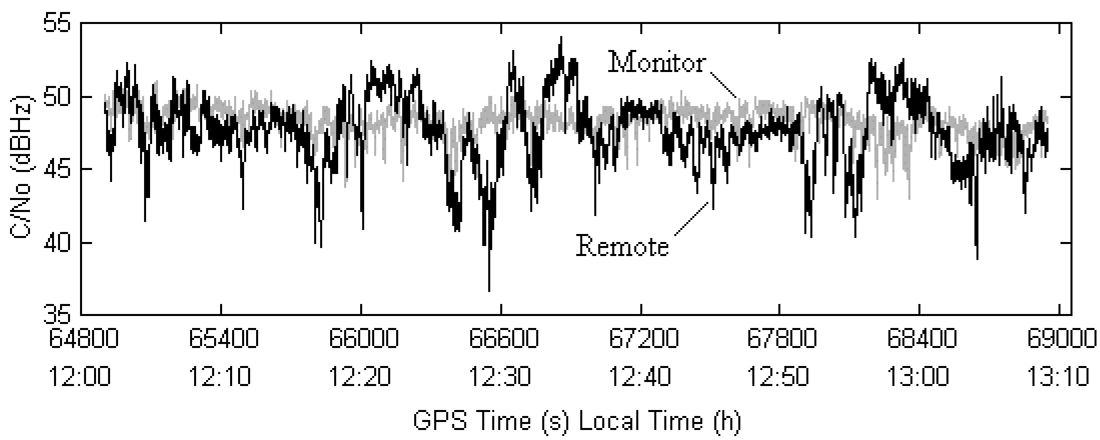

Figure 5.9 Glenmore Reservoir. PL C/N_0 as Measured By Reference and Remote.

5.1.1 Changes to DGPS Availability, Accuracy and Reliability Measures

Figures 5.10, 5.11 and 5.12 illustrate the number of satellites tracked (SVs), the Horizontal Dilution of Precision (HDOP), and the Maximum Horizontal Error (MHE) for the Glenmore Reservoir data set, using a constant mask angle of 10°. The horizon due to local topography or man-made structures was less than the 10° mask angle. The following three configurations are assessed: unaugmented GPS with no height constraint (HC), PL augmented GPS with no HC, and PL augmented GPS with a HC. The average number of satellites tracked for the unaugmented scenario was 7.08, whereas for the PL augmented scenario it was

8.08. As shown in Figure 5.10, the actual number of satellites tracked remained fairly constant throughout the data set, with only one short segment where the number of satellites dropped to 5 (or 6 for the PL augmented cases). Note that this figure shows only the actual number of satellites tracked and not “observations”, which would include the height constraint quasi-observation.

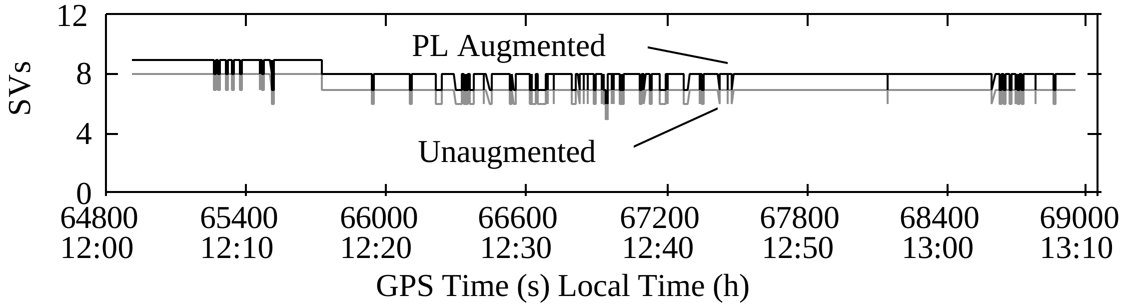

Figure 5.10 Glenmore Reservoir. Number of Satellites Tracked. Unaugmented and PL Augmented GPS Constellations. Mask Angle 10°. No Satellites Rejected.

The HDOP plots for the three configurations are presented in Figure 5.11. The values for the HDOPs are quite good throughout the period, with only one small excursion that occurs when the number of satellites for the unaugmented case drops to 5. The average HDOP for the three configurations are 1.25, 1.11 and 1.03, respectively.

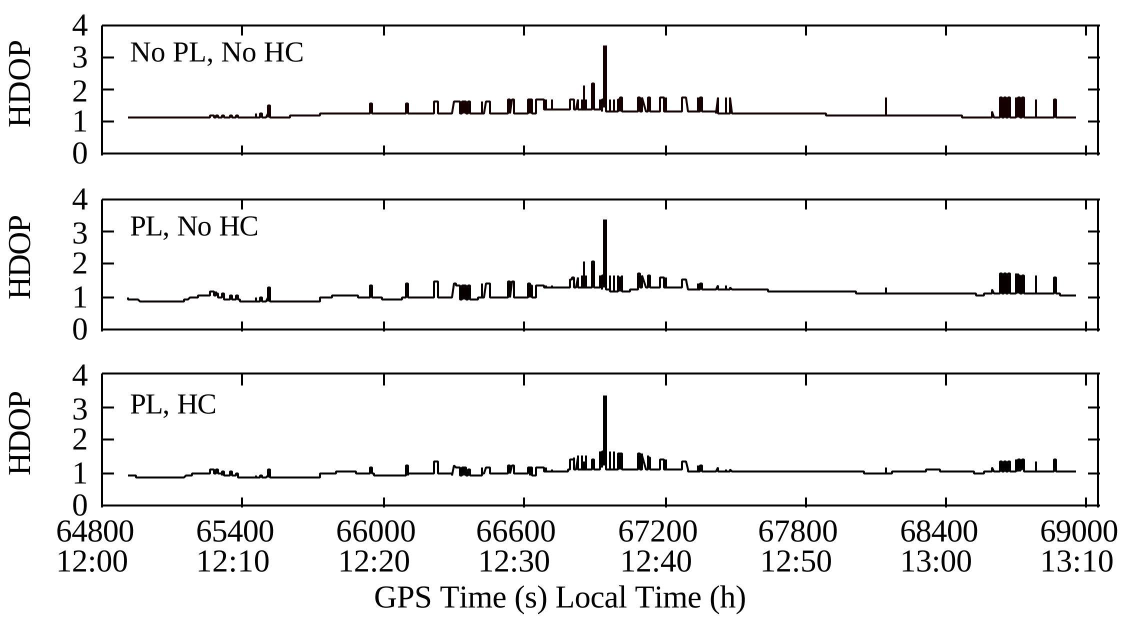

Figure 5.11 Glenmore Reservoir. HDOP. Unaugmented and PL Augmented GPS Constellations. Mask Angle 10°. No Satellites Rejected.

The MHE envelopes for the three cases are shown in Figure 5.12. There is slightly more separation between the three plots, with the three configurations averaging 7.59 m, 5.96 m, and 3.97 m, respectively. Note that the inclusion of PL information has a fairly significant effect during the first half of the data set, whereas, during the second half of the data set, this extra information does not reduce significantly the magnitude of the MHE. This is due to the geometrical dependency of the reliability measure. What is most notable, however, is the dramatic effect that this extra information can have on the reliability measure when the geometry becomes poor from a reliability perspective. Consider GPS time 66894 (approximately 12:35 local time) where the number of GPS satellites tracked drops from 7 to 6 due to the loss of satellite 3 for seven epochs. This corresponds to the middle "spike" on the MHE plot. Comparing the unaugmented to the augmented case (both with unconstrained height), it is found that the HDOP decreases slightly from 1.33 to 1.27, which is not very significant. The MHE, on the other hand, decreases from over 54 m to 18.5 m, which is very significant. In fact, from an integrity monitoring point of view, an alert would have to be presented to the GPS operator for the unaugmented case, indicating that an undetected blunder could occur with GPS that would result in a horizontal position error in excess of the 20 m marine requirement [FRP, 1994]. This alert would not have to be issued for the PL augmented case. Less than one minute later, however, the situation is quite different. At GPS time 66940 (approximately 12:36 local time) the number of satellites tracked drops from 6 to 5 (corresponding to the right "spike" on the MHE plot) with the loss of satellite 31 for ten epochs. This time, the HDOP decreases from 1.69 to 1.66, and the MHE decreases from 39.0 m to 31.1 m. An integrity alert would have to be issued for both the unaugmented and PL augmented cases. The use of a height constraint improves this situation considerably, as the HDOP and MHE are reduced to 1.61 and 13.8 m, respectively.

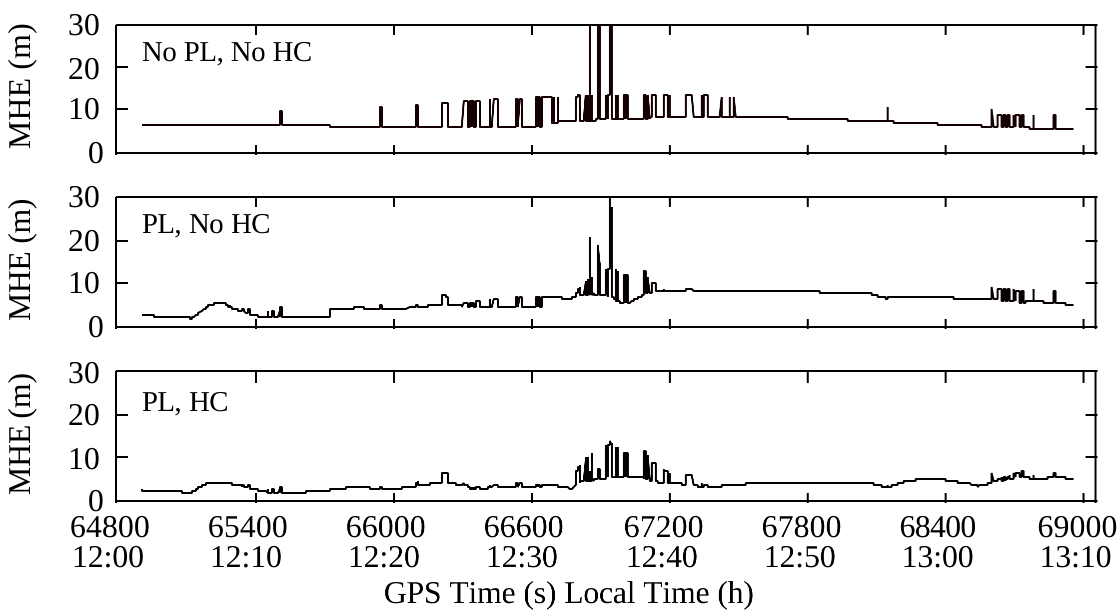

Figure 5.12 Glenmore Reservoir. MHE. Unaugmented and PL Augmented GPS Constellations. Mask Angle 10°. No Satellites Rejected.

For the next series of plots, the satellite elevation mask angle was increased from 10° to 20°. All other parameters for the three configurations remained the same. As expected, there was a decrease in the number of satellites tracked, and a corresponding increase in the HDOP and MHE measures. Figure 5.13 shows the number of satellites tracked for a 20° mask angle. The average for the unaugmented case is over one satellite less than for the 10° mask angle case (6.02 versus 7.08). The appearance of this plot is somewhat different than Figure 5.10, where there was frequent loss of lock of GPS signals from satellites near the 10° cut off, but not for signals near the 20° cut off.

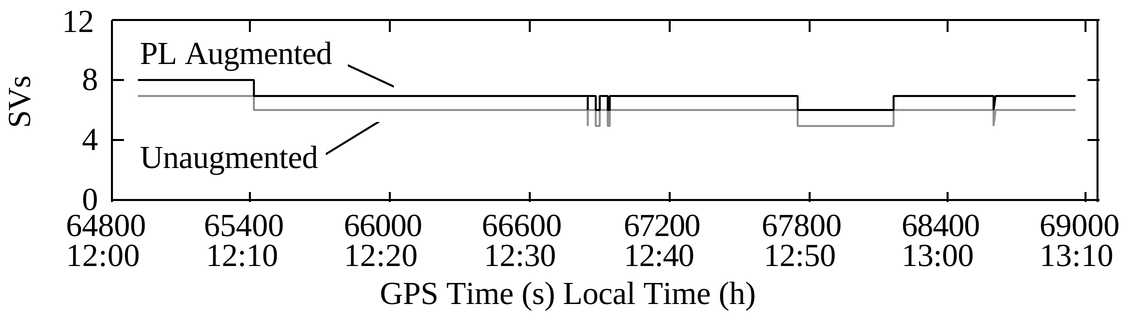

Figure 5.13 Glenmore Reservoir. Number of Satellites Tracked. Unaugmented and PL Augmented GPS Constellations. Mask Angle 20°. No Satellites Rejected.

The HDOP plot shown in Figure 5.14 indicates that, even with a 20° mask angle, the geometric strength of the unaugmented GPS constellation (with respect to precision) was quite strong, with an average HDOP of 1.71, compared to an average HDOP of 1.52 for the PL augmented case. The addition of a height constraint did not make a significant difference to the HDOP, except from GPS time 67800 to 68200 when the number of satellites tracked dropped from 6 to 5. The average HDOP for the PL augmented and height constrained configuration was reduced to 1.26.

There is, however, a marked difference between the three cases when the reliability measure is compared, as shown in Figure 5.15. For much of the data set, there is a difference between the MHE for an unaugmented constellation versus a PL augmented constellation of over 3 m. In fact, the average MHE has been reduced from 11.6 m to just under 8 m. The incorporation of a height constraint makes even more of a difference, especially during the latter half of the data set. The average MHE for the PL augmented and height constrained case is only 4.9 m.

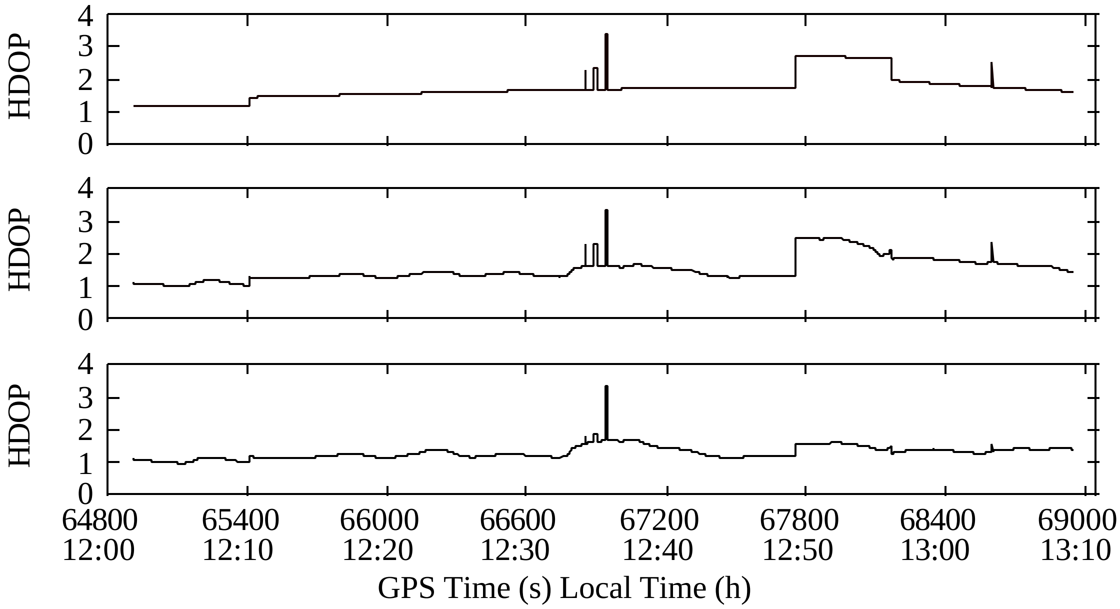

Figure 5.14 Glenmore Reservoir. HDOP. Unaugmented and PL Augmented GPS Constellations. Mask Angle 20°. No Satellites Rejected.

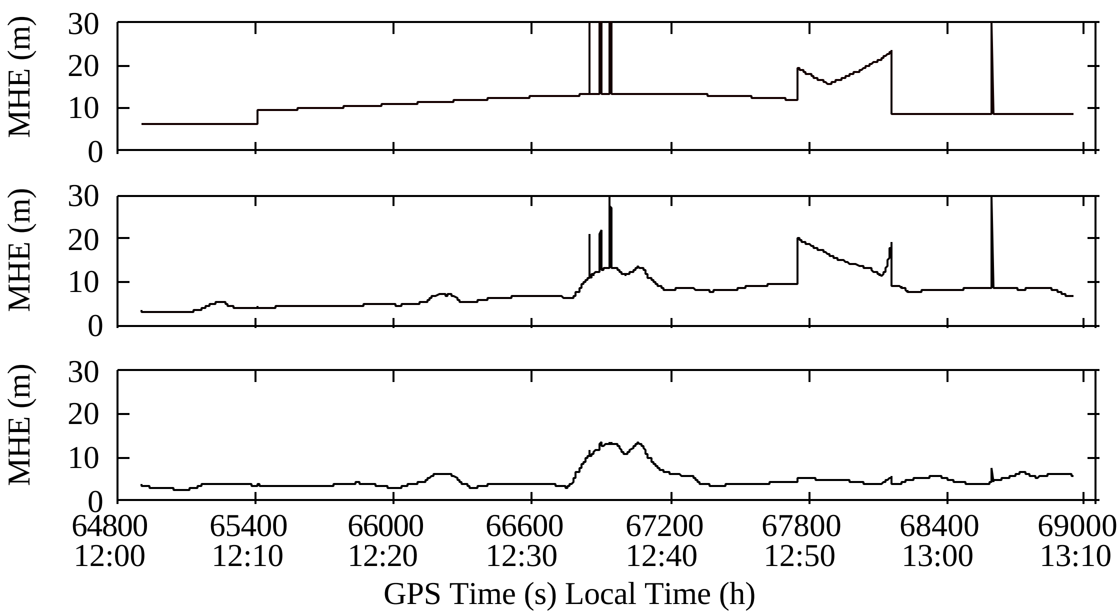

Figure 5.15 Glenmore Reservoir. MHE. Unaugmented and PL Augmented GPS Constellations. Mask Angle 20°. No Satellites Rejected.

As there is always a possibility under operational conditions that one or more satellites could be unavailable for use (due, for example, to unserviceability or old/no ephemeris information), the data set for the 10° mask angle was reprocessed, but with one satellite, namely PRN 31, rejected. The plot of the number of satellites tracked for this degraded scenario is shown in Figure 5.16.

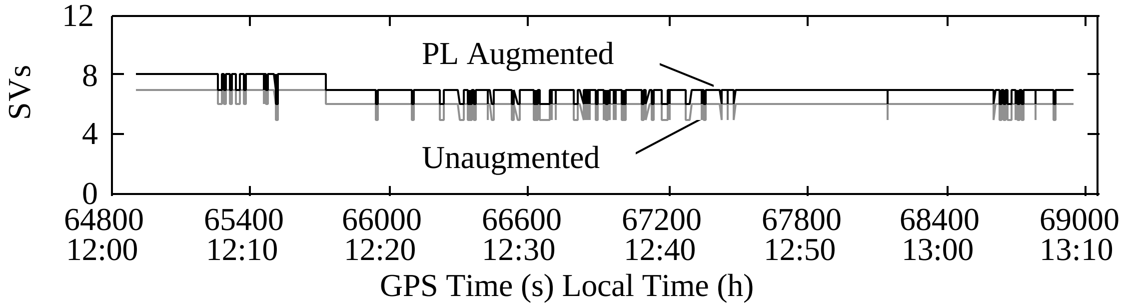

Figure 5.16 Glenmore Reservoir. Number of Satellites Tracked. Unaugmented and PL Augmented GPS Constellations. Mask Angle 10°. Satellite 31 Rejected.

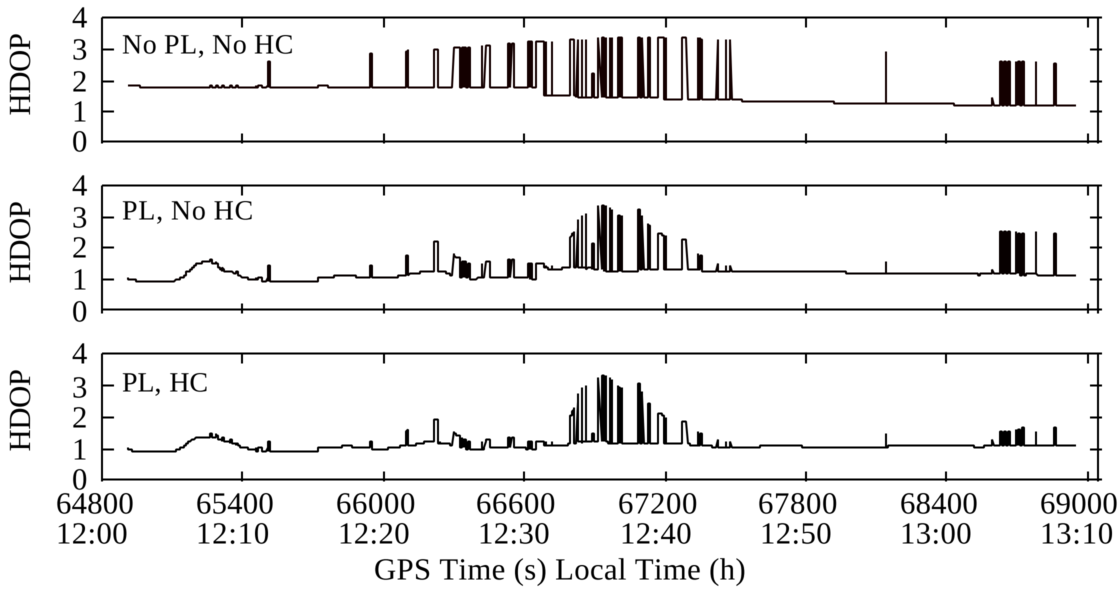

Figure 5.17 Glenmore Reservoir. HDOP. Unaugmented and PL Augmented GPS Constellations. Mask Angle 10°. Satellite 31 Rejected.

The HDOP plot presented in 5.17 shows a general increase in the HDOP values for the unaugmented and unconstrained case, with rather pronounced excursions in the HDOP whenever lock was broken on a low elevation satellite. The PL augmented cases for both the unconstrained and constrained height also show this trend, which is an indication of the sensitivity of the geometry to satellite 31.

The MHE plot for the 10° mask angle with satellite 31 rejected is shown in 5.18. The difference between this plot and the 10° mask angle plot that includes satellite 31 (Figure 5.12) is striking. This MHE plot is even worse than the 20° mask angle case (Figure 5.15), even though the number of satellites tracked is similar (between five and seven), and the HDOPs are generally two or less. In fact, in Figure 5.18, 127 of the 4045 epochs (3.1%) had an MHE greater than 100 m. The average MHEs for the three configurations are: 17.9 m, 8.6 m, and 5.8 m, respectively. Note that for the computation of the average MHE, if the calculated MHE exceeded 100 m, it was set equal to 100 m. There were no MHE excursions over 100 m for either of the PL augmented scenarios. Results for the number of satellites tracked, the mean HDOP and the mean MHE for all of the above scenarios are summarized at Table 5.1.

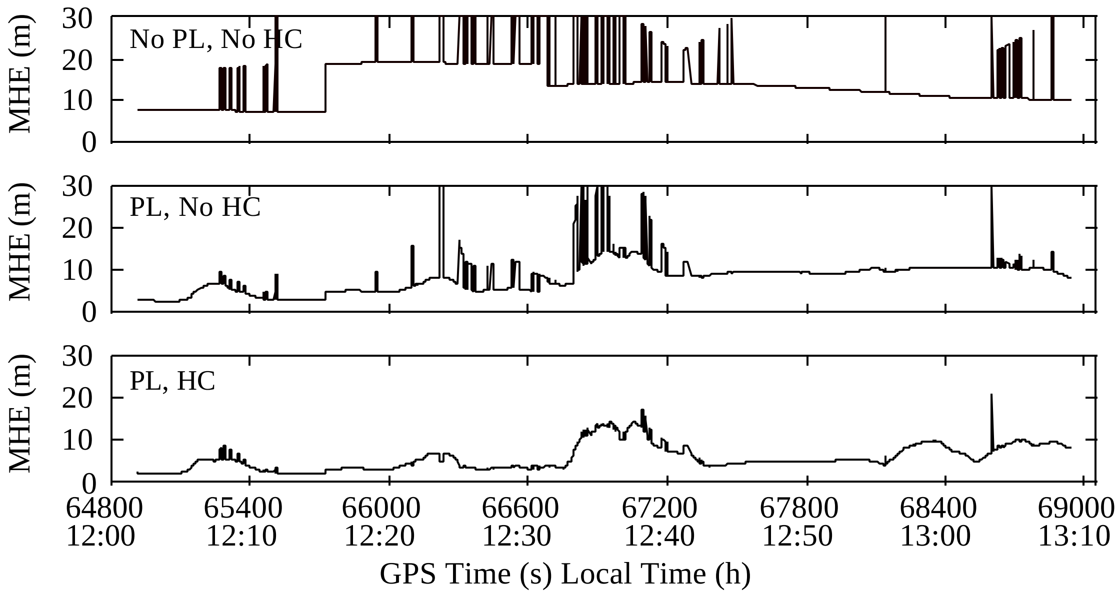

Figure 5.18   Glenmore Reservoir. MHE. Unaugmented and PL Augmented GPS Constellations. Mask Angle 10°. Satellite 31 Rejected.

Table 5.1 Glenmore Reservoir. Summary of Number of Satellites Tracked, Average HDOP and Average MHE. Various Mask Angles. Various Configurations.

Mask Angle	PL Used	1 m^2 HC Used	Rejected SV	Mean SVs	Mean HDOP	Mean MHE (m)
10°	No	No	None	7.08	1.25	7.59
	Yes	No		8.08	1.11	5.96
	Yes	Yes		8.08	1.03	3.97
20°	No	No	None	6.02	1.71	11.63
	Yes	No		7.02	1.52	7.97
	Yes	Yes		7.02	1.26	4.91
10°	No	No	31	6.08	1.69	17.94*
	Yes	No		7.08	1.26	8.56
	Yes	Yes		7.08	1.15	5.80

* Includes 3.1% of epochs with an MHE greater than 100 m.

5.1.2 Changes to DGPS Positioning

To assess the absolute accuracy of the C^3NAVPL position results, an epoch by epoch comparison was made against the FLYKIN™ fixed integer ambiguity reference trajectory. The resulting differences in latitude, longitude and height could then be easily established. For the Glenmore Reservoir data set, the positioning analysis was completed for only raw pseudoranges, and the analysis was conducted for three configurations (all with a 10° mask angle and no satellites rejected): a) no PL and no height constraint, b) one PL and no HC, and c) one PL and a HC.

Figure 5.19 illustrates the C^3NAVPL latitude, longitude and height errors for both the unaugmented and PL augmented GPS constellations. The unaugmented case, shown in gray, appears very much as expected, with good results for the longitude component as compared to the latitude, and the poorest performance in the vertical. The means for all three error components are generally near zero, indicating a non-systematic distribution for any error sources. The PL augmented case, shown in black, has a noticeable bias with the latitude and height errors. The latitude bias is approximately 0.60 m, and the height bias is approximately 1.6 m. Statistics for the two configurations are included in Table 5.2.

As described in Chapter 3, pseudolite signals are very susceptible to distortion caused by multipath [Ford, *et al*., 1996]. For this test, ideal conditions exist for multipath interference, especially between the PL and the reference station. Also, the pseudolite elevation was less than one degree, as observed by the reference station, and between three and 13 degrees as observed by the remote receiver. The signal to noise ratio of the received signal can have a dramatic effect on the accuracy of the GPS (or pseudolite) measurements. As shown previously in Figure 4.24, the pseudolite signal, as recorded at the reference station, showed some variation in received strength, suggesting that the actual transmitted power from the pseudolite was not entirely constant. The remote receiver recorded a much greater variation in the received pseudolite signal, due primarily to the movement of the canoe with respect to the pseudolite.

Table 5.2 Glenmore Reservoir. C^{3}NAVPL Raw Code Errors. Mask Angle 10°. Various Configurations. No Satellites Rejected.

PL Used	1 m^2 HC Used	Latitude		Longitude		Height	
		mean	95 %	mean	95 %	mean	95 %
No	No	-0.062	1.563	0.114	0.868	0.228	1.956
Yes	No	-0.640	2.066	0.039	1.045	1.597	3.786
Yes	Yes	-0.848	2.279	0.095	0.998	0.541	1.296

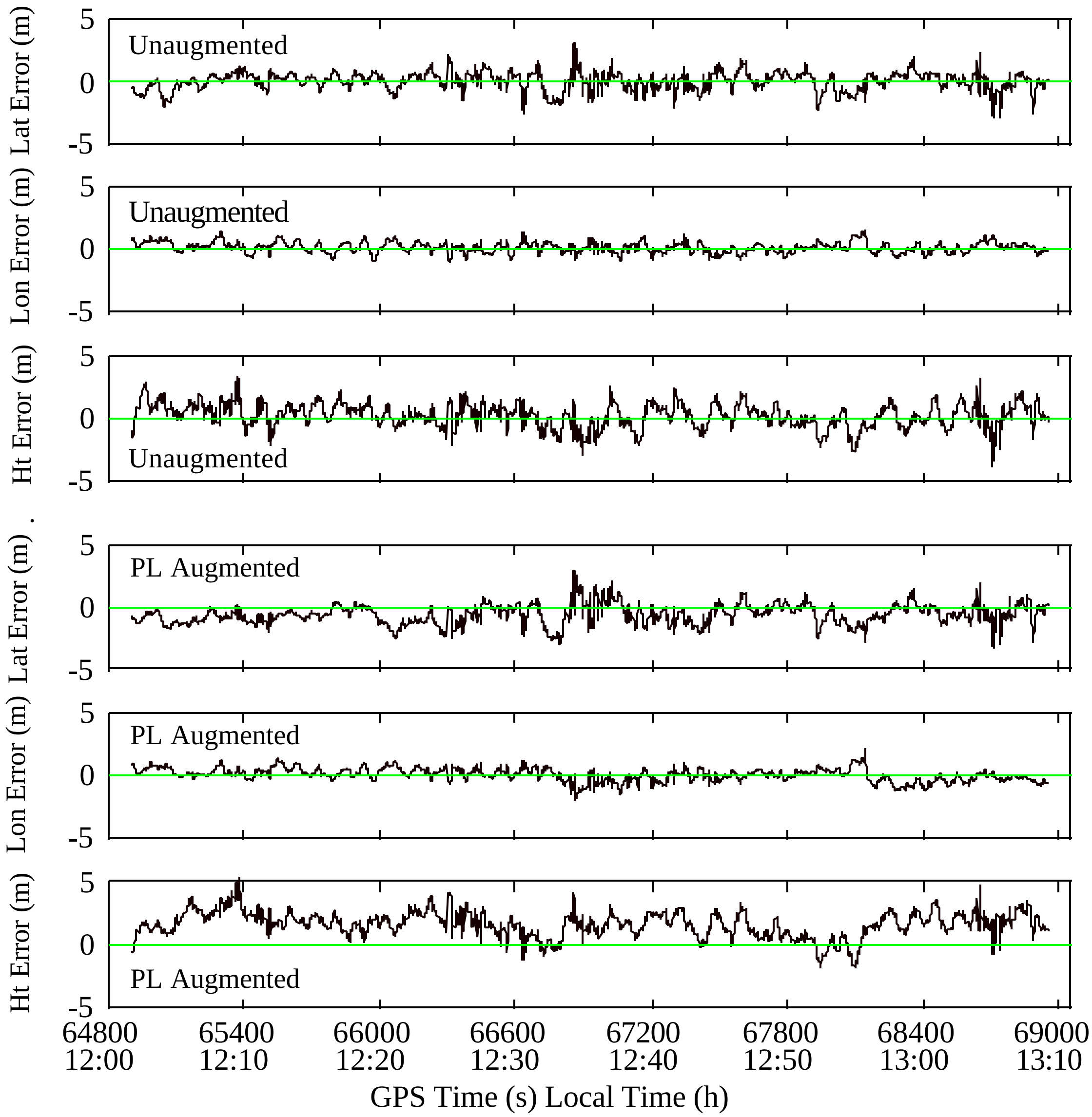

Figure 5.19 Glenmore Reservoir. C^{3}NAVPL Raw Code Error Comparison Between Unaugmented and PL Augmented GPS Constellations. Mask Angle 10°. Unconstrained Height. No Satellites Rejected.

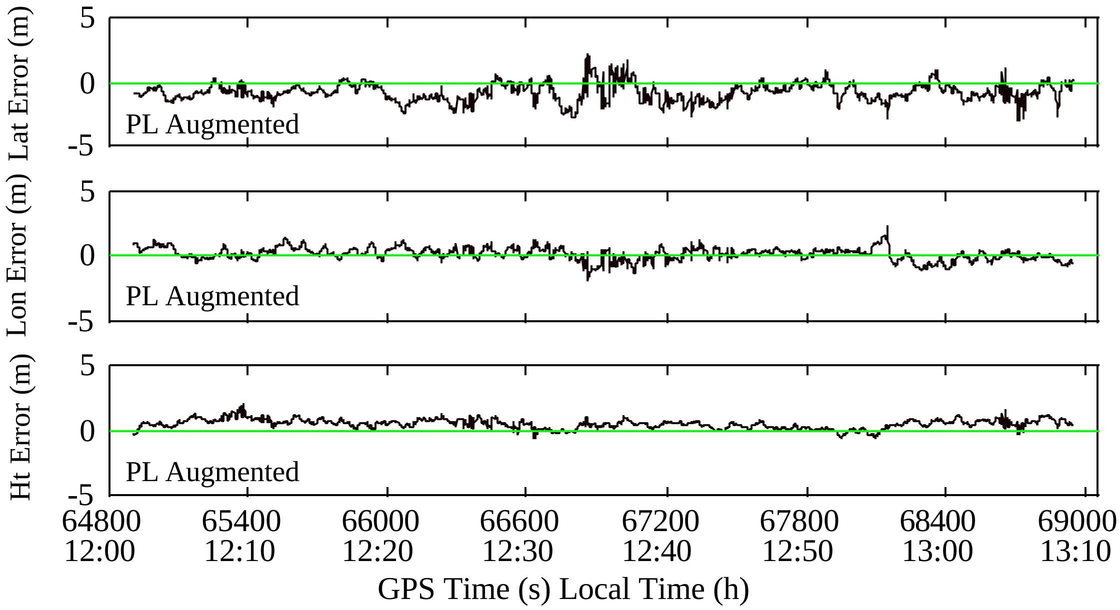

Figure 5.20 Glenmore Reservoir. C^3NAVPL Raw Code Error Comparison Between PL Augmented GPS Constellations. Mask Angle 10°. With HC.

It was anticipated that the use of a height constraint as a quasi-observation would improve the position solution in both the vertical and horizontal directions. Unfortunately (and somewhat counter-intuitively), for this test, the use of a height constraint worsened slightly the latitude error from 2.07 m to 2.28 m (2DRMS), as summarized in Table 5.2. By constraining a biased height, the 1.6 m non-systematic error component (from the PL to the reference receiver) is forced from the vertical to the horizontal direction. The height constraint has improved the vertical positioning, but at the expense of the horizontal.

The cumulative frequency distribution for the three cases is shown in Figure 5.21 and Table 5.3. PL augmentation did not improve the horizontal positioning performance when compared to the unaugmented case. The horizontal position error for the PL augmented case is worse than for the unaugmented case, and the PL augmented case with a height constraint is worse than the PL augmented case with no height constraint. By estimating the systematic multipath error induced in the differential corrections, it may be possible to reduce or eliminate the biases in the latitude, longitude and height errors, and improve the horizontal positioning capability. This concept is demonstrated on the Lake Okanagan field test data set, presented in section 5.2.3.

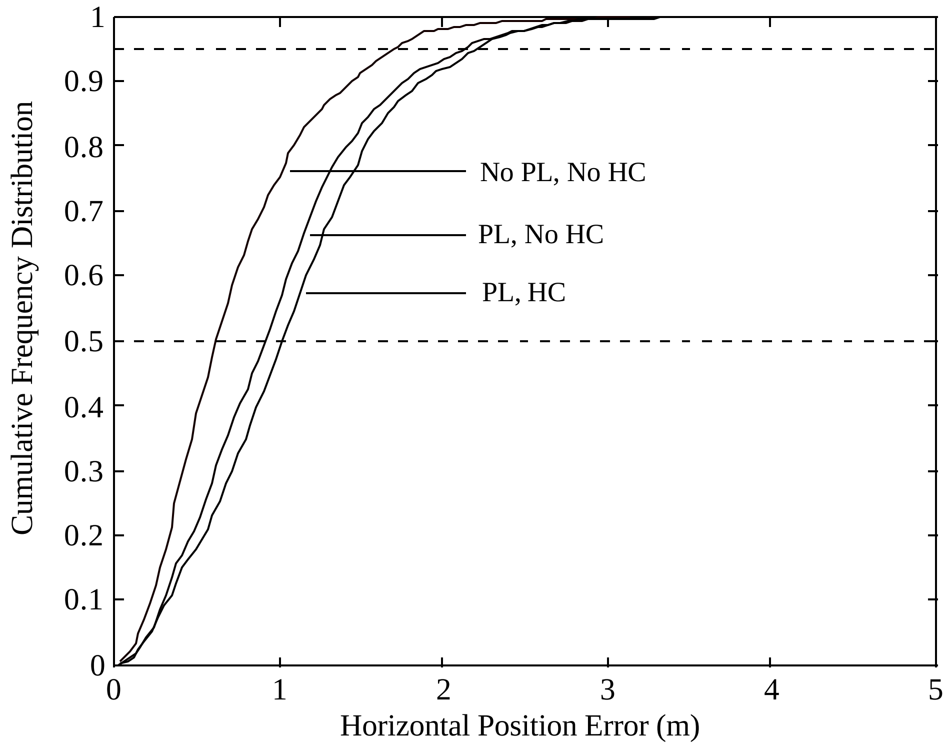

Figure 5.21 Glenmore Reservoir. C^{3}NAVPL Raw Code Cumulative Frequency Distribution of Horizontal Position Error. Unaugmented and PL Augmented GPS Constellations. Mask Angle 10°.

Table 5.3 Glenmore Reservoir. C^{3}NAVPL 50th and 95th Percentile Horizontal Position Error and 2DRMS Horizontal Accuracy. Mask Angle 10°. No Satellites Rejected.

Configuration	50th percentile	95th percentile	2DRMS (m)
No PL, No HC	0.624	1.700	1.770
PL, No HC	0.919	2.124	1.928
PL and 1 m^2 HC	1.022	2.204	1.810

As observed in the previous three figures, the PL range data has introduced errors into the least squares adjustment which manifest themselves primarily in the vertical direction. An analysis of the C^{3}NAVPL raw code single difference residuals indicates that for satellite PRNs 01 and 09, the residuals for the unaugmented constellation are essentially unbiased. For the PL augmented case, the residuals are now not only biased (by -40 cm and 64 cm, respectively), but their standard deviations have increased (by 9 cm and 14 cm, respectively). This is a strong indicator of both multipath on the PL signal (resulting in the observed bias) and noisier PL measurements (resulting in the increase in standard deviation). The residuals for the PL show a mean of -89 cm and a standard deviation of 53 cm. The residuals are shown in Figure 5.22, and summarized in Table 5.4.

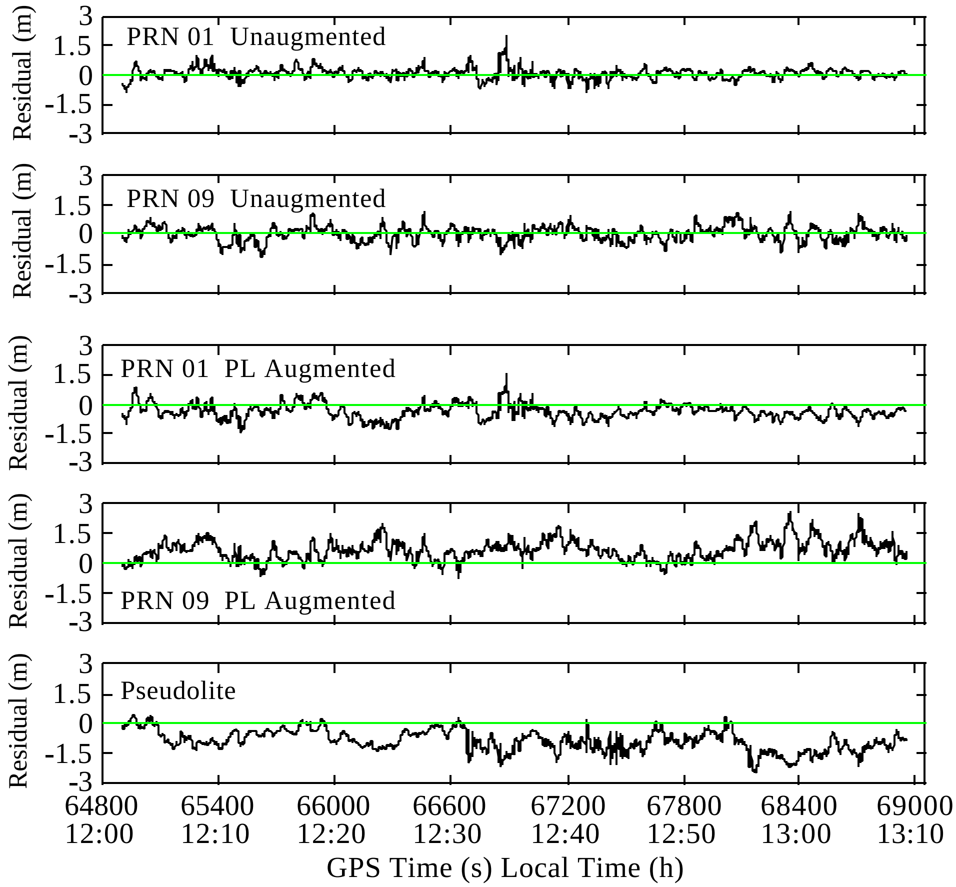

Figure 5.22 Glenmore Reservoir. C^{3}NAVPL Raw Code Residuals for Unaugmented and PL Augmented GPS Constellations. Mask Angle 10°. No HC.

Table 5.4 Glenmore Reservoir. C^{3}NAVPL Raw Code Residual Statistics.

PRN (elev)	Unaugmented		PL Augmented	
	Mean (m)	RMS (m)	Mean (m)	RMS (m)
01 (24° - 78°)	0.052	0.289	-0.402	0.551
09 (18° - 29° - 23°)	-0.016	0.374	0.637	0.815
PL	N/A	N/A	-0.892	1.037

5.2 Lake Okanagan Field Test - Overview

The second and final field test was conducted on November 7, 1996 at Lake Okanagan, British Columbia. Two NovAtel OEM-2 (RT20) L1 GPS receivers were used at both the reference and remote stations. Each receiver used a 501 L1 antenna with chokering. The reference station was located on a rocky bluff, approximately 80 m above the surface of the lake. The coordinates of the reference station were determined with C^{3}NAV™ using precise orbit and clock information. The expected absolute accuracy of the reference coordinates are 1 m (horizontal) and 2 m (vertical) [Henriksen, *et al*., 1996].

The remote station was located on a large boat. The L1 antenna and chokering were attached to a range pole which was securely fastened to the upper deck railing. The antenna was located approximately 1.8 m above the upper deck, and 4.5 m above the surface of the lake. The PL was located at the top of Knox Mountain, approximately 260 m above the lake, and 180 m above the reference station. The PL antenna was securely fastened to an aluminum mounting bracket which was, in turn, attached to a tripod. The mounting bracket was adjusted so as to tilt the PL antenna approximately 25° towards the reference station. The PL antenna was centered over a hydrographic survey marker. Photographs of the boat and the PL location are shown in Figures 5.23 and 5.24. The coordinates of the hydrographic survey marker with respect to the reference coordinates were determined using SEMIKIN™. The slant range between the PL and the reference locations was found to be 670 m, and the PL elevation as observed by the reference was 15.7°.

Figure 5.23 Lake Okanagan. Photograph of Remote Platform.

Two data sets were collected on November 7, 1996. During the morning session, two hours and twenty minutes of continuous PL data were recorded. In the afternoon session approximately one hour of non-continuous PL data were recorded. During this session, the boat was intentionally driven away (or toward) the PL until the signal was lost (or regained) to assess the PL tracking and reacquisition performance. Only the data set from the morning session will be used in this chapter, as it is representative of both data sets.

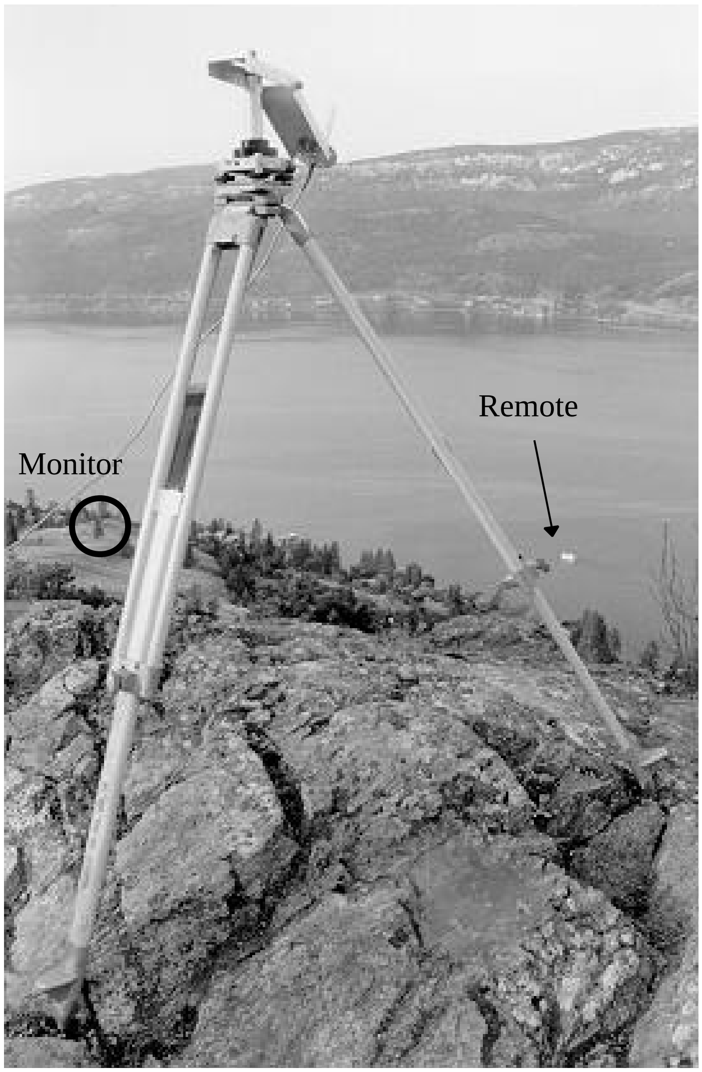

Figure 5.24 Lake Okanagan. Photograph at PL Location.

The locations of the PL, the reference station, the approximate shoreline, and the reference trajectory of the remote antenna on the boat are shown in Figures 5.25 to 5.29. As before, the reference trajectory for the remote station was determined using FLYKIN™ fixed integer on-the-fly solution, with an expected 3D accuracy of better than 10 cm [Lachapelle, 1995]. The GPS times are indicated every 180 seconds, from the beginning of the data set (408400 seconds) to the end of the data set (416700 seconds).

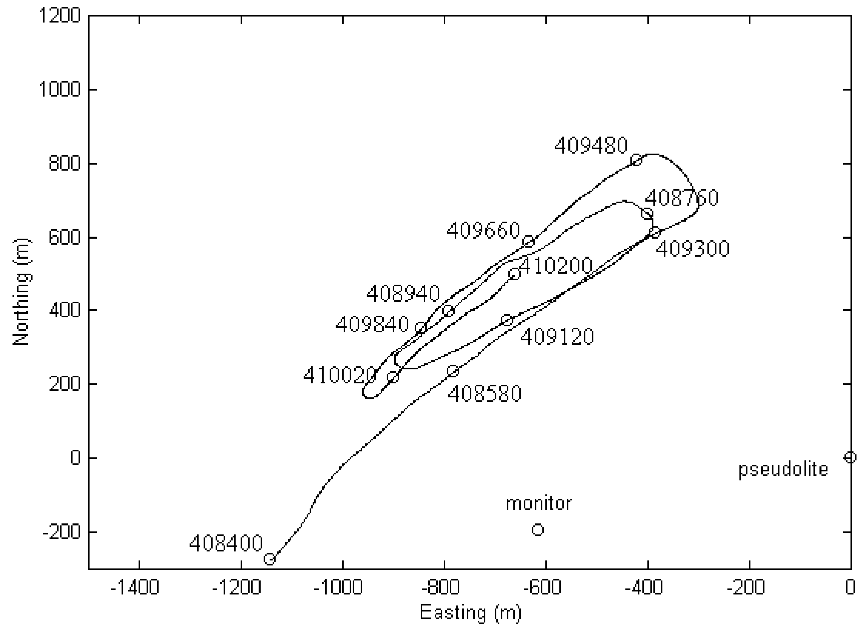

Figure 5.25 Lake Okanagan. Reference Trajectory. (GPS Time 408400 to 410200)

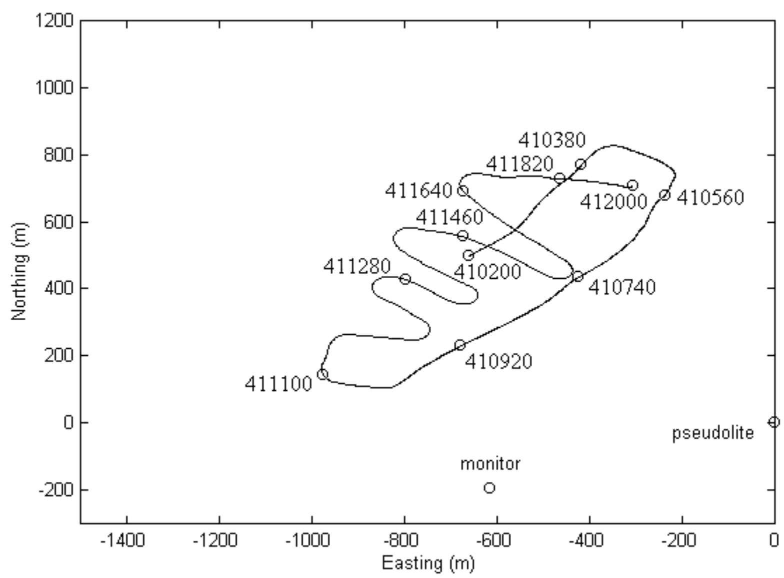

Figure 5.26 Lake Okanagan. Reference Trajectory. (GPS Time 410200 to 412000)

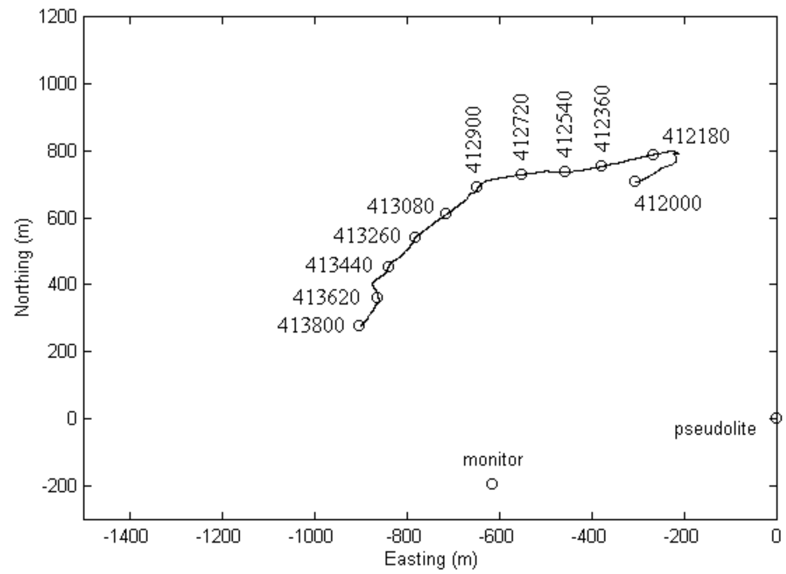

Figure 5.27 Lake Okanagan. Reference Trajectory. (GPS Time 412000 to 413800)

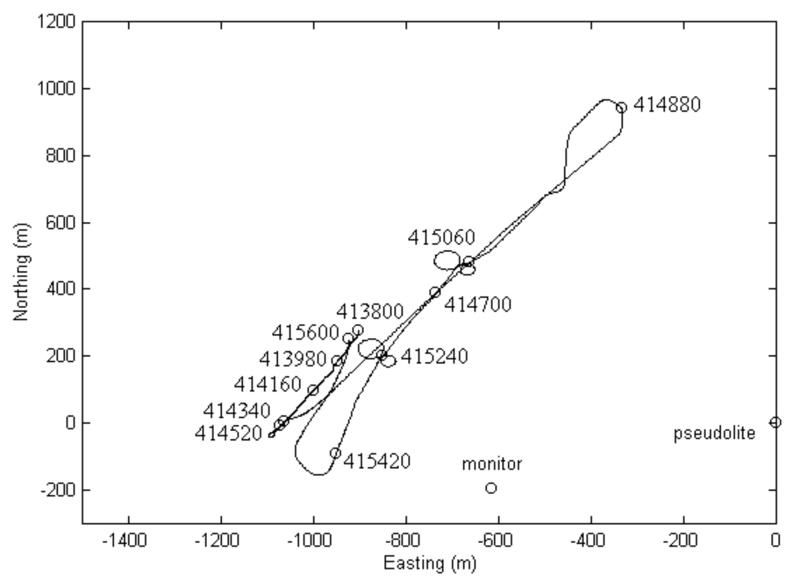

Figure 5.28 Lake Okanagan. Reference Trajectory. (GPS Time 413800 to 415600)

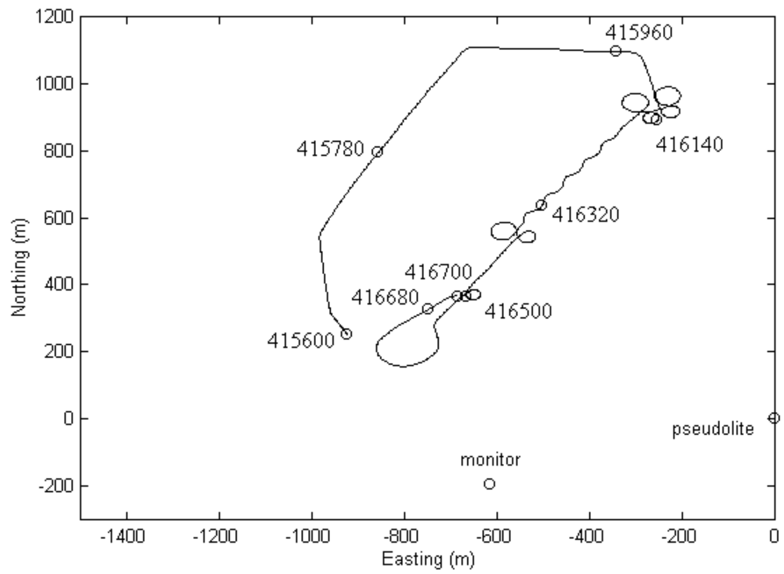

Figure 5.29 Lake Okanagan. Reference Trajectory. (GPS Time 415600 to 416700)

The fixed ambiguity height solution is included in Figure 5.30. The mean height during the morning session was found to be 332.03 m, with a standard deviation of 2 cm. The horizontal velocity of the reference station is presented in Figure 5.31. The speed of the boat during this test ranged from 0.3 to 3.9 m/s.

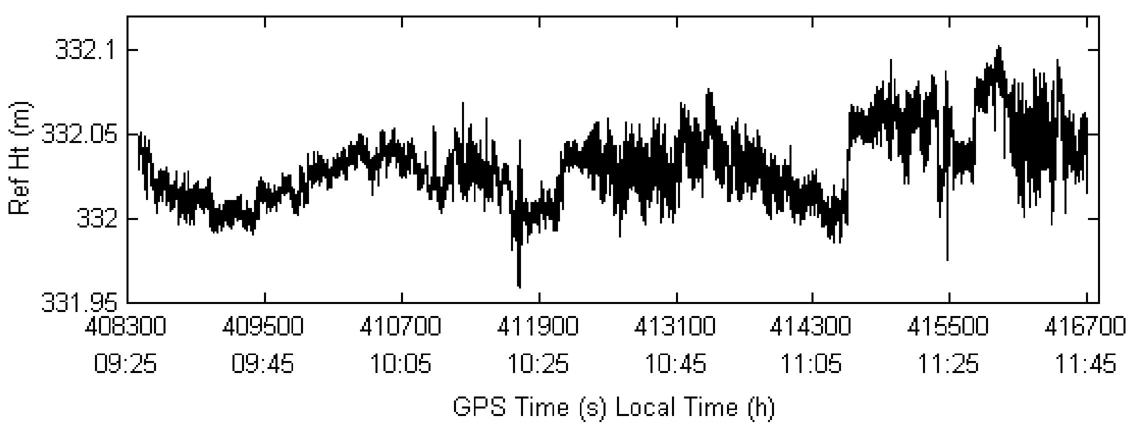

Figure 5.30 Lake Okanagan. Fixed Ambiguity Height Solution.

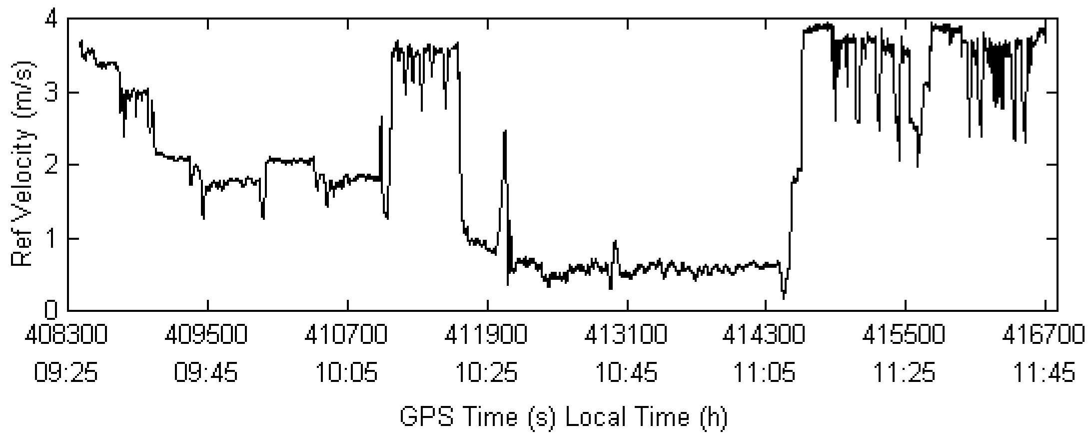

Figure 5.31 Lake Okanagan. Fixed Ambiguity Horizontal Velocity.

The calculated slant ranges from the remote platform to both the reference station and the PL location are shown in Figures 5.32 and 5.33. The separation between the remote and the reference varied between approximately 400 m and 1350 m, while the distance between the remote and the PL varied between approximately 700 m and 1350 m.

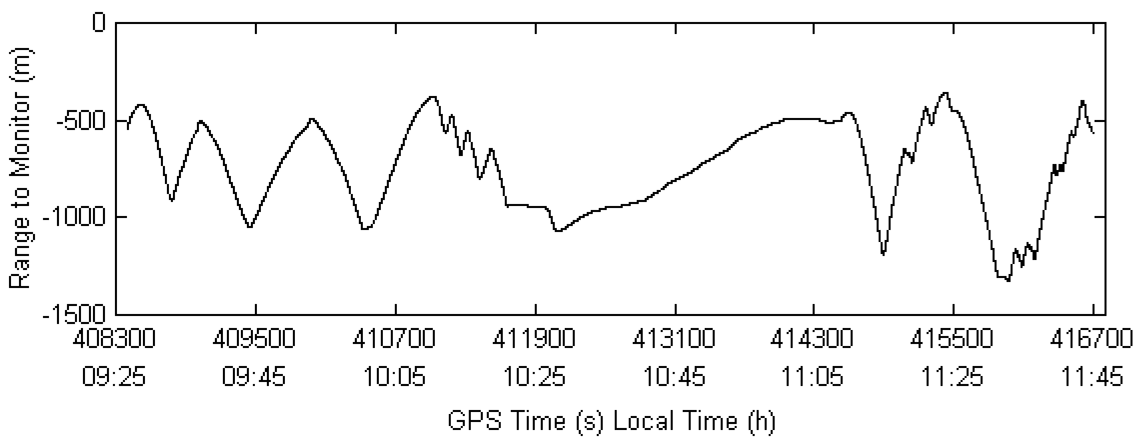

Figure 5.32 Lake Okanagan. Slant Range Between Reference and Remote.

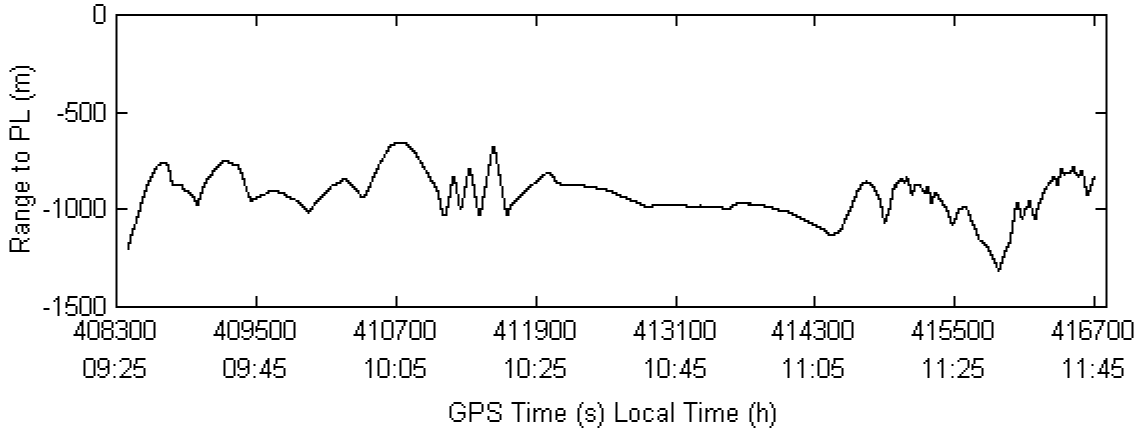

Figure 5.33 Lake Okanagan. Slant Range Between PL and Remote.

A plot of the PL elevation, as observed by the remote receiver, is given in Figure 5.34. The average PL elevation for the morning session was 16.4°, with a maximum elevation of just over 23°. A plot of the PL signal to noise ratio (C/N_o), as measured by the remote receiver, is shown in Figure 5.35. The C/N_o of the PL, as measured by the reference station, is also shown in this figure for reference. The average PL C/N_o for the remote receiver was 42.4 dB-Hz, and for the reference receiver was 46.3 dB-Hz.

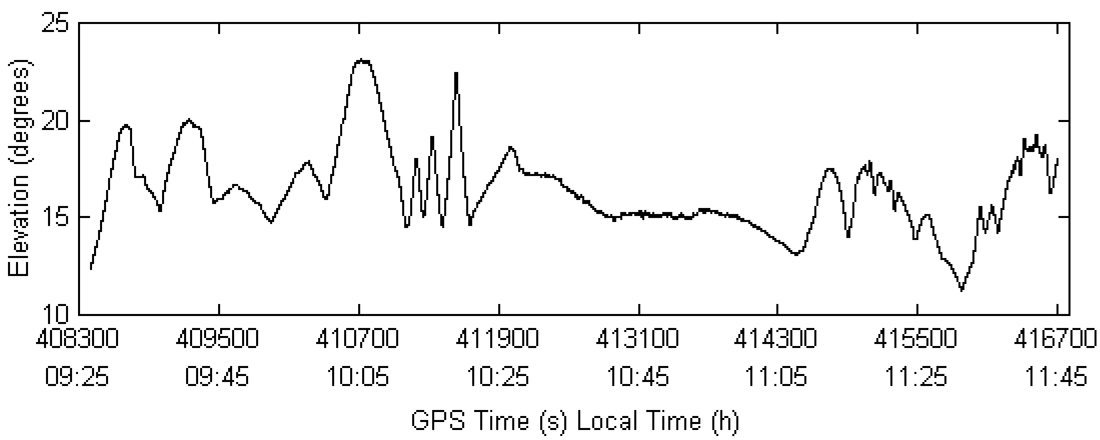

Figure 5.34 Lake Okanagan. Elevation of PL as Observed by Remote.

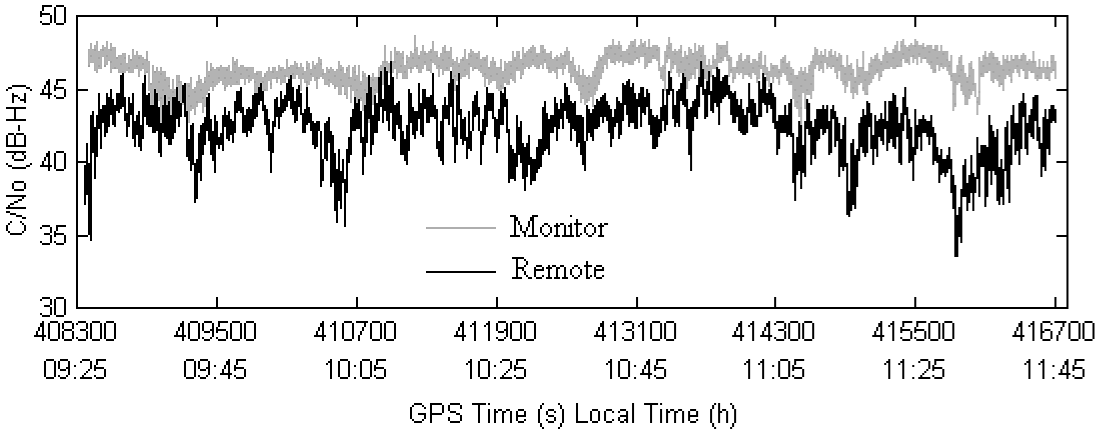

Figure 5.35 Lake Okanagan. PL C/N_0 as Measured by Reference and Remote.

A representative Lake Okanagan horizon, as measured by an observer on the boat, is shown at Figure 5.36. The longitudinal axis of the lake is oriented roughly North/South, and this horizon was measured at a location corresponding to the middle of the reference trajectory. The approximate locations of the reference station and PL are indicated.

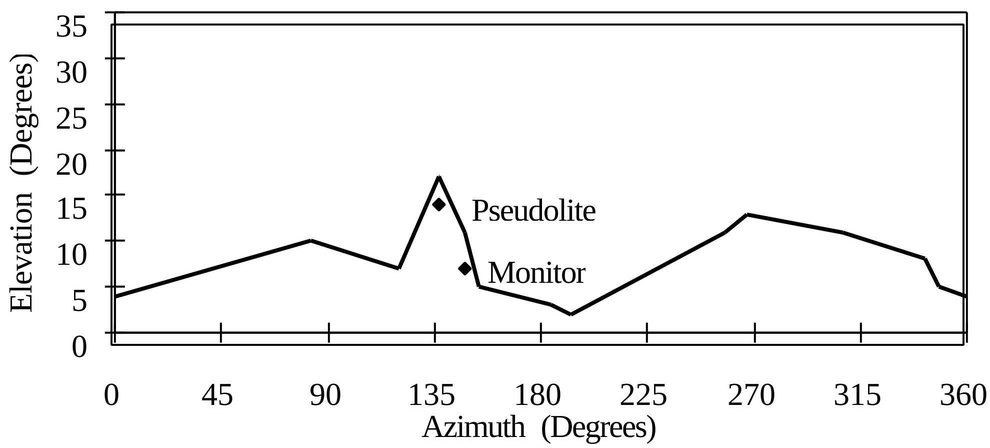

Figure 5.36 Lake Okanagan. Horizon as Measured From the Remote.

5.2.1 Changes to DGPS Availability, Accuracy and Reliability Measures

The number of satellites observed during the morning session at Lake Okanagan is shown in Figure 5.37. A mask angle of 10° was used. The unaugmented constellation was reasonably stable throughout the data collection period, and the average number of satellites tracked was 6.31. The PL was tracked by both the reference and remote receivers for the entire two hour and twenty minute data set.

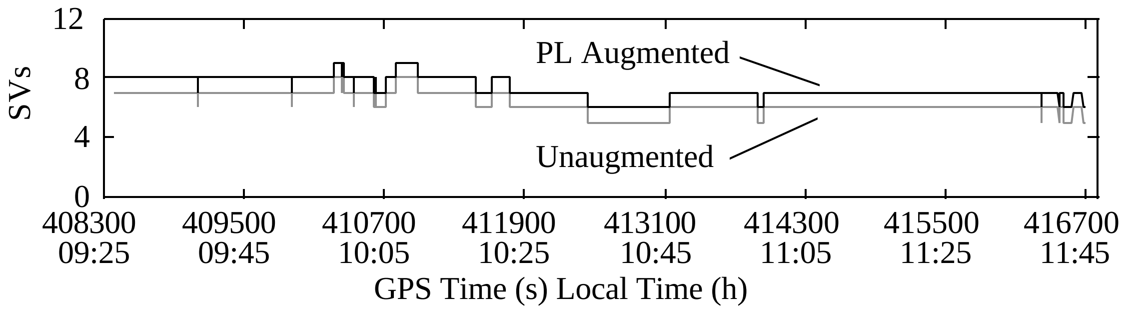

Figure 5.37 Lake Okanagan. Number of Satellites Tracked. Unaugmented and PL Augmented GPS Constellations. Mask Angle 10°. No Satellites Rejected.

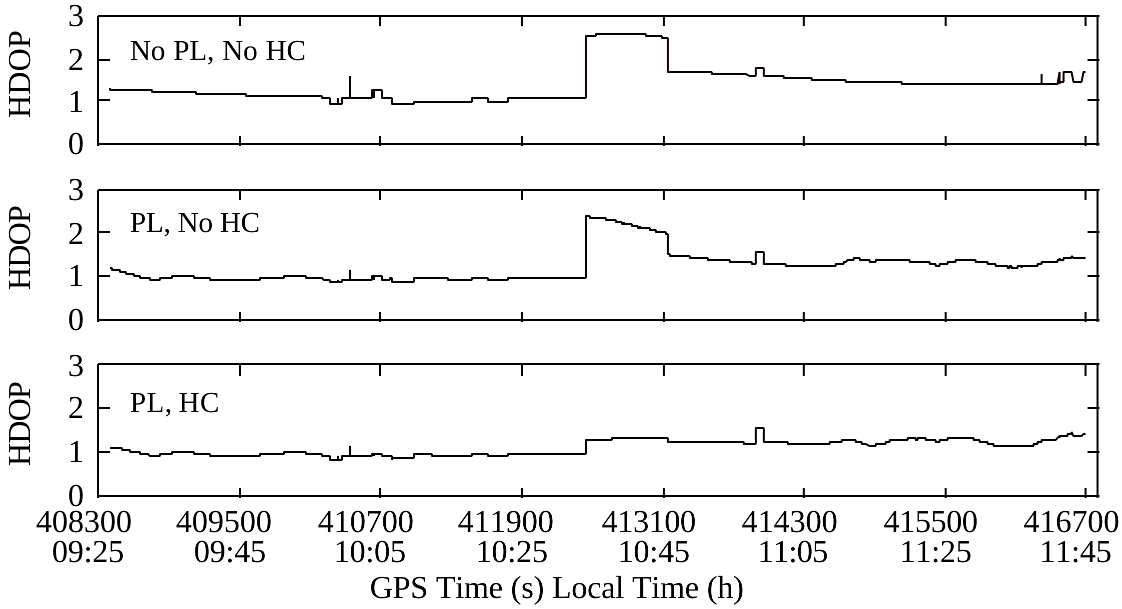

Figure 5.38 Lake Okanagan. HDOP. Unaugmented and PL Augmented GPS Constellations. Mask Angle 10°. No Satellites Rejected.

The HDOP plot for the three configurations is presented in Figure 5.38. For the unaugmented case, the HDOP was quite good, even when the number of satellites dropped to only five for approximately ten minutes in the middle of the data set. The PL augmented configuration shows a slight improvement in HDOP throughout the plot. The height constraint has little additional effect on the HDOP for most of the data set, except for the period where the number of satellites drops to five. During this critical window the height constraint limits the HDOP to less than 1.5.

The MHE plot, given in Figure 5.39, shows a much greater variation between the three configurations. For the unaugmented configuration, the MHE varies between approximately 5 and 10 metres for most of the data set. Two obvious exceptions occur when the number of satellites tracked drops to five. For the first excursion (GPS Time 412438 to 413142), the MHE for the unaugmented configuration jumps from 10.5 m to 31.9 m. Not until over 700 seconds later does the MHE drop from 112.1 m to 8.9 m. The PL augmented configuration shows a small jump in the MHE from 9.8 m to 12.0 m. At time 413142 the MHE drops from 17.5 m to 6.0 m. During this period, the value of the HDOP for both configurations is between 2.2 and 2.6. The height constraint reduces the magnitude of the MHE envelope further still. In fact, the MHE does not exceed 5 m for the entire 700 second period where the number of satellites in view drops to five.

The second excursion occurs from 413893 to 413947 where, again, the number of satellites drops to five. This time, the additional information provided by the PL does not result in the same dramatic improvement in reliability as during the first excursion. The MHE for the unaugmented constellation jumps from 7.9 m to 33.8 m (at time 413893), then drops from 31.5 m to 7.7 m (at time 413947). The MHE for the pseudolite augmented constellation jumps from 6.3 m to 33.6 m, then drops from 30.8 m to 6.7 m. Finally, the MHE for the PL augmented and height constrained constellation jumps from 4.5 m to 21.6 m, and drops from 21.8 m to 4.9 m. The sensitivity of the MHE measure to geometry is illustrated by the following observation. During this excursion, the remote platform was located to the west of the pseudolite. Had the remote platform been directly north of the pseudolite, the MHE for the PL augmented configuration would have jumped to only 16.1 m (determined by simulation). The use of a height constraint would have decreased this value further to only 10.3 m.

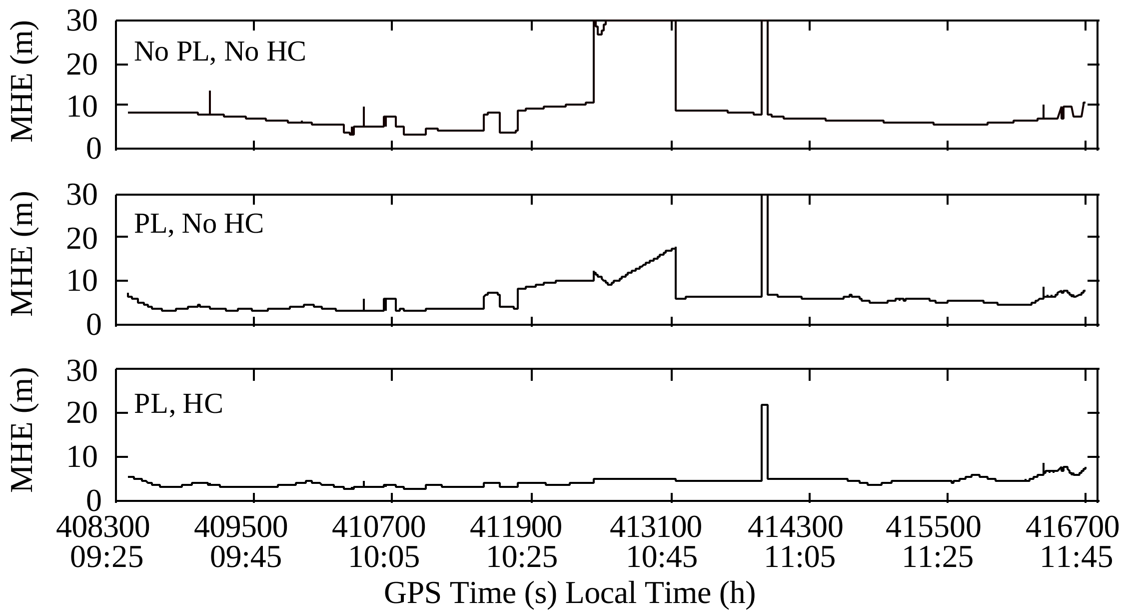

Figure 5.39 Lake Okanagan. MHE. Unaugmented and PL Augmented GPS Constellations. Mask Angle 10°. No Satellites Rejected.

Table 5.5 Lake Okanagan. Summary of Number of Satellites Tracked, Average HDOP and Average MHE. Mask Angle 10°. Various Configurations.

Mask Angle	PL Used	1 m^2 HC Used	Rejected SV	Mean SVs	Mean HDOP	Mean MHE
10°	No	No	None	6.31	1.38	12.03*
	Yes	No		7.31	1.21	6.11
	Yes	Yes		7.31	1.10	4.37

* Includes 3.2% of epochs with an MHE greater than 100 m.

5.2.2 Changes to DGPS Positioning - Full Constellation

The analysis for the Lake Okanagan field tests is conducted in the same manner as the Glenmore Reservoir field test. The C^3NAVPL results are compared to the FLYKIN™ fixed integer reference trajectory to produce errors in latitude, longitude and height for each epoch. Figure 5.40 shows the C^3NAVPL results for the unaugmented and PL augmented GPS constellations. The results for this test are very similar to the Glenmore field test, with the unaugmented constellation showing essentially unbiased latitude, longitude and height errors. Again, the PL augmented configuration shows a marked bias in the height component, and lesser biases in both the latitude and longitude errors. The magnitude of the height bias is half of what was observed at the Glenmore field test. This is a strong indicator that the non-systematic constant multipath distortion of the pseudorange signal from the PL to the reference station was considerably less during the Okanagan data collection. Having the PL at an elevation of 15.7° with respect to the reference station (versus only 0.95° for the Glenmore Reservoir test) has probably reduced the PL multipath considerably.

Again, a height constraint was applied to the PL augmented results, and again, a significant improvement in the vertical position solution was observed, as shown in Figure 5.41. For this data set, however, the latitude and longitude 2DRMS values both showed an improvement over the unconstrained configuration. Because the height bias (-0.79 m) was smaller than the height constraint (1.0 m^2), the constraint tended to improve the solution, instead of forcing the height bias from the vertical to the horizontal. Summary statistics for the three configurations are included in Table 5.6.

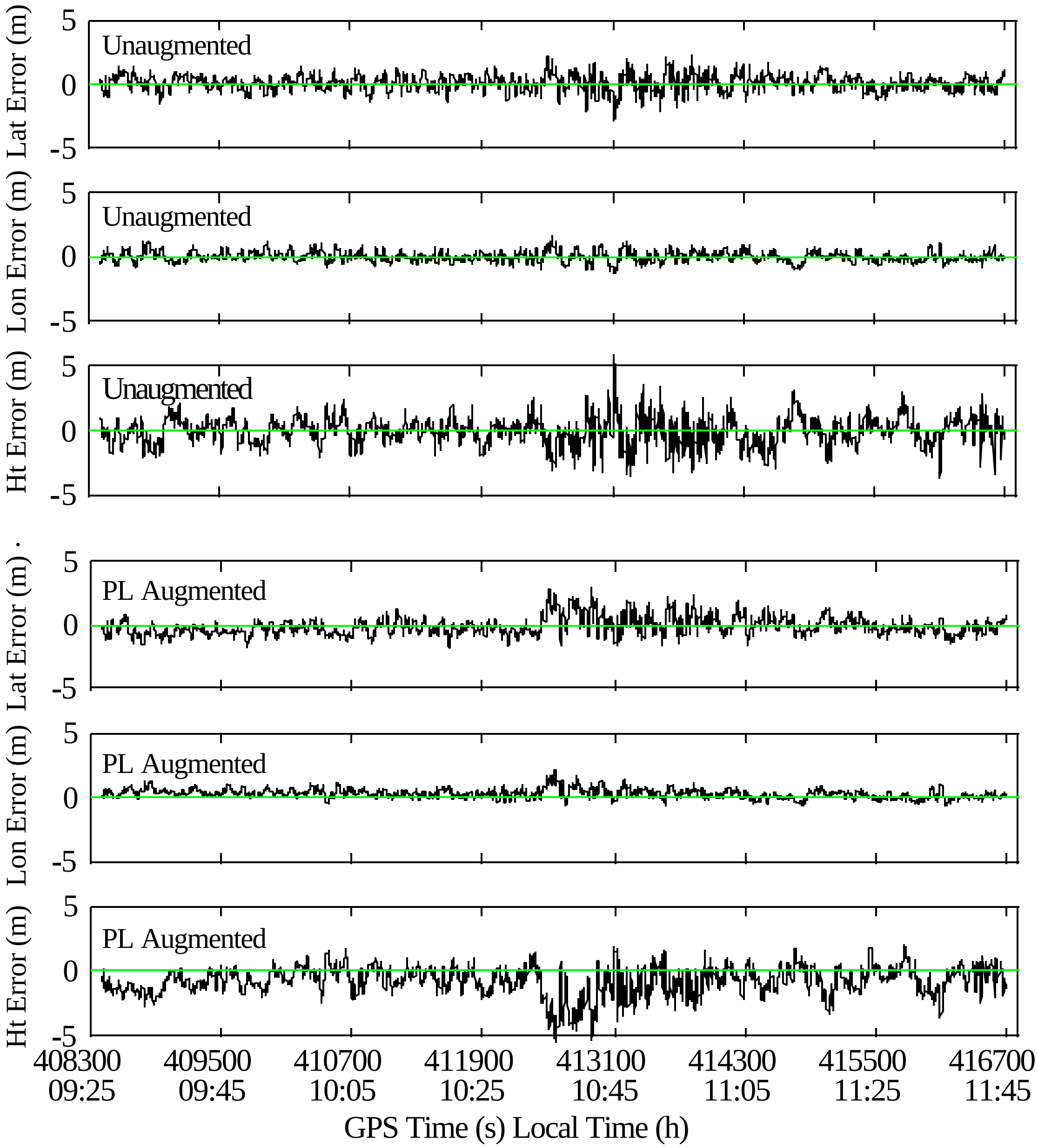

Figure 5.40 Lake Okanagan. C^{3}NAVPL Raw Code Error Comparison Between Unaugmented and PL Augmented GPS Constellations. Mask Angle 10°. Unconstrained Height. No Satellites Rejected.

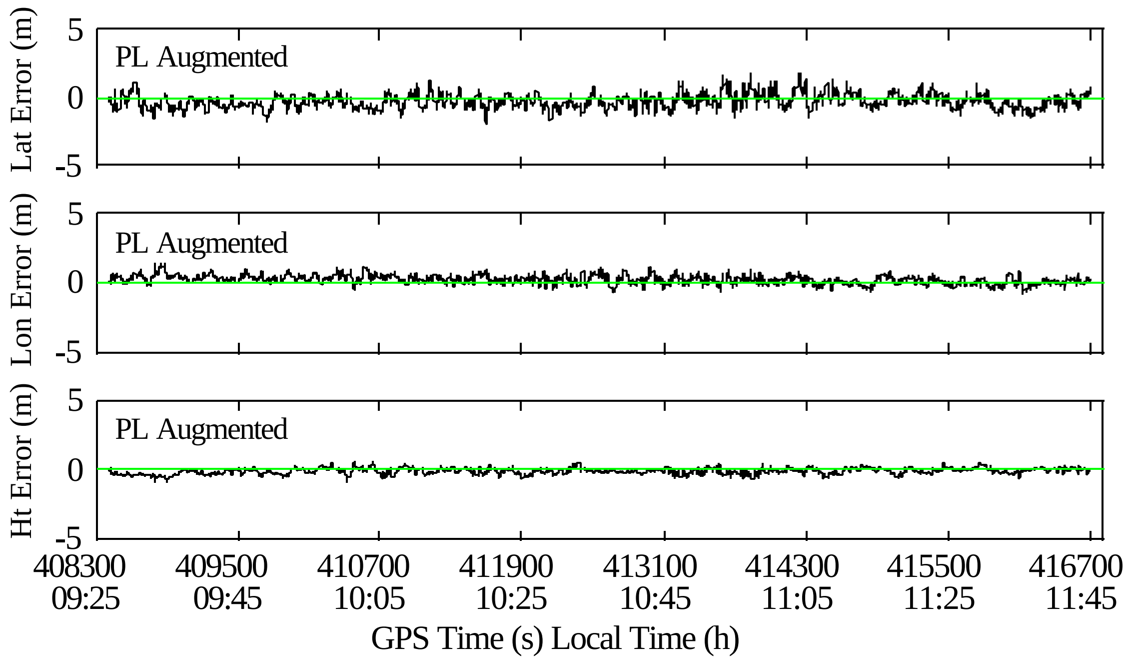

Figure 5.41 Lake Okanagan. C^{3}NAVPL Raw Code Errors for PL Augmented GPS Constellation Using a HC. Mask Angle 10°.

Table 5.6 Lake Okanagan. C^{3}NAVPL Raw Code Errors. Mask Angle 10°. Various Configurations. No Satellites Rejected.

PL	1 m^2 HC	Latitude		Longitude		Height	
Used	**Used**	**mean**	**95 %**	**mean**	**95 %**	**mean**	**95 %**
No	No	0.056	1.253	0.018	0.763	-0.062	2.130
Yes	No	-0.148	1.456	0.287	0.944	-0.792	2.638
Yes	Yes	-0.301	1.263	0.231	0.812	-0.177	0.582

A plot of the horizontal position error frequency distribution for the three configurations is shown below, in Figure 5.42. Note that the performance of the PL augmented (unconstrained height) configuration is inferior to the performance of the unaugmented GPS constellation, as was observed at the Glenmore Reservoir field test. The addition of a 1 m^2 height constraint, however, improves the horizontal positioning performance of the PL augmented configuration, when compared to the PL augmented configuration with no height constraint. The height constrained and PL augmented configuration also shows some improvement over the unaugmented configuration for the larger magnitude (i.e. greater than approximately 1.2 m) horizontal errors. This occurs because the larger magnitude latitude and longitude errors correlate to the period when the height solution is relatively poor, from approximately 10:35 to 11:05 (local time). Summary statistics for Figure 5.42 are given in Table 5.7

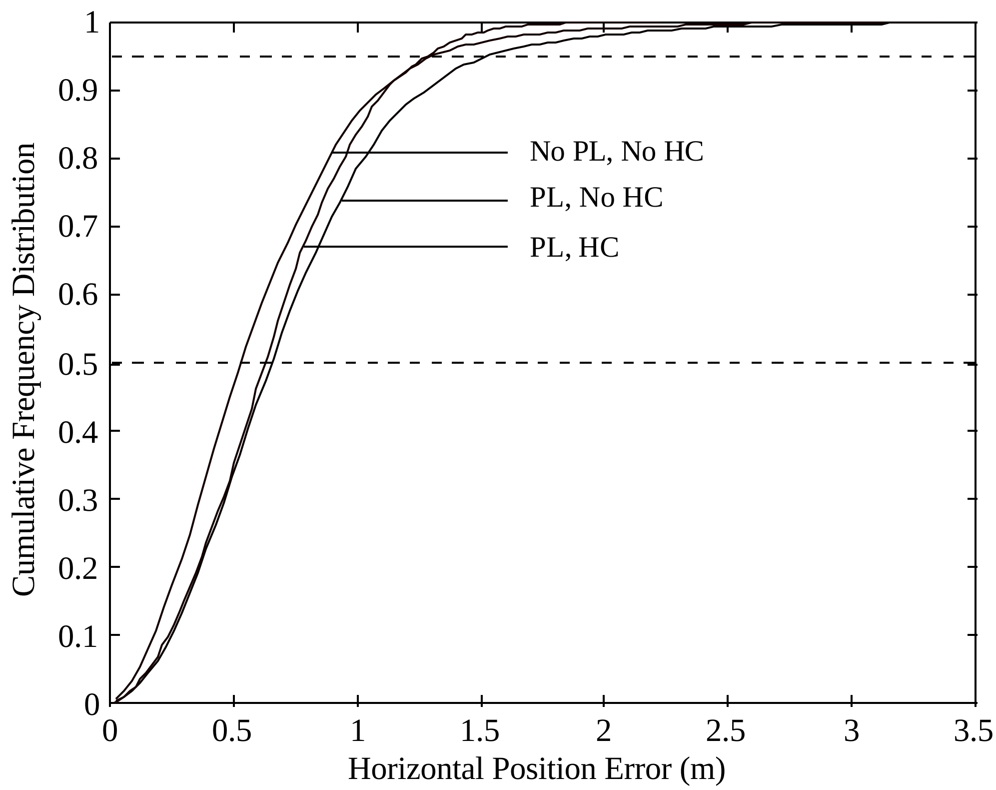

Figure 5.42 Lake Okanagan. C^3NAVPL Raw Code Cumulative Frequency Distribution of Horizontal Position Error. Unaugmented and PL Augmented GPS Constellations. Mask Angle 10°.

Table 5.7 C^3NAVPL 50th and 95th Percentile Horizontal Position Error and 2DRMS Horizontal Accuracy. Mask Angle 10°. No Satellites Rejected.

Configuration	50th percentile	95th percentile	2DRMS (m)
No PL, No HC	0.530	1.296	1.468
PL, No HC	0.653	1.521	1.736
PL and 1 m^2 HC	0.627	1.279	1.502

An analysis of the Lake Okanagan C^3NAVPL single-difference residuals for the raw code show similar trends to those experienced at the Glenmore Reservoir. Again, the residuals for the unaugmented configuration are essentially unbiased, and again, the inclusion of the PL data has introduced a bias and noise into the least squares adjustment, as shown in Figure 5.43. Summary statistics for the raw code residuals are given in Table 5.8.

Table 5.8 Lake Okanagan. C^3NAVPL Raw Code Residual Statistics.

	Unaugmented		PL Augmented	
PRN (elev)	Mean (m)	RMS (m)	Mean (m)	RMS (m)
01 (71° - 43°)	-0.014	0.246	0.025	0.277
15 (16° - 58°)	-0.002	0.280	0.199	0.379
PL	N/A	N/A	0.559	0.730

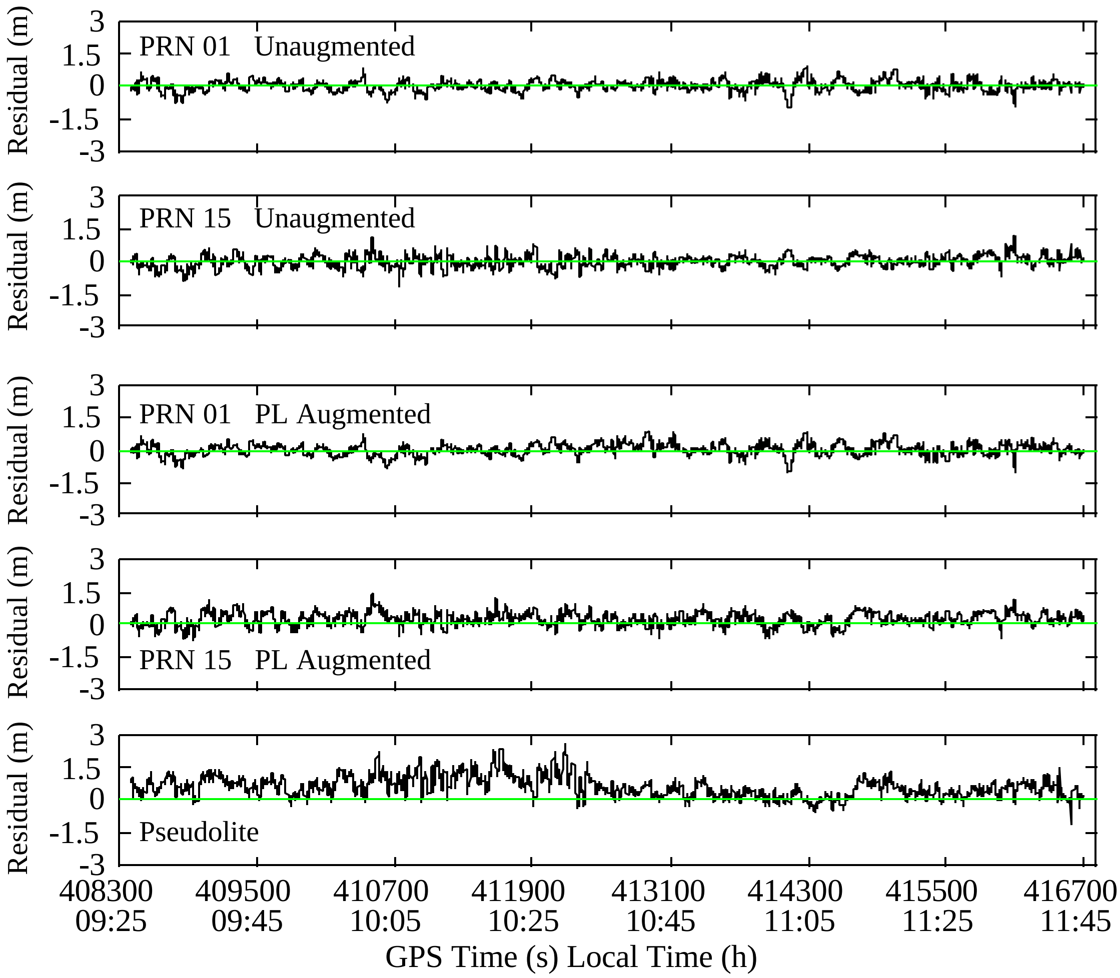

Figure 5.43 Lake Okanagan. C^3NAVPL Raw Code Residuals for Unaugmented and PL Augmented GPS Constellations. Mask Angle 10°. Unconstrained Height.

5.2.3 Pseudolite Multipath Estimation at the Reference Station

There can exist many transmission paths from the PL to the reference receiver, in addition to the direct path signal. As described in section 2.2.3, multipath can cause correlation errors on the pseudorandom noise code and distortion of the carrier phase. As the multipath signals always have a longer transmission path when compared to the direct line-of-sight signal, they will delay the pseudorandom noise code auto-correlation peak in time. This shift results in an error for the pseudorange measurement. The magnitude of this error is a function of many variables, including surrounding environment, user equipment and GPS receiver processing techniques.

For the Glenmore and Okanagan field tests, both the PL and the reference receiver were static. As the relative geometry between the two locations is unchanging, the multipath environment will also be essentially unchanging, resulting in a constant multipath error from epoch to epoch. As observed at each field test, the inclusion of PL code data has a generally deleterious effect on the positioning performance. If PL to reference multipath is the root cause of this degradation, and if this multipath component is reasonably constant, it should be possible to "correct" the differential corrections for the PL pseudorange measurements.

To determine the constant multipath component, the Okanagan data set was processed several times with different PL correction terms, ranging from 0 to 2 metres. A running total was kept of the sum of squares (SoS) for the residuals and for the horizontal error components for the entire data set. Figure 5.44 shows the two resulting curves. Note that all data points for the residual and horizontal error curves have been normalized by dividing by the respective value of the 0 metre correction data point. Both curves indicate a minimum when the PL correction term is 1.25 m. The use of this correction term should improve the PL augmented results, assuming that the observed biases are caused primarily by non-systematic multipath from the PL to the reference station.

The approximate geometry between the pseudolite and the reference station at Lake Okanagan is shown in Figure 5.45. Knowing that the separation between the two antennas is 670 m, it is possible to estimate the approximate offset of a reflecting surface to yield a signal path which is 1.25 m longer than the line-of-sight path. For this test, the offset was found to be slightly greater than 20 m, which is quite achievable, considering the local geometry and terrain as shown in the photograph at Figure 5.24. In reality, there will be many reflecting surfaces, each of which will contribute to the overall multipath effect, but this example is sufficient to illustrate the feasibility of the 1.25 m multipath component for this test configuration.

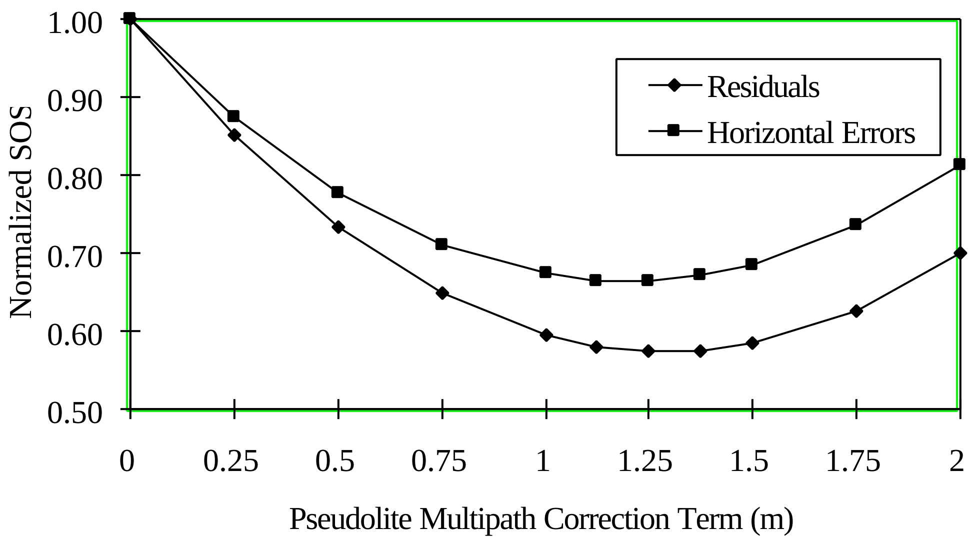

Figure 5.44 Lake Okanagan. Normalized Sum of Squares for C^{3}NAVPL Raw Code Residuals and Horizontal Error Components for Various PL Multipath Correction Terms.

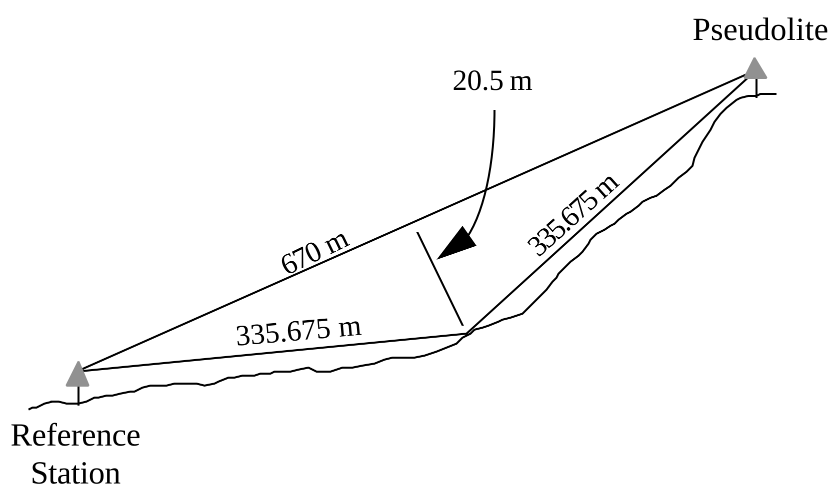

Figure 5.45 Lake Okanagan. Possible Multipath Geometry Between PL and Reference Station.

A plot of the latitude, longitude and height errors for the PL augmented (no correction) and PL augmented (with 1.25 m multipath correction) constellations is included in Figure 5.46. Note that the estimation of the non-systematic multipath error has reduced significantly the latitude, longitude and height biases, and improved the performance of the PL augmented GPS constellation. Statistics for Figure 5.46 are given in Table 5.9.

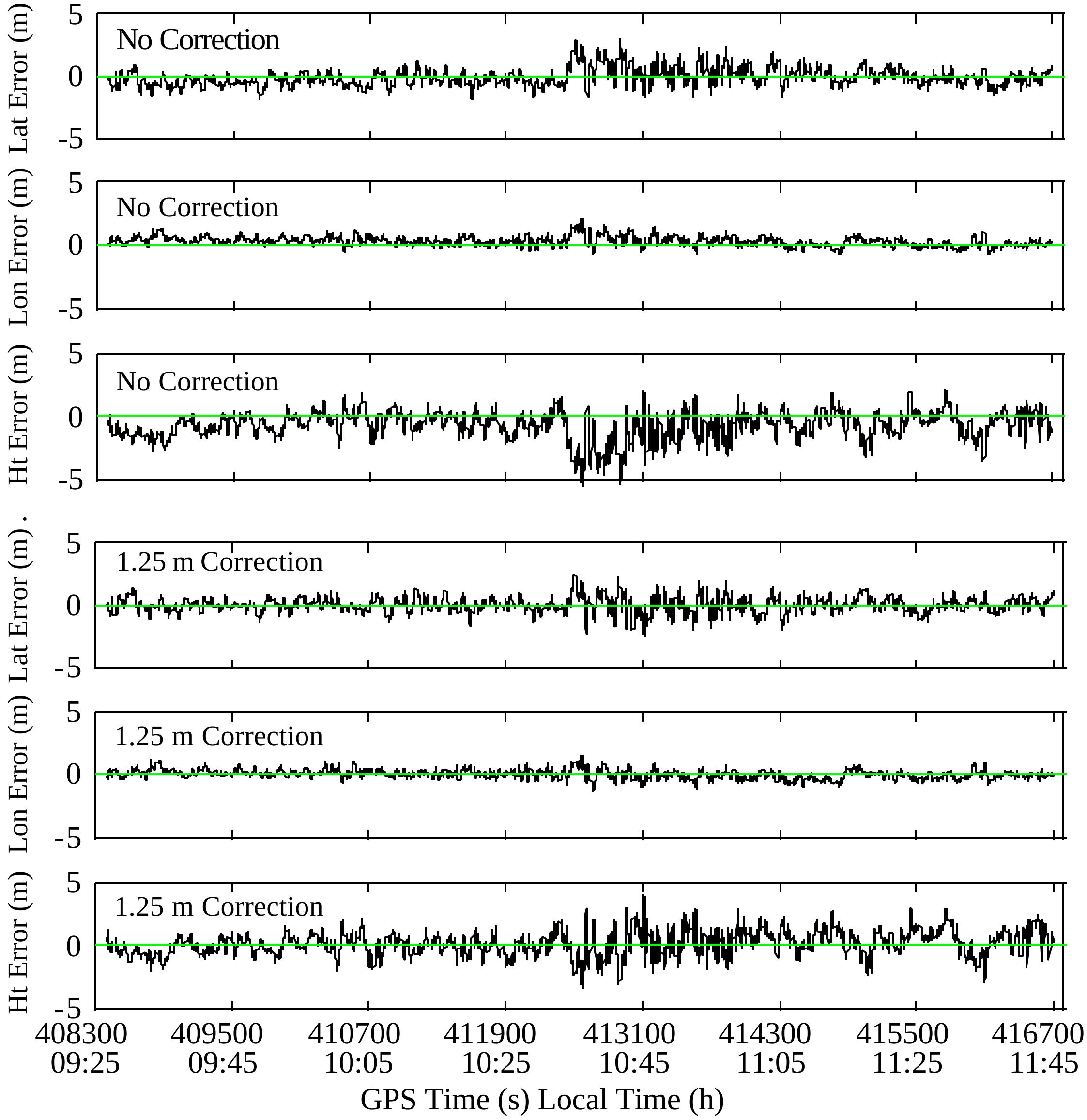

Figure 5.46 Lake Okanagan. C^{3}NAVPL Raw Code Error Comparison Between Unaugmented and Multipath Corrected PL Augmented GPS Constellations. Mask Angle 10°. Unconstrained Height.

Table 5.9 Lake Okanagan. C^3NAVPL Raw Code Errors. Mask Angle 10°. Various Configurations. No Satellites Rejected. PL Multipath Corrected.

1.25 m Multipath Correction Used	**Latitude**		**Longitude**		**Height**	
	mean	**95 %**	**mean**	**95 %**	**mean**	**95 %**
No	-0.148	1.456	0.287	0.944	-0.792	2.638
Yes	-0.054	1.223	-0.020	0.713	0.072	1.901

Plots for four cumulative frequency distributions are shown in Figure 5.47. The unaugmented and PL augmented configurations are shown for reference. Also shown are the multipath corrected PL augmented configurations for an unconstrained and height constrained case. Note that the horizontal position error curves generated for the multipath corrected PL augmented configurations are consistently better than the unaugmented case. Additionally, the use of a height constraint with the multipath corrected PL pseudoranges produces the best horizontal positioning capability. Statistics for Figure 5.47 are presented in Table 5.10.

Table 5.10 Lake Okanagan. C^3NAVPL 50^{th} and 95^{th} Percentile Horizontal Position Error and 2DRMS Horizontal Accuracy. Mask Angle 10°. No Satellites Rejected. Uncorrected and Multipath Corrected PL Pseudoranges.

Configuration	50^{th} percentile	95^{th} percentile	2DRMS (m)
No PL, No HC	0.530	1.296	1.468
PL, No HC	0.653	1.521	1.736
PL (Corrected), No HC	0.510	1.302	1.415
PL (Corrected), 1 m^2 HC	0.480	1.065	1.222

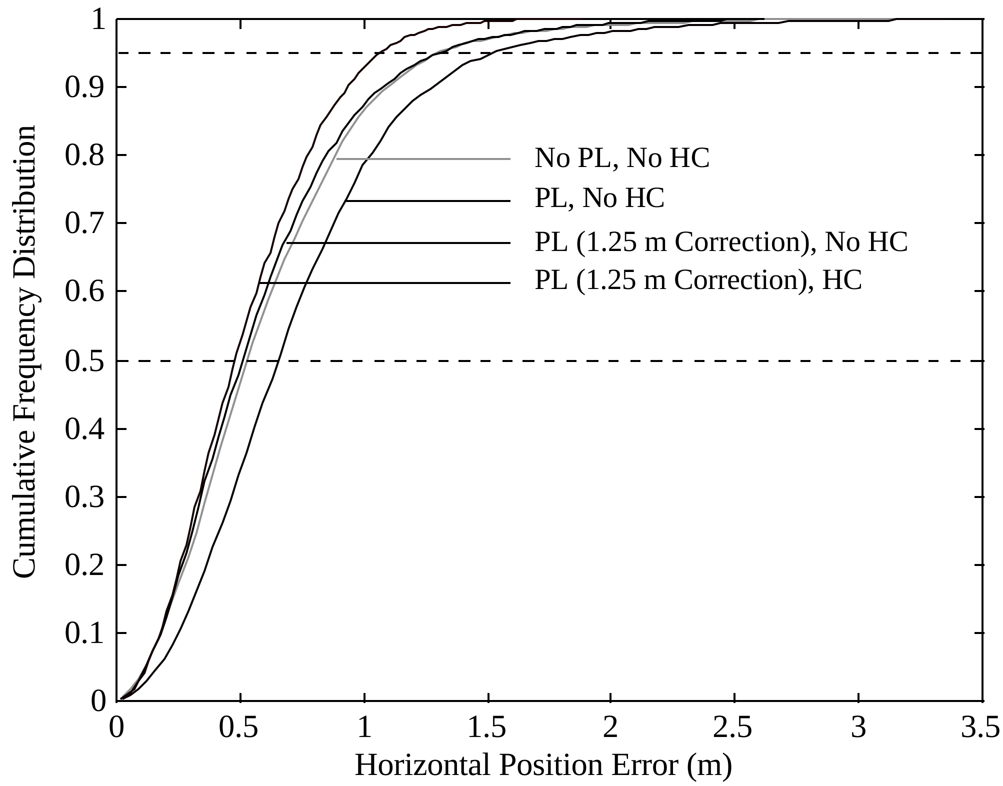

Figure 5.47 Lake Okanagan. C³NAVPL Raw Code Cumulative Frequency Distribution of Horizontal Position Error. Unaugmented and PL Augmented (Uncorrected and Multipath Corrected) GPS Constellations. Mask Angle 10°.

Residuals for the uncorrected and multipath corrected PL augmented configurations are shown in Figure 5.48. Note that, again, the use of a correction for an average 1.25 metre multipath effect has essentially removed the biases from the residual plots. Statistics for these plots are included in Table 5.11.

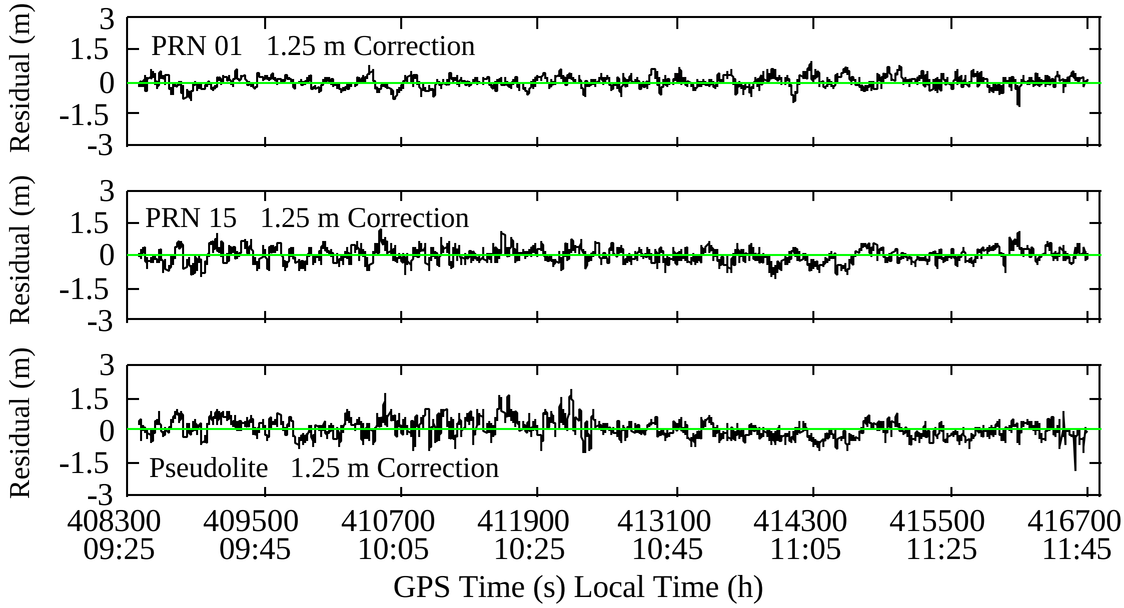

Figure 5.48 Lake Okanagan. C^3NAVPL Raw Code Residuals for Uncorrected and Multipath Corrected PL Augmented GPS Constellations. Mask Angle 10°. Unconstrained Height.

Table 5.11 Lake Okanagan. C3NAVPL Raw Code Residual Statistics. Uncorrected and Multipath Corrected PL Pseudoranges.

PRN	PL (No Correction)		PL (1.25 m Correction)	
(elev)	Mean (m)	RMS (m)	Mean (m)	RMS (m)
01 (71° - 43°)	0.025	0.277	0.000	0.261
15 (16° - 58°)	0.199	0.379	-0.020	0.326
PL	0.559	0.730	0.021	0.406

5.2.4 Changes to DGPS Positioning - Degraded Constellation

An analysis was conducted for a degraded constellation (satellite PRN 15 (elevation 16° to 58°) rejected) to determine the changes to the DGPS availability, accuracy, and reliability measures, and the C^3NAVPL single difference positioning performance. As before, a 10° mask angle was used, and the height constraint variance (when used) was 1 m^2. A 1.25 m multipath correction term was applied to the PL differential correction terms generated by the reference receiver. Figure 5.49 shows the number of satellites tracked for the degraded constellation for both the unaugmented and PL augmented configurations. There are several periods where the unaugmented constellation drops to only four satellites in view. The average number of satellites tracked for this configuration was only 5.31.

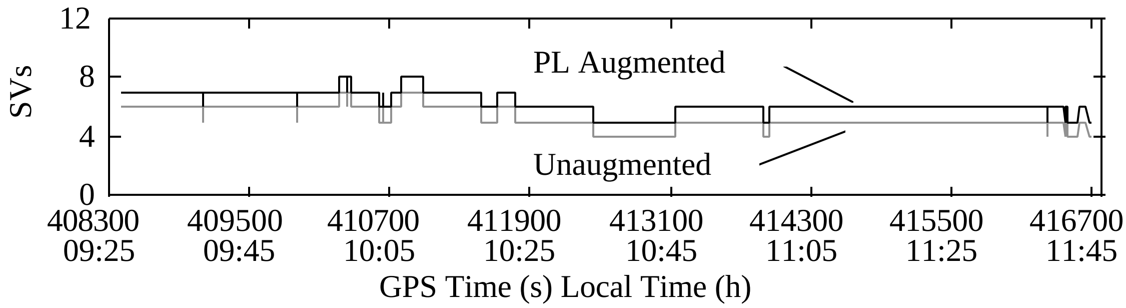

Figure 5.49 Lake Okanagan. Number of Satellites Tracked. Unaugmented and PL Augmented GPS Constellations. Mask Angle 10°. Satellite 15 Rejected.

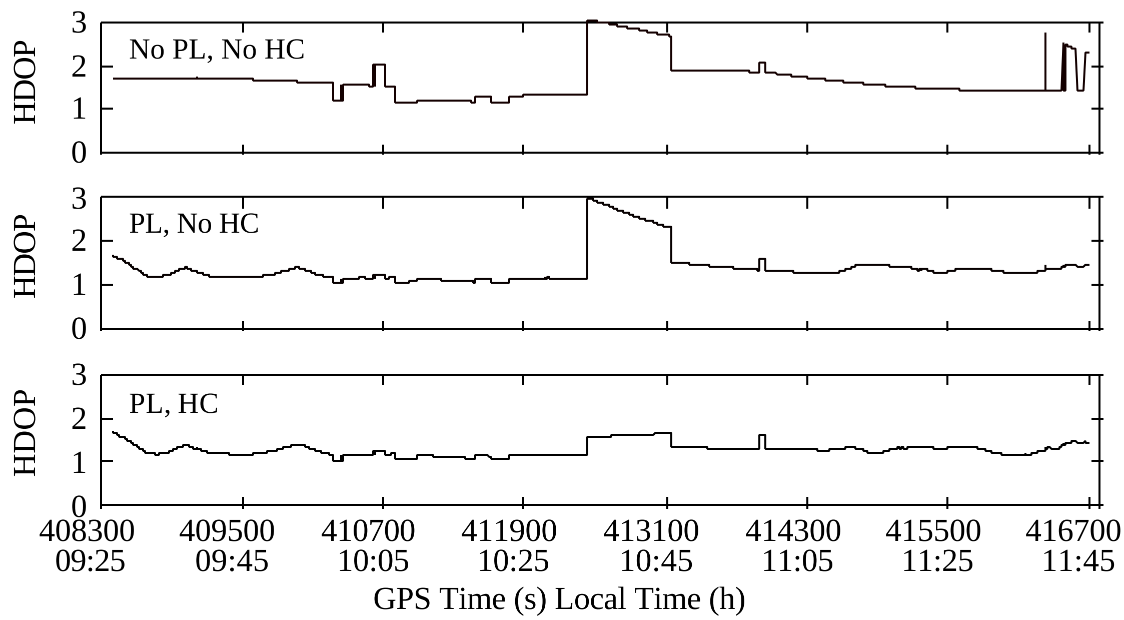

Figure 5.50 Lake Okanagan. HDOP. Unaugmented and PL Augmented GPS Constellations. Mask Angle 10°. Satellite 15 Rejected.

The HDOP plots for three different configurations in shown in Figure 5.50. The PL augmented case shows a slight improvement over the unaugmented case. The use of a height constraint reduces significantly the magnitude of the HDOP during those periods when the number of satellites is only four.

As illustrated in Figure 5.51, the augmentation of GPS with a PL has reduced the external reliability measure substantially for the degraded constellation. The unaugmented constellation contains periods where no reliability assessment is possible (10.7% of epochs with only four satellites available), and periods where, even with more than four satellites, the magnitude of the MHE envelope exceeds 100 metres (8.3% of epochs). Even though the HDOP measure is reasonable, the satellite constellation is very weak from a reliability perspective. A comparison of the PL augmented configurations show a dramatic improvement in the ability to detect an erroneous observation by analyzing the residuals. For both PL augmented configurations, no periods exist where the magnitude of the MHE exceeds 100 metres. For the PL augmented and unconstrained height MHE plot, the maximum MHE (70 metres) occurs at time 413140, just before the number of observations increases from 5 to 6. The maximum MHE for the height constrained MHE (22 metres) occurs at 413945, when the number of observations drops from 6 to 5. The average MHEs for the three configurations are: 36.70 m (with 19.0% of the values set to 100 m), 12.19 m and 6.76 m, respectively. The MHE was set to 100 metres during any periods where there was no reliability assessment available or during any periods where the MHE exceeded 100 metres.

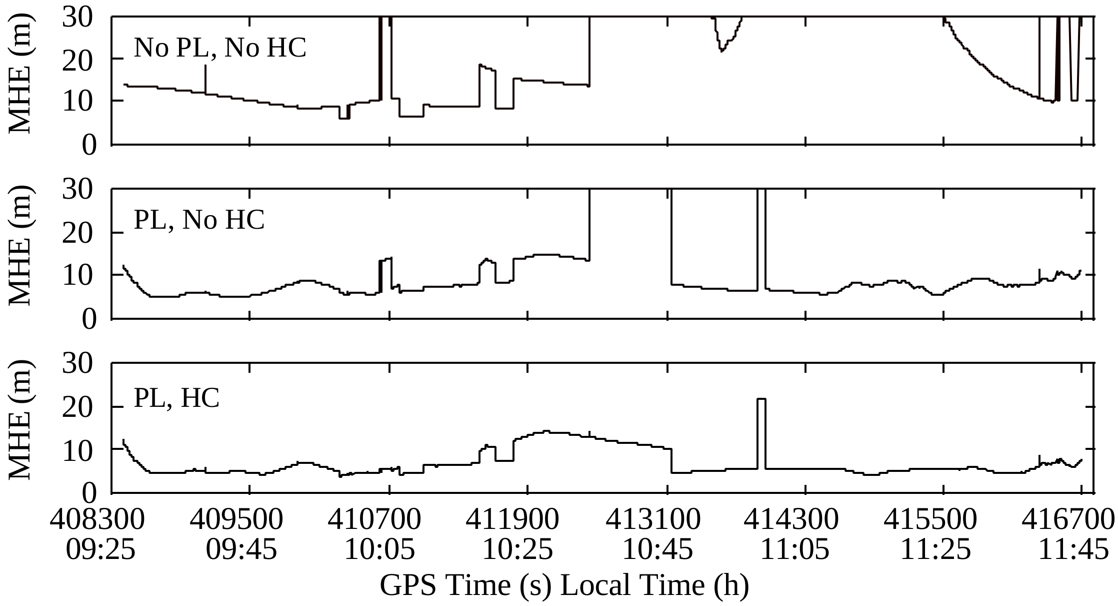

Figure 5.51 Lake Okanagan. MHE. Unaugmented and PL Augmented GPS Constellations. Mask Angle 10°. Satellite 15 Rejected.

Table 5.12 Lake Okanagan. Summary of Number of Satellites Tracked, Average HDOP and Average MHE. Mask Angle 10°. Various Configurations. Satellite 15 Rejected.

Mask Angle	PL Used	1 m^2 HC Used	Rejected SV	Mean SVs	Mean HDOP	Mean MHE
10°	No	No	15	5.31	1.68	36.70*
	Yes	No		6.31	1.39	12.19
	Yes	Yes		6.31	1.26	6.76

* Includes 19.0% of epochs with an MHE greater than 100 m.

The latitude, longitude and height errors for the degraded constellation are shown in Figure 5.52. The plots below show the three error components for an unaugmented and pseudolite augmented (multipath corrected) configuration. As expected, with the loss of one satellite, the ability to accurately position the remote receiver is reduced. All three error components show a decrease in the 2DRMS accuracy (Table 5.13) when compared to the results obtained with a full constellation (Table 5.10, row 1 for the unaugmented case, rows 3 and 4 for the PL augmented configurations without and with HC). The plots of the cumulative frequency distribution of horizontal error (Figure 5.53) shows a similar degradation in horizontal position accuracy, with the 95th percentile horizontal error for the unaugmented configuration (no height constraint) increasing from 1.296 m to 1.714 m (32.2 %). The pseudolite augmented (unconstrained height) case increased from 1.302 m to 1.528 m (17.4 %), while the pseudolite augmented and height constrained case increased from 1.065 m to 1.291 m (21.2 %). Statistics for this analysis are presented in Table 5.14.

Table 5.13 Lake Okanagan. C^{3}NAVPL Raw Code Errors. Mask Angle 10°. Various Configurations. No Satellites Rejected.

PL	1 m^2 HC	Latitude		Longitude		Height	
Used	**Used**	**mean**	**95 %**	**mean**	**95 %**	**mean**	**95 %**
No	No	0.114	1.561	0.000	0.980	-0.154	2.543
Yes	No	-0.025	1.455	-0.024	0.837	0.077	2.259
Yes	Yes	-0.066	1.233	0.017	0.769	0.000	0.460

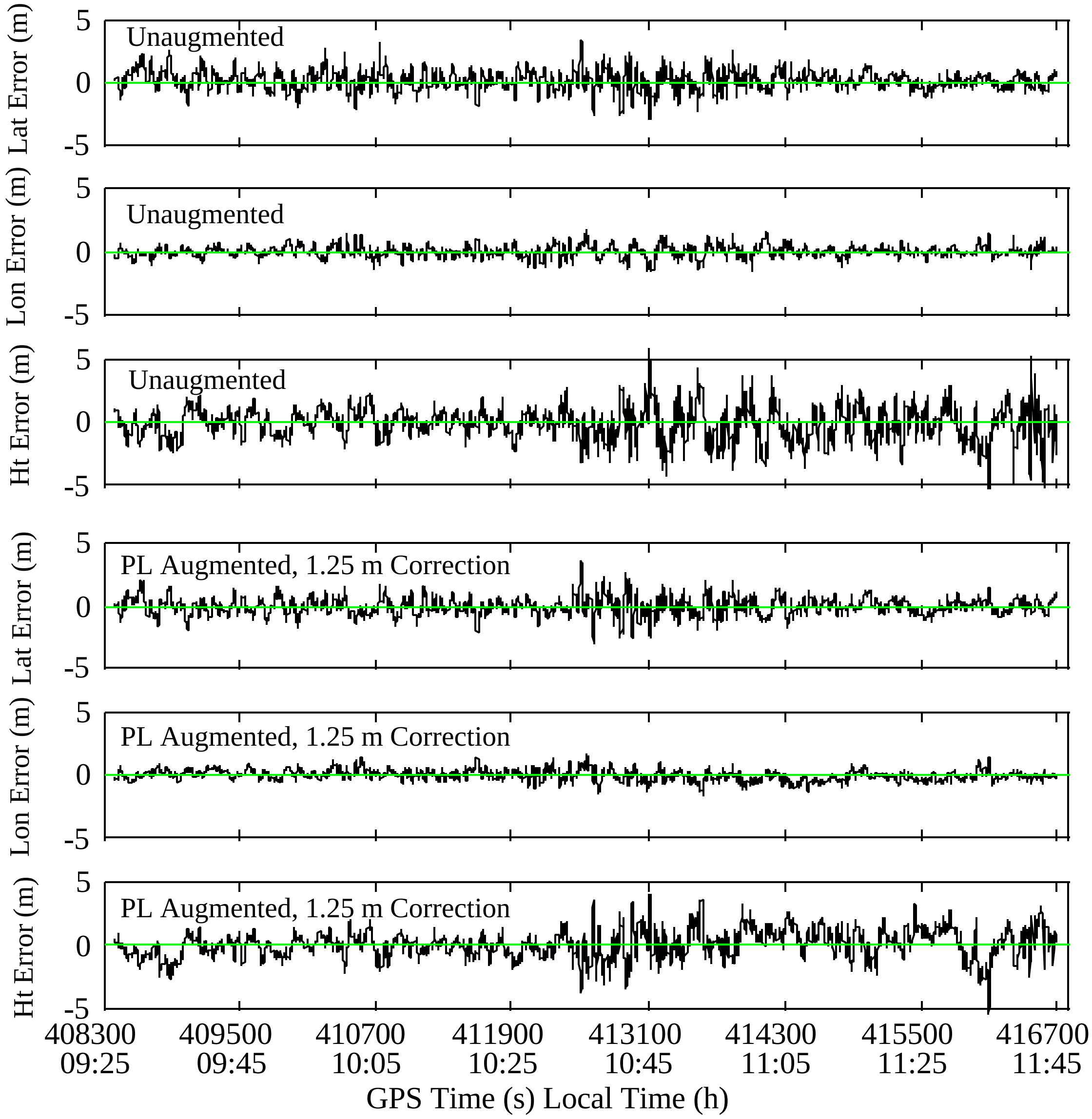

Figure 5.52 Lake Okanagan. C^{3}NAVPL Raw Code Error Comparison Between Unaugmented and Multipath Corrected PL Augmented GPS Constellations. Mask Angle 10°. Satellite 15 Rejected.

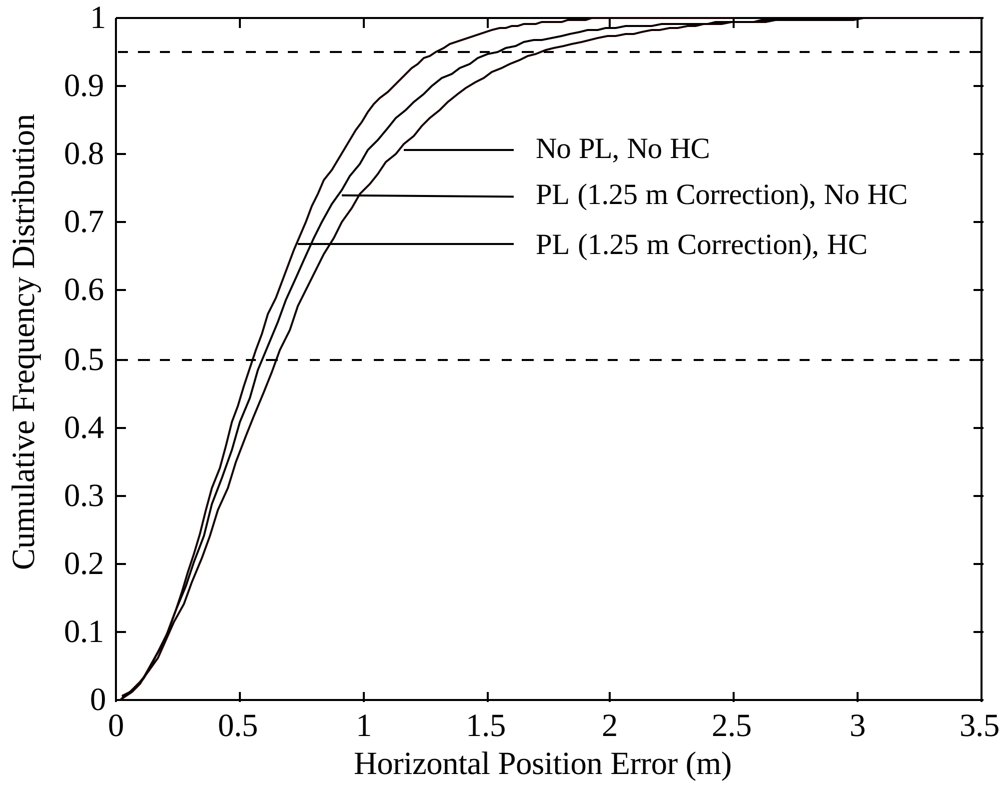

Figure 5.53 Lake Okanagan. C^3NAVPL Raw Code Cumulative Frequency Distribution of Horizontal Position Error. Unaugmented and Multipath Corrected PL Augmented GPS Constellations. Mask Angle 10°. Satellite 15 Rejected.

Table 5.14 Lake Okanagan. C^3NAVPL 50th and 95th Percentile Horizontal Position Error and 2DRMS Horizontal Accuracy. Mask Angle 10°. No Satellites Rejected. Uncorrected and Multipath Corrected PL Pseudoranges.

Configuration	50th percentile	95th percentile	2DRMS (m)
No PL, No HC	0.651	1.714	1.843
PL (Corrected), No HC	0.594	1.528	1.680
PL (Corrected), 1 m^2 HC	0.558	1.291	1.455

5.2.5 Changes to DGPS Carrier Phase Smoothed Code Positioning - Full Constellation

The Lake Okanagan morning data set was reprocessed to illustrate the effects of carrier phase smoothing of the pseudoranges on the single difference DGPS position solution. The smoothing ramp reset time, as described in section 2.3.1 was set to 400 epochs. The latitude, longitude and height errors for three configurations are shown in Figure 5.54: unaugmented, PL augmented with no multipath correction, and

PL augmented with a 1.25 m multipath correction of the pseudoranges as measured by the reference receiver. Note that the first 100 epochs, where the carrier phase smoothing filter is initializing, are not plotted, nor are these first 100 epochs incorporated into the statistics. A height constraint was not used for this analysis. The results are very much as anticipated, with the uncorrected pseudolite results being biased due to the time invariant multipath component. The unaugmented and pseudolite augmented (multipath corrected) plots are very similar. Statistics for the three configurations are summarized in Table 5.15.

Table 5.15 Lake Okanagan. C^3NAVPL Smoothed Code Errors. Mask Angle 10°. Various Configurations. No Satellites Rejected. PL Multipath Corrected. No HC.

PL Used?	1.25 m Multipath Correction Used?	Latitude		Longitude		Height	
		mean	95 %	mean	95 %	mean	95 %
No	N/A	0.043	0.380	0.036	0.289	-0.062	0.869
Yes	No	-0.416	0.920	0.363	0.769	-0.707	1.726
Yes	Yes	-0.065	0.345	0.106	0.310	-0.203	0.860

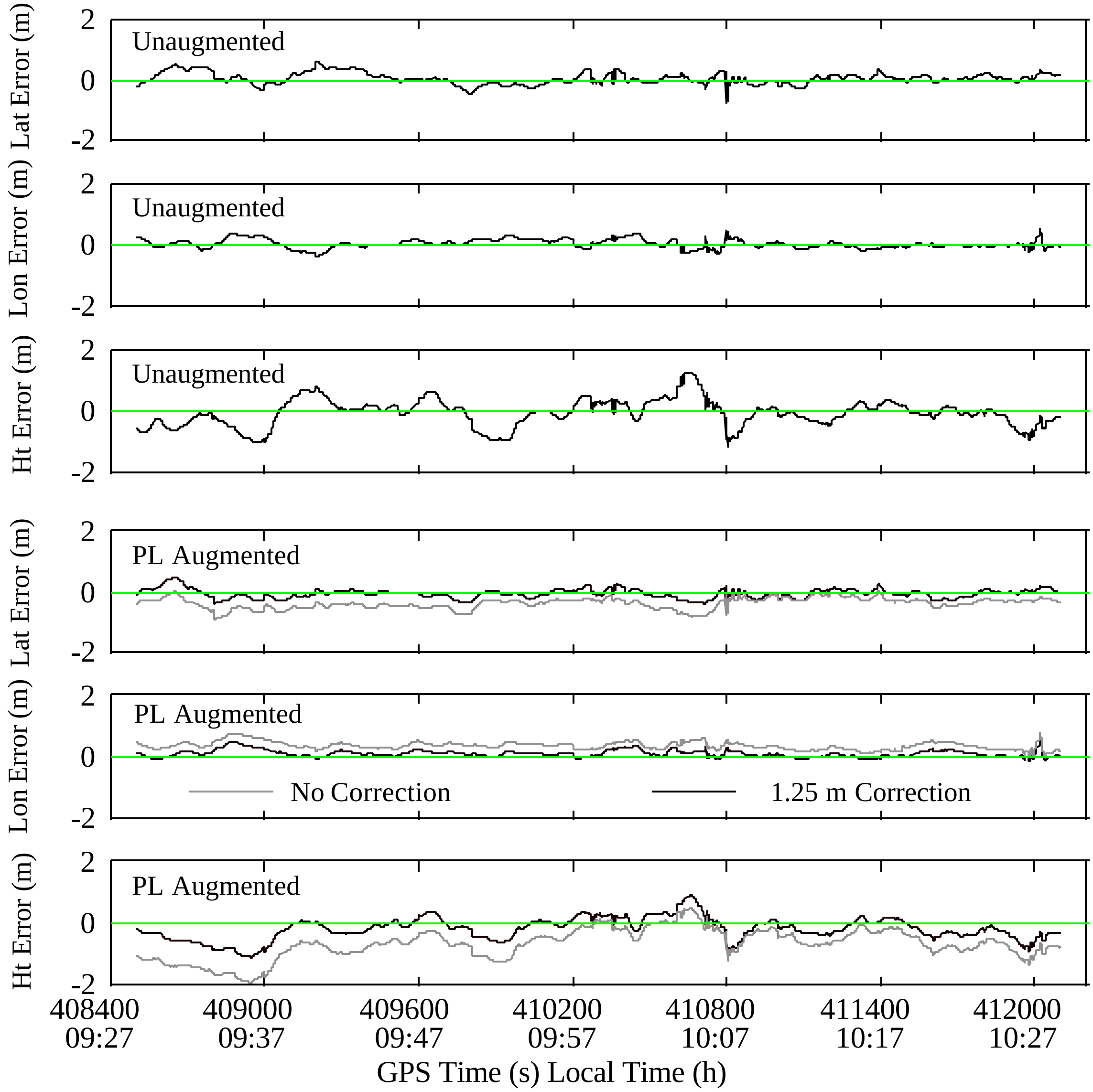

Figure 5.54 Lake Okanagan. C³NAVPL Smoothed Code Error Comparison Between Unaugmented and PL Augmented (Uncorrected and Multipath Corrected) GPS Constellations. Mask Angle 10°. Unconstrained Height.

A plot of the cumulative frequency distribution of the horizontal position error for the carrier phase smoothed code is shown in Figure 5.55, with statistics for the 50th and 95th percentile horizontal errors and the 2DRMS horizontal error summarized in Table 5.16. The unaugmented and PL augmented (multipath corrected) results are virtually identical, whereas the results for the PL augmented (uncorrected) configuration are considerably worse. Carrier phase smoothing of the pseudoranges has reduced the 95th percentile horizontal position error for the PL augmented (multipath corrected) configuration with no height constraint, from 1.528 m (Table 5.14) to 0.438 m (Table 5.16).

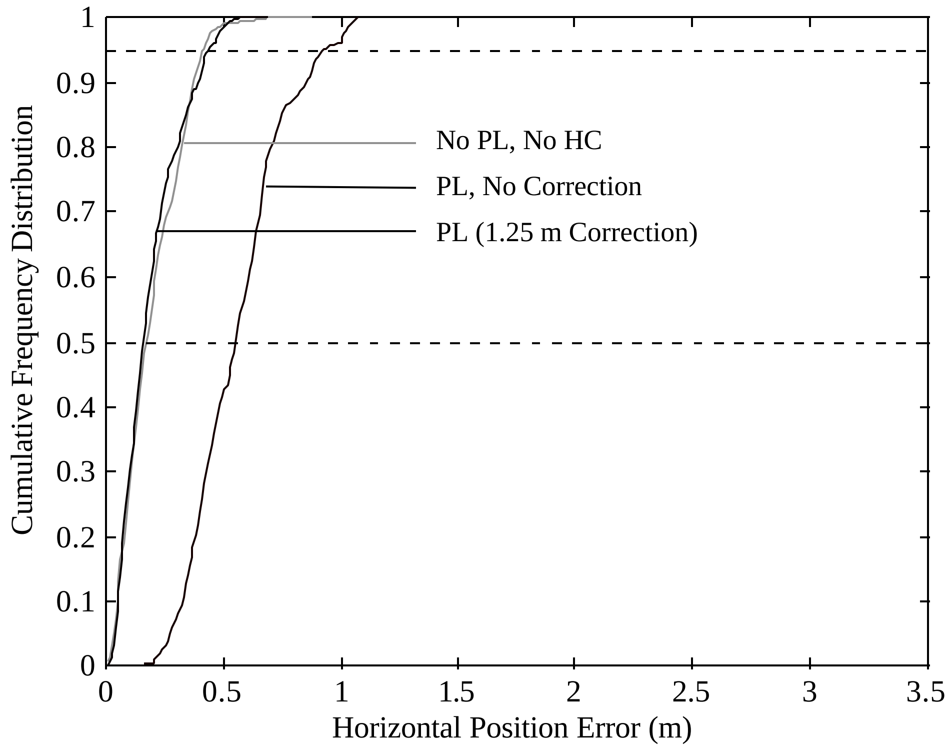

Figure 5.55 Lake Okanagan. C^3NAVPL Smoothed Code Cumulative Frequency Distribution of Horizontal Position Error. Unaugmented and PL Augmented (Uncorrected and Multipath Corrected) GPS Constellations. Mask Angle 10°.

Table 5.16 Lake Okanagan. C^3NAVPL Smoothed Code 50th and 95th Percentile Horizontal Position Error and 2DRMS Horizontal Accuracy. Mask Angle 10°. No Satellites Rejected. No HC.

Configuration	50th percentile	95th percentile	2DRMS (m)
No PL	0.171	0.416	0.477
PL (Uncorrected)	0.558	0.923	1.198
PL (Corrected)	0.157	0.438	0.463

Finally, the residuals for two satellites and the pseudolite for the above three configurations are plotted in Figure 5.56 and summarized in Table 5.17. The three different configurations show almost identical results for the residuals of satellite PRN 01. The uncorrected pseudolite configuration shows a marked bias in the residual plots for PRN 09 and the PL. The unaugmented and multipath corrected PL augmented configurations are essentially unbiased for all three plots.

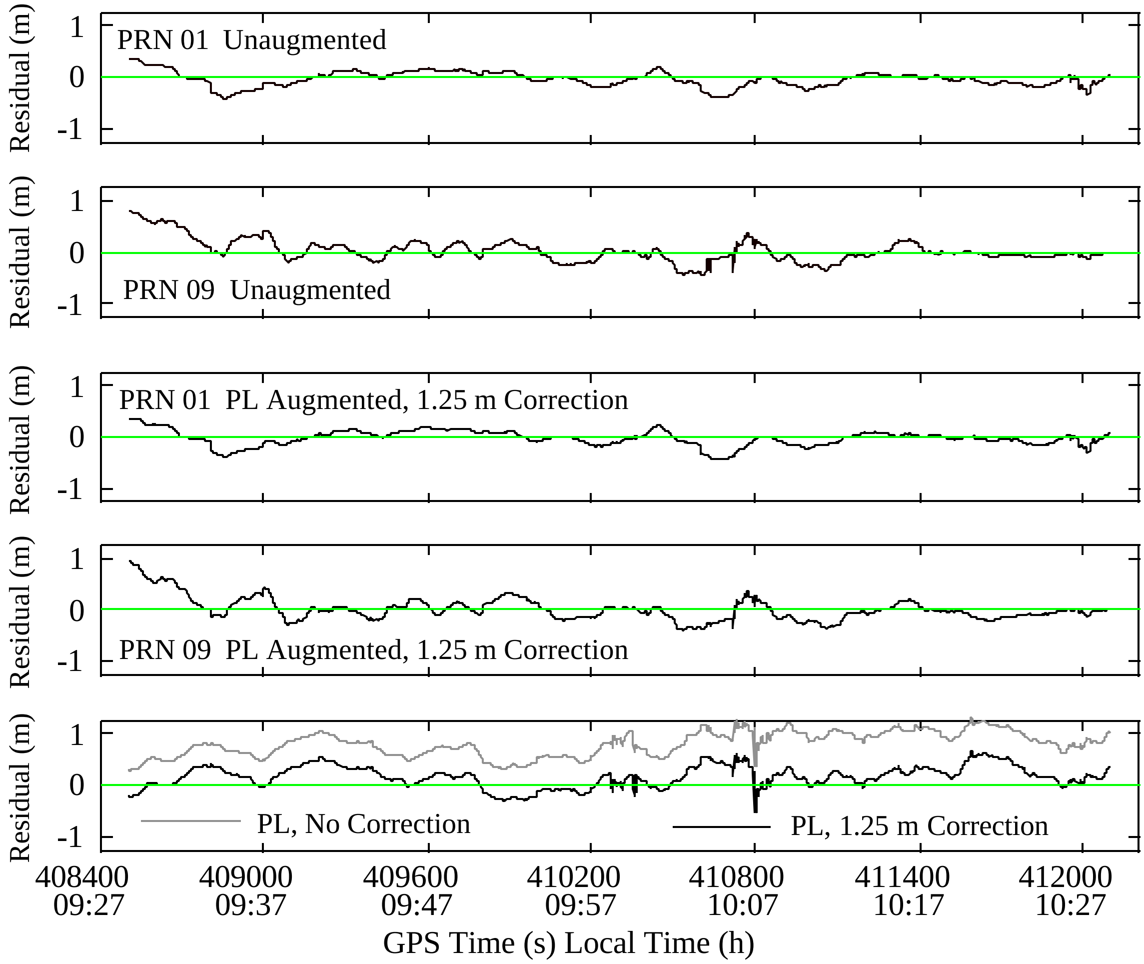

Figure 5.56 Lake Okanagan. C^{3}NAVPL Smoothed Code Residuals for Unaugmented and Multipath Corrected PL Augmented GPS Constellations. Mask Angle 10°. Unconstrained Height.

Table 5.17 Lake Okanagan. C^{3}NAVPL Smoothed Code Residual Statistics. Uncorrected and Multipath Corrected PL Pseudoranges. No HC.

PRN	No PL		PL (Uncorrected)		PL (1.25 m Correction)	
(elev)	Mean (m)	RMS (m)	Mean (m)	RMS (m)	Mean (m)	RMS (m)
01 (71°-53°)	-0.044	0.151	-0.040	0.163	-0.046	0.156
09	0.039	0.219	-0.141	0.263	0.005	0.233
PL	N/A	N/A	0.781	0.815	0.159	0.259

5.2.6 Effect of a Simulated Blunder on DGPS Fault Detection and Exclusion

To illustrate the beneficial effect of PL augmentation on the performance of a simple fault detection and exclusion (FDE) algorithm, a simulated blunder was introduced into the remote receiver's pseudorange measurement for PRN 21. The profile of the induced error is shown in Figure 5.57. At time 413200 the error was initiated, growing in magnitude at a rate of 0.25 metre per second. Once the induced error reached 15 m, it was held constant for 5 minutes (until 413560), then allowed to decrease to zero (at time 413620), at a rate of 0.25 metre per second.

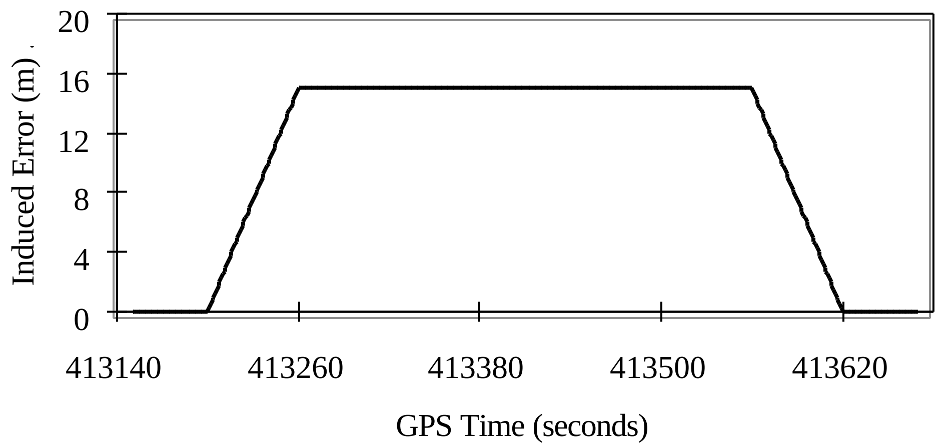

Figure 5.57 Simulated Error Profile for PRN 21.

There are several methods by which the C^3NAVPL raw code residuals can be tested for gross errors, or blunders. The method developed by Baarda [1967, 1968] tests the standardized residual (i.e the i^{th} estimated residual divided by the estimated standard deviation of the i^{th} residual) against a critical value, 'c'. Using this method, 'c' is determined by the values selected for α (type I error) and β (type II error). As developed previously in section 2.4, for an α of 0.001 and a β of 0.1, the critical value 'c' (or the non-centrality parameter δ_o) is 4.57.

The statistical testing technique implemented in this FDE algorithm is described by Vanicek and Krakiwsky [1981]. Again, the absolute value of the standardized estimated residuals are compared against a test statistic, as follows:

$$\hat{r}_i^* = \left| \frac{\hat{r}_i}{\hat{\sigma}_{\hat{r}_i}} \right| \tag{5.1}$$

where $\hat{r}_i$ ... is the estimated residual of the i^{th} observation,

$\hat{\sigma}_{\hat{r}_i}$ ... is the estimated standard deviation of the i^{th} observation,

and $\hat{r}_i^*$ ... is the standardized estimated residual of the i^{th} observation.

The null hypothesis (i.e. that $\hat{r}_i$ is free of gross errors or blunders) is rejected whenever the absolute value of the estimated standardized residual exceeds a test statistic. Normally, this test statistic is associated with a (1-α) confidence level, where each residual is considered individually, or out of context of the other residuals. For an α of 0.001, the test statistic for $\alpha/2$ is approximately 3.29. To consider the entire set of residuals "in context" with each other, the $\alpha/2$ term is replaced by $\alpha/2N$ where 'N' is the number of residuals [Steeves & Fraser, 1987]. Thus, for 6 residuals, $\alpha/2N$ corresponds to a test statistic of approximately 3.67.

At every epoch the FDE algorithm compares the estimated standardized residual for each observation against the test statistic (3.67). If the magnitude of the estimated standardized residual is greater than the test statistic, a blunder is declared. If only one blunder is declared at a given epoch, the appropriate observation is rejected, and the least squares solution is recomputed. If there is more than one blunder declared during a particular epoch, the observation with the greatest difference between the estimated standardized residual and the test statistic is rejected.

Figure 5.58 shows the C^3NAVPL raw code standardized residuals for PRN 21 for the unaugmented and PL augmented configurations. Note that these residuals were produced by disabling the FDE algorithm implemented in C^3NAVPL to illustrate the relations between the standardized residuals for the two configurations. When the residual exceeds the corresponding test statistic (3.67), a blunder will be declared. The deleterious effects of a blunder will be absorbed by the residuals of all observations in the least squares adjustment [Leick, 1995]. It is quite possible that a blunder on one observation could cause the residual of another observation to exceed the test statistic first, leading to an erroneous fault detection, and the subsequent rejection of a good observation.

As shown in Figure 5.58, PL augmentation has two obvious benefits: first, the rate at which the pseudorange error is absorbed by the residual is increased; and second, the amount of error absorbed by the residual is increased. For the unaugmented constellation, the PRN 21 estimated standardized residual exceeds the test statistic after approximately 31 seconds of error growth (i.e. a 7.75 metre blunder). For the PL augmented case, the estimated standardized residual exceeds the test statistic after only 19 seconds (i.e. a 4.75 metre blunder).

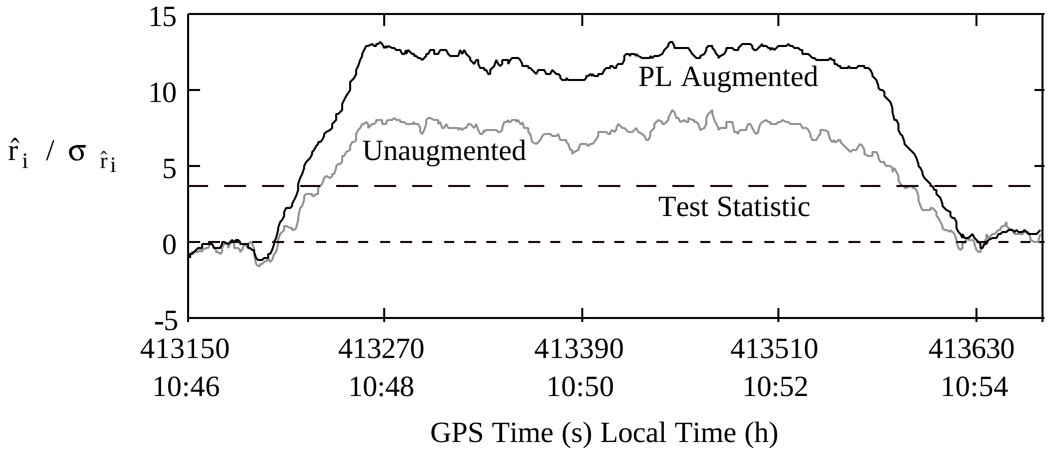

Figure 5.58 Test Statistic (3.67) and PRN 21 C^{3}NAVPL Raw Code Estimated Standardized Residuals for Unaugmented and PL Augmented GPS Constellations. Simulated Error on PRN 21.

Plots for the latitude, longitude and height errors for a nine minute data segment are shown in Figure 5.59. The pseudorange error for PRN 21 is initiated at 413200, and grows to 15 metres according to Figure 5.57. The induced error is reduced to zero at time 413620. For both the unaugmented and PL augmented configurations, the FDE algorithm successfully identifies and rejects PRN 21 from the least squares adjustment. For the unaugmented case, the initial blunder detection occurs at time 413231. PRN 21 is continuously rejected until time 413587, where it is accepted for three epochs. PRN 21 is then rejected for one epoch (413590), and then accepted for the remainder of the test. The performance for the PL augmented configuration is noticeably better than that of the unaugmented configuration. A blunder detection is declared at time 413219, and satellite PRN 21 is continuously rejected until time 413599 when the FDE algorithm accepts all observations as blunder free. For the error induced condition, the maximum horizontal error for the unaugmented configuration is 9.42 m, whereas the maximum horizontal error for the PL augmented configuration is 3.67 m.

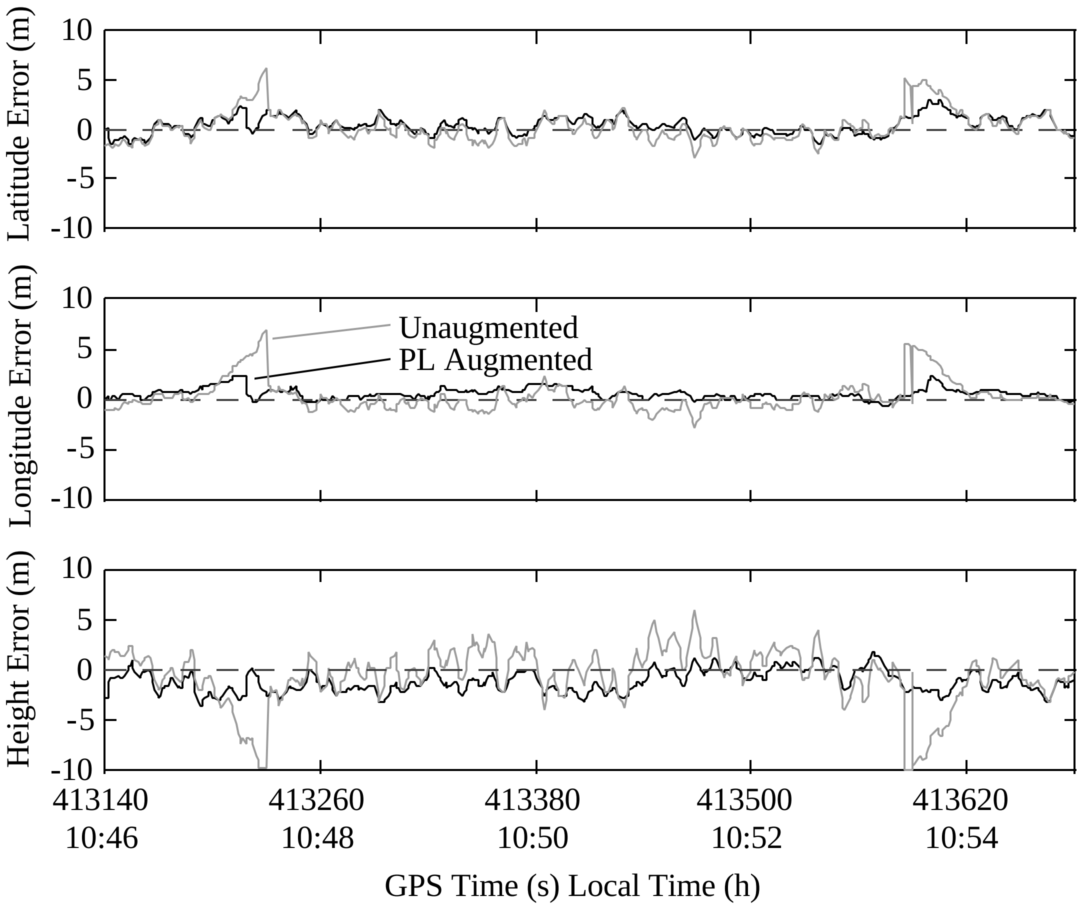

Figure 5.59 Lake Okanagan. C^{3}NAVPL Raw Code Error Comparison Between Unaugmented and PL Augmented GPS Constellations. Mask Angle 10°. Simulated Error on PRN 21.

While this simple algorithm was not designed as a robust fault exclusion function, it illustrates effectively the significant advantages achievable through the augmentation of GPS with a PL. If a robust fault exclusion algorithm was to be designed, the following quality control improvements could be implemented to minimize the probability of rejecting a valid observation and accepting a degraded observation: firstly, once a blunder has been detected by comparing the estimated standardized residuals to the test statistic, sequentially reject all observations, one at a time, and compute the sum of squares of the residuals for all subsets. If the subset with the smallest sum of squares of the residuals corresponds to the same satellite that caused the blunder detection in the first place, one can be reasonably certain that this is the correct satellite to reject. Lastly, before a previously rejected satellite is re-accepted as valid, it should have to pass all statistical testing for a specified number of epochs.

CHAPTER 6

EFFECT OF PSEUDOLITE AUGMENTATION ON OTF INTEGER AMBIGUITY RESOLUTION PERFORMANCE

As summarized in Table 1.2, most marine GPS applications require positioning information primarily in the horizontal plane, to an accuracy usually no better than 5 m. Some marine applications, however, such as 3D seismic work or the movement of vessels through constricted waterways, have a requirement for very accurate horizontal and vertical positioning. As described in section 2.3.2, sub-decimetre GPS accuracies (horizontal and vertical) can be achieved if the carrier-phase double-difference ambiguities can be successfully and reliably determined [Weisenburger and Cannon, 1997]. For virtually all marine applications it will be impossible or highly impractical to conduct a static initialization, therefore the ambiguities must be resolved using on-the-fly (OTF) techniques. The time required to determine the integer ambiguities is a function of many variables, including: the equipment used (single or dual frequency), the separation between the reference and the remote receivers, the number of satellites available (a minimum of five are required to solve for the ambiguities), the strength of the satellite geometry, the atmospheric conditions, the multipath environment (which will degrade the pseudorange measurements and distort the carrier phase signal), and the ambiguity search method(s) used [Lachapelle, 1995].

The augmentation of GPS with a PL can have a dramatic affect not only on the time to ambiguity resolution, but in the reliability of that solution. This chapter investigates the performance enhancements achieved by using the extra information provided by the PL. Results from two data sets (Okanagan morning and Okanagan afternoon) are presented. The November 7, 1996 morning data set is initially analyzed to determine the optimal PL carrier phase noise required to reliably solve for the integer ambiguities. Following this, the morning data set is analyzed under two conditions: a GPS constellation using all available satellites, and a GPS constellation with one satellite rejected. Results for both the unaugmented and PL augmented cases are summarized. Finally, the afternoon data set is analyzed to illustrate the correlation between the reference and remote distance and the integer ambiguity resolution time.

The University of Calgary software package SEAFLY (a modified version of FLYKIN™) was further modified (termed SFLYPL) to accept pseudolite data and process the field test data [Weisenburger, 1997]. The following are the most significant modifications of SFLYPL: default coordinates for the pseudolite instead of calculated coordinates via a pseudolite ephemeris record, implementation of user-defined variances for pseudolite code and carrier measurements, user-defined adjustment of the process noise, disabling of the ionospheric corrections for pseudolite measurements, constant index of refractivity for the tropospheric delay correction, and adjustment of the filter reset parameters to account for noisier residuals.

6.1 Lake Okanagan Field Test - Morning Session

The data set described in section 5.2 was processed using SFLYPL to assess the changes in ambiguity resolution time and reliability due to PL augmentation. As mentioned previously, the time to resolve the integer ambiguities is affected by many factors. It was decided to repeatedly process this data set, using different start times, and record the time to integer ambiguity resolution, and whether the initial ambiguity set was correct. The "correct" ambiguities were determined using a 10 cm height constraint and observing the calculated residuals of the SFLYPL output for the entire data set. The base satellite was PRN 01 for all subsets, and the mask angle used was 10° plus local terrain. The data were recorded and processed at 1 Hz.

6.1.1 Lake Okanagan - Full Constellation

The initial start time was chosen to be 408400 (GPS time), and the data set was processed until the ambiguities were solved. The next start time was set 100 seconds later, at 408500 (GPS time), and the process repeated. The last start time was 416300 (GPS time) resulting in a total of 80 different start times. This was completed for the unaugmented case, and for the PL augmented cases using three different carrier phase noise variances (0.5 cm^2, 1.0 cm^2, 2.0 cm^2). For comparison, the SFLYPL software uses a carrier phase variance of 0.5 cm^2 for a satellite observation. Carrier phase multipath cannot exceed one quarter of a wavelength, or approximately 5 cm on L1 [Lachapelle, 1995]. Additionally, the code phase noise variance for the pseudolite was set at 36 m^2 (as compared to 16 m^2 for a satellite). By de-weighting the PL code observations (which were shown in section 5.2.3 to contain time invariant errors due to multipath) the integer ambiguity search volume is defined primarily by satellite code measurements, and thus, should not be affected adversely by the biased PL code measurements [Ford, *et al*., 1996].

The results for the above analysis are summarized in Figure 6.1. The unaugmented case had an average integer ambiguity resolution time of 209 seconds, and a success rate of 95.0% (76 out of 80). Note that this statistic includes results only for the cases where the integer ambiguities were successfully resolved on the initial attempt. The RMS ambiguity resolution time provides an indication of the temporal variation for the various cases. Quite an improvement in average ambiguity resolution time was achieved (from 206.9 to 114.3 seconds) when the PL carrier phase noise was set to 0.5 cm^2 (identical to the phase noise on the satellite observations). Unfortunately, it also resulted in only a slight improvement in the initial success rate, solving correctly the first time 97.5% of the time (78 out of 80 attempts). A higher carrier phase noise (2.0 cm^2) yielded similar results, solving in an average of 150.1 seconds, with an initial success of 98.8% (79 out of 80 attempts). A reasonable value for the carrier phase noise for the pseudolite appears to be around 1.0 cm^2, for this case. The value of 1.0 cm^2 is a function of PL noise and the local carrier phase multipath conditions due to the environment. A 100% success rate was achieved, along with a reduction in average ambiguity resolution time of 38% (from 206.9 to 129.1 seconds). For the remainder of this chapter, a PL phase noise of 1.0 cm^2 is used.

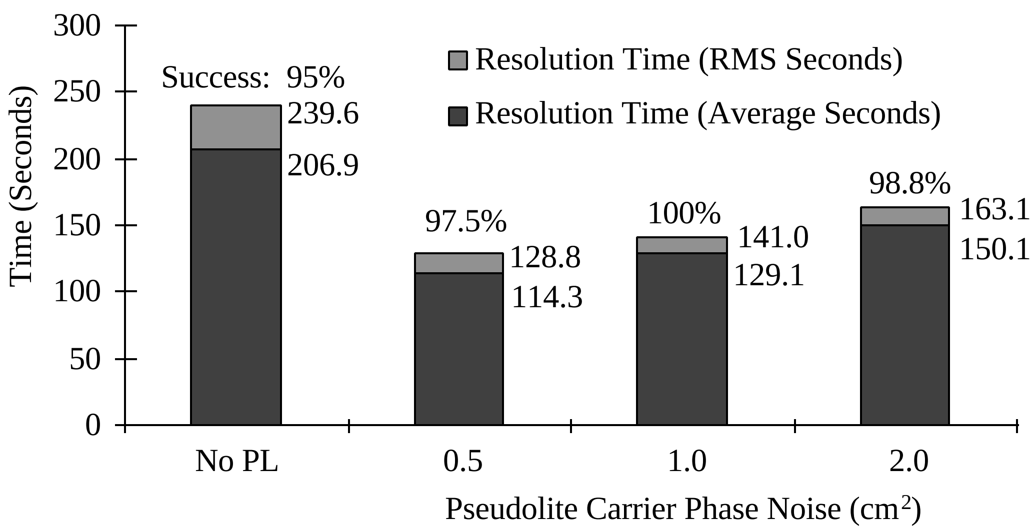

Figure 6.1 Effect of PL Augmentation and SFLYPL PL Phase Noise on Integer Ambiguity Resolution Time and Resolution Reliability.

A plot of the integer ambiguity resolution time results for the unaugmented and PL augmented cases is shown in Figure 6.2. Note that the four epochs where the unaugmented case had an incorrect initial ambiguity solution have been assigned values of 800 epochs (for illustration purposes only), and that all four of these epochs occur one after the other. This is a strong indication that there is an identical underlying cause for these occurrences. A closer inspection of Figure 5.37 shows that the number of satellites tracked during this portion of the data set dropped from six to five for approximately 700 seconds. As the four incorrect initial solutions all occur after the loss of satellite PRN 09 (which descended below the 10° mask angle at 412436), it was weak satellite geometry that caused the poor performance of the integer ambiguity resolution algorithm. As described previously, signals from low elevation satellites are particularly prone to distortion by multipath. Note that the data set that starts at 412400 (just as PRN 09 is setting) takes 747 epochs to solve correctly for the ambiguities. The code and phase information from satellite PRN 09 was distorted sufficiently to affect adversely the performance of the FASF algorithm, even though this information was available for only 36 seconds. The data set that begins at time 412900 starts when there are only five satellites available, but fixes correctly only 16 seconds after satellite PRN 14 (which ascended above the 10° mask angle at 413140) is incorporated into the algorithm. During this same period, the PL augmented case results in four correct resolutions.

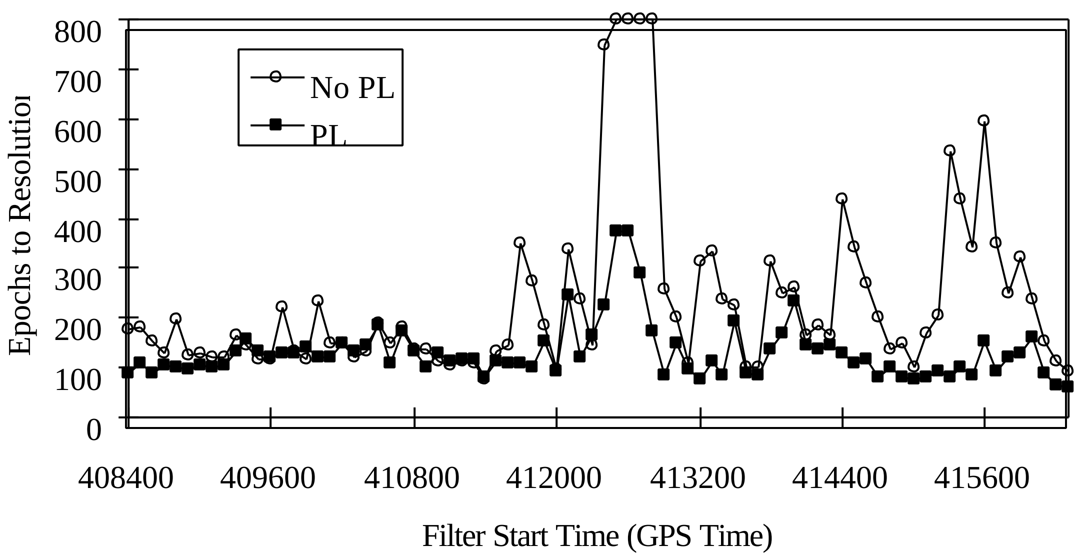

Figure 6.2 Comparison of SFLYPL Integer Ambiguity Resolution Times for the Unaugmented and PL Augmented GPS Constellations. Mask Angle 10°. PL Phase Noise 1.0 cm^2. (Four Incorrect Initial Fixes Assigned a Value of 800)

The SFLYPL program performs several tests on the fixed ambiguity solution to try and ensure that the ambiguity set chosen is indeed the correct set. Tests are performed on the carrier phase residuals to detect any growth which would indicate an incorrect ambiguity set has been chosen. If the baseline distance between the reference and the remote station is less than 1 km, a warning flag is set for every carrier phase residual that exceeds a residual test value of 2.0 cm during a given epoch. For baseline distances in excess of 1 km, the residual test is set to 3.0 cm. If two or more satellites have residuals that exceed the test value, the integer ambiguity set is assumed to be incorrect, and the FASF algorithm is reset. A test is also conducted between the float solution and the fixed solution. If any coordinate (or combination of coordinates) of the fixed ambiguity solution differs from the corresponding float solution coordinates by more than 3σ for three consecutive epochs, the FASF algorithm is reset. Figure 6.3 is a slightly modified version of Figure 6.2. In this plot, the SFLYPL program was allowed to run until correct ambiguities were found for all start times. For those four epochs that had incorrect initial ambiguity solutions, the program had to complete three steps: firstly, it had to recognize that an incorrect ambiguity set had been chosen, secondly it had to reset the FASF algorithm and thirdly, it had to resolve for the ambiguities. A summary of the initial (incorrect) fix times, the time required to reset the filter after an incorrect set was chosen (reset time) and the total time required to solve for the correct ambiguity set is included in Table 6.1.

In addition to the geometric effects described above, there appears to be periods in which an increased ambiguity resolution time correlates to the monitor-remote baseline distance. For example, near the end of the data set, and as shown in Figure 5.32, there are two periods where the boat was over 1 km from the reference station. Figures 6.2 and 6.3 indicate that, at approximately these time, the integer ambiguity resolution times increase markedly. The satellite constellation during these periods was very stable, with 6 satellites in view. Results from the afternoon session (presented in section , where the monitor-remote separation exceeds 2.5 km will better illustrate this relationship.

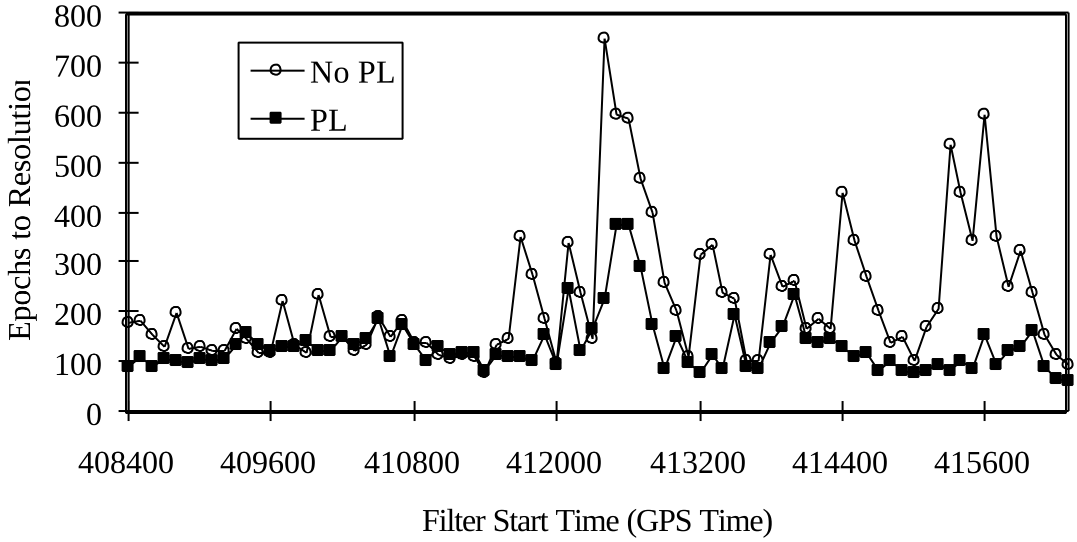

Figure 6.3 Comparison of SFLYPL Integer Ambiguity Resolution Times for the Unaugmented and PL Augmented GPS Constellations. Mask Angle 10°. PL Phase Noise 1.0 cm^2. Times to Reach Correct Ambiguity Solution.

Table 6.1 Summary of Time to First (Incorrect) Fix, Time to Filter Reset, and Time to Correct Fix. Unaugmented Configuration.

Start Time (GPS Time)	**Time to Initial Fix (s)**	**Reset Time (s)**	**Time to Correct Fix (s)**
412500	93	385	594
412600	91	415	586
412700	86	187	465
412800	171	212	399
Average	*110.3*	*299.8*	*511.0*

A plot of the SFLYPL carrier phase residuals for PRN 21 and the PL are shown in Figure 6.4. Summary statistics for this figure are included in Table 6.2. The PRN 21 carrier phase residuals for the unaugmented configuration have been offset by 4 cm for clarity. An increase in the phase noise of PRN 21 is evident as the satellite descends from 70° to 22°. The pseudolite residuals are substantially noisier than those of the satellite, which was expected with a relatively low elevation angle resulting in increased carrier phase multipath. The use of a 1.0 cm^2 phase noise is well justified. Also, the PL residual is unbiased, as are the residuals for PRN 21 for the unaugmented and PL augmented configurations. This infers that, while the PL carrier phase measurements are slightly noisier, they are not distorted with non-systematic errors to the same degree as the code measurements.

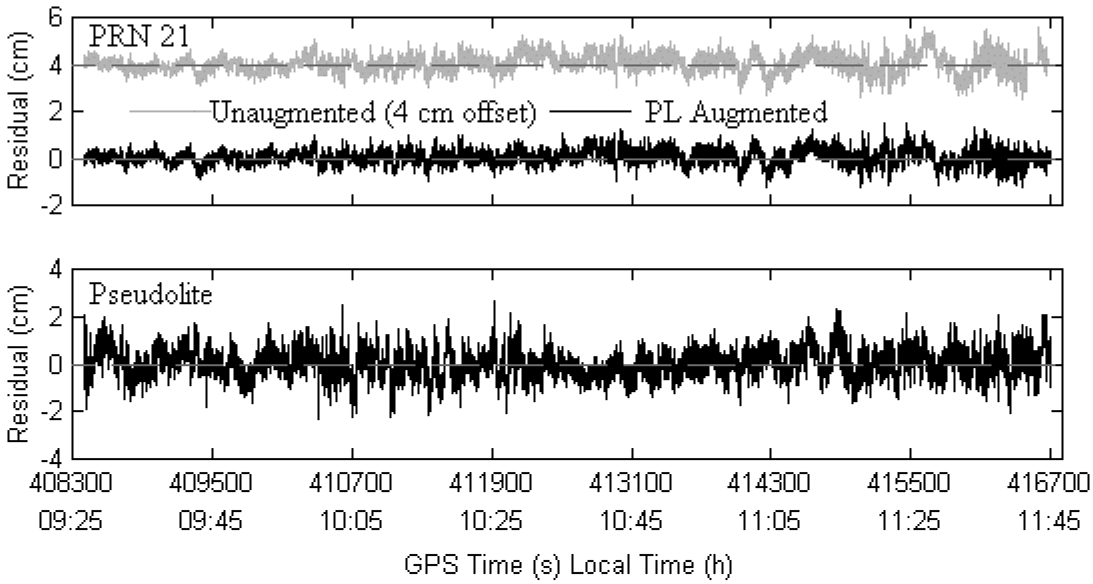

Figure 6.4 Lake Okanagan Morning Session. SFLYPL Carrier Phase Residuals. Base Satellite PRN 01. Mask Angle 10°.

Table 6.2 Lake Okanagan. SFLYPL Carrier Phase Residual Statistics.

	Unaugmented		PL Augmented	
PRN	Mean (cm)	RMS (cm)	Mean (cm)	RMS (cm)
21	0.088	0.408	0.087	0.368
PL	N/A	N/A	0.021	0.631

6.1.2 Lake Okanagan - Degraded Constellation

The above analysis was repeated, but with one satellite (PRN 15) rejected to simulate a failure. The number of satellites tracked and the HDOP were shown previously in Figures 5.49 and 5.50. Figure 6.5 presents a summary of this analysis. This time, there were many more incorrect initial solutions, which have been assigned a value of 1600 (for illustration purposes only). Additionally, the incorrect solutions are fairly evenly distributed with respect to filter start time. For the unaugmented case, there was a total of 16 incorrect solutions, for a success rate of 79.0 % (60 out of 76). For the PL augmented case, the success rate was 93.4% (71 out of 76). The last four subsets, which were included in the previous analysis, were not included in this analysis, as the unaugmented constellation was not able to successfully solve for the integer ambiguities before the end of the data set.

A period existed where, for the unaugmented case, the number of available satellites dropped to four. If the ambiguities were not fixed prior to the number of satellites dropping to four, the unaugmented case would have to "coast" for over 700 epochs until a fifth satellite was available. The pseudolite augmented case had a minimum five signals available for the entire data set. Statistics derived from a direct comparison of these times would not be overly meaningful. On the other hand, an operational system must be prepared to operate during periods of satellite unserviceability. It was therefore decided to present the results under two conditions: Condition 'A' omits any results which are affected by the satellite constellation dropping to four. Condition 'B' includes all filter start times, and allows the FASF algorithm to "coast" as required.

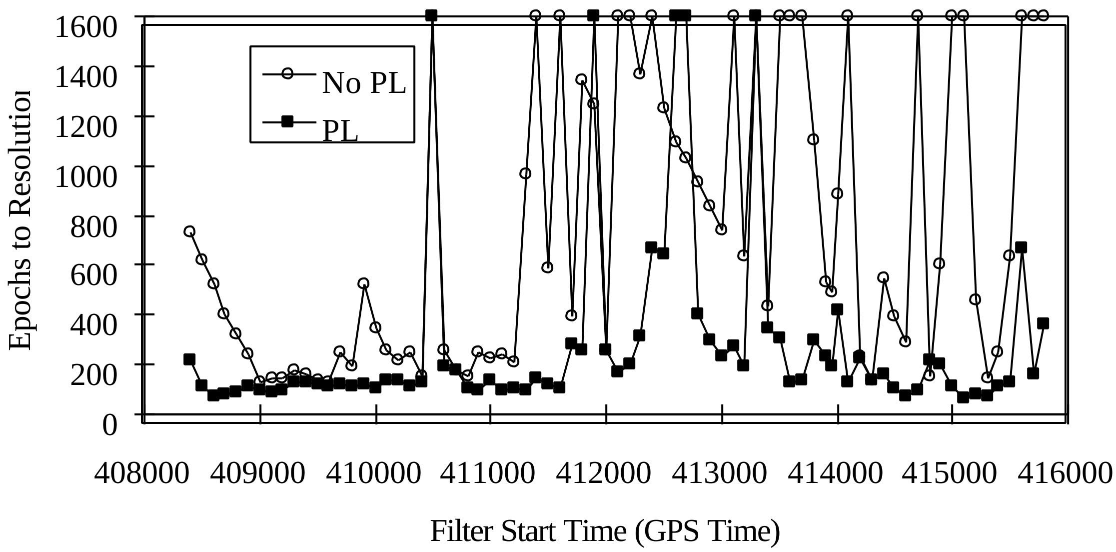

Figure 6.5 Comparison of SFLYPL Integer Ambiguity Resolution Times for the Unaugmented and PL Augmented Configurations. Mask Angle 10°. PL Phase Noise 1.0 cm^2. Satellite 15 Rejected. (Incorrect Initial Fixes Assigned a Value of 1600)

Figure 6.6 shows the results under Condition 'A', where all epochs affected by the number of satellites dropping to four have been omitted for both the unaugmented and augmented cases. As for the previous analysis, the PL augmented case shows a consistent improvement over the unaugmented case.

The complete data set (Condition 'B'), including periods of four satellites, is shown in Figure 6.7. Both the unaugmented and PL augmented cases show an increase in the integer ambiguity resolution time when the number of satellites decreases to four. Also note that two data points were omitted for each case, corresponding to times 413500 and 413700. For these two times, the unaugmented case was unable to solve for the ambiguities before the end of the data set. The float solution was within approximately 20 cm of the reference trajectory position, but the FASF algorithm was unable to collapse the solution to integers.

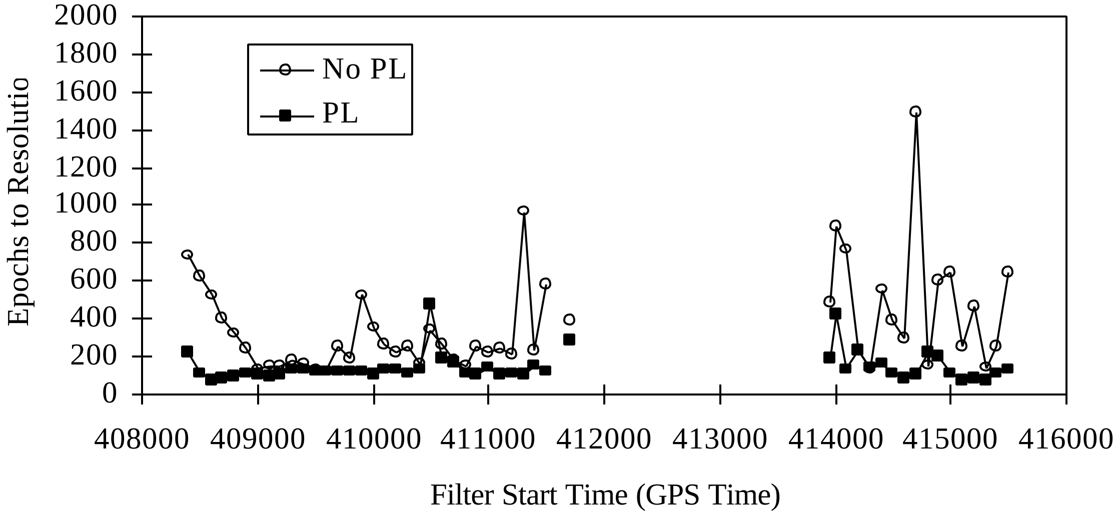

Figure 6.6 Comparison of SFLYPL Integer Ambiguity Resolution Times for the Unaugmented and PL Augmented Configurations. Mask Angle 10°. PL Phase Noise 1.0 cm^2. Satellite 15 Rejected. All Epochs Affected by Dropping to Four Satellites Removed.

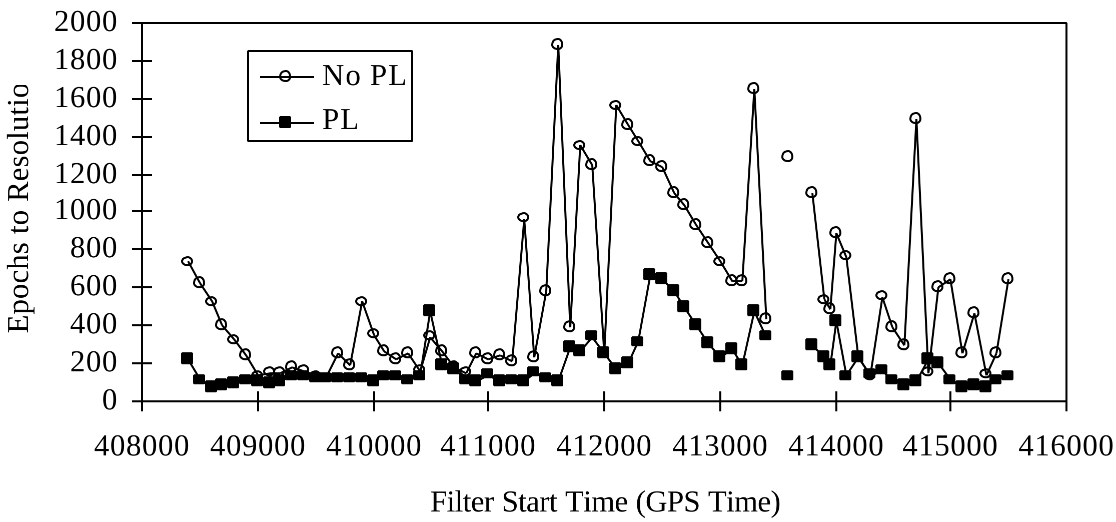

Figure 6.7 Comparison of SFLYPL Integer Ambiguity Resolution Times for the Unaugmented and PL Augmented Cases. Mask Angle 10°. PL Phase Noise 1.0 cm^2. Satellite 15 Rejected. Times to Reach Correct Ambiguity Solution for All Epochs.

Summary statistics for the number of incorrect initial solutions, filter reset times, and times to reach correct solutions for the two conditions both with and without PL augmentation, are shown in Table 6.3. The use of a PL has resulted in a dramatic reduction in the time required to detect that an incorrect ambiguity set has been selected, and a corresponding reduction in the time required to solve for the correct ambiguity set.

Plots of the average and RMS integer ambiguity resolution times for the two conditions are shown in Figure 6.8. For the full GPS constellation, PL augmentation resulted in a 37.6 % reduction in the integer ambiguity resolution time. For a degraded constellation, PL augmentation reduced the integer ambiguity resolution time by 61.9 % for Condition ‘A’, and 66.0 % for Condition ‘B’.

Table 6.3 Summary of Number of Incorrect Initial Ambiguity Solutions, Average Times to Filter Reset, and Average Times to Correct Fix. Unaugmented and PL Augmented Configurations. Mask Angle 10°. PL Phase Noise 1.0 cm^2. Satellite 15 Rejected.

Condition	Incorrect Initial Solutions	Average Reset Time (s)	Average Time to Fix Correctly (s)
A - no PL	10 (18.8 %)	261.5	616.3
A - PL	1 (1.9 %)	220	472
B - no PL	16 (21.1 %)	454.4	1028.5
B - PL	5 (6.6 %)	118.6	470.8

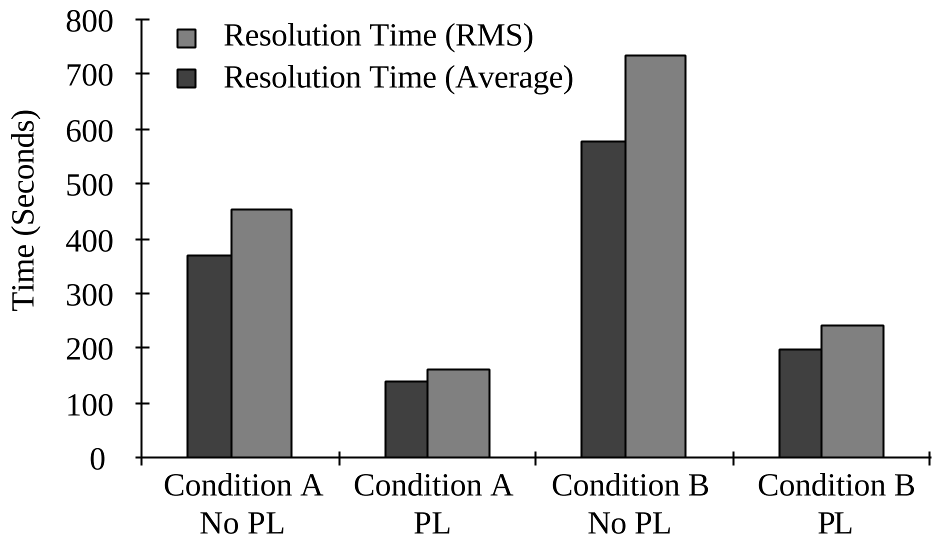

Figure 6.8 Average and RMS Integer Ambiguity Resolution Times Under Various Conditions and Configurations.

6.2 Okanagan Field Test - Afternoon Session

Approximately one hour of PL augmented GPS data was collected on Lake Okanagan on the afternoon of November 7, 1996. The equipment used and test configuration was identical to the morning data collection. The purpose of the afternoon test was to operate the remote platform at increasing ranges until loss of lock on the PL occurred. The reference trajectory for this session is shown in Figure 6.9. Initially, the boat was steered to the west, away from the PL and reference station, until the PL signal was too weak to track. The boat was then turned around and steered towards the two stations. Once near the shore, the boat was turned to the north, and the procedure repeated. The final leg was in a southward direction, again until the PL signal was lost. The height of the remote antenna is shown in Figure 6.10. The average height for the afternoon data set was 332.07 m, with a standard deviation of 3 cm. The throttle on the boat was held constant for most of the hour, resulting in a fairly constant velocity profile as shown in Figure 6.11. The average velocity was 3.75 m/s.

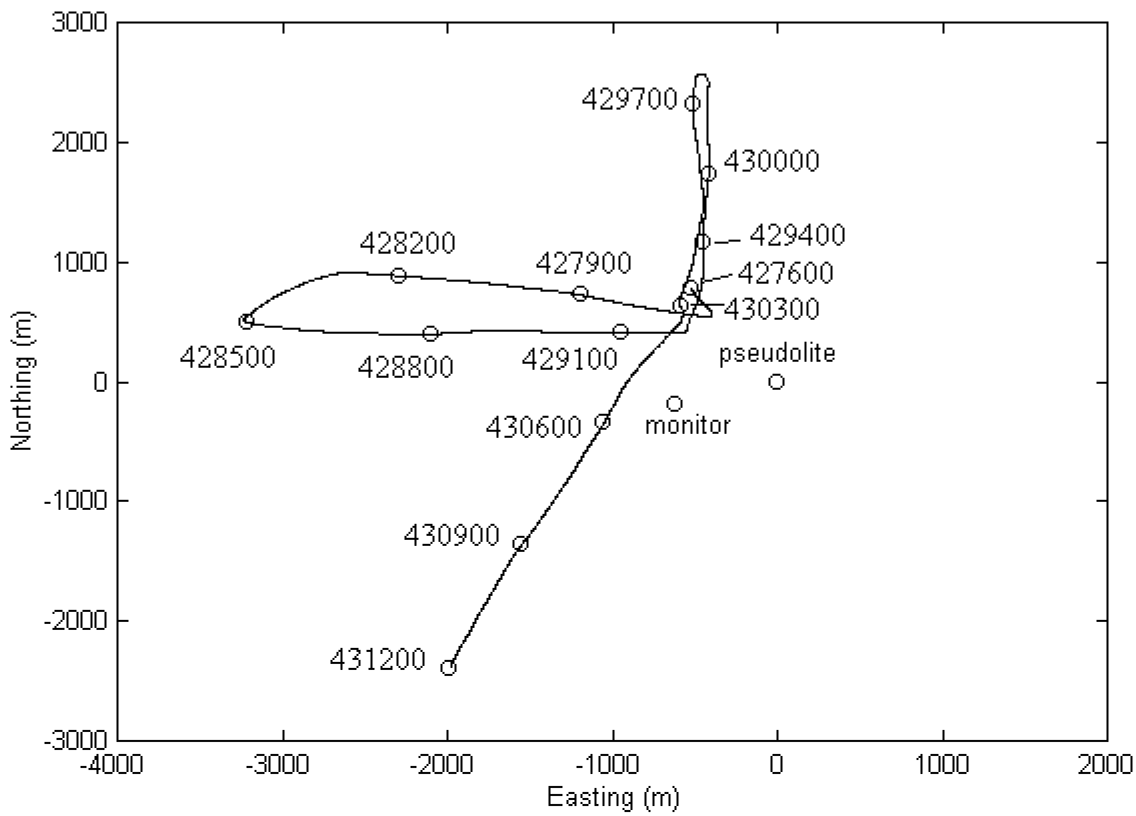

Figure 6.9 Lake Okanagan (P.M.) Fixed Ambiguity Reference Trajectory.

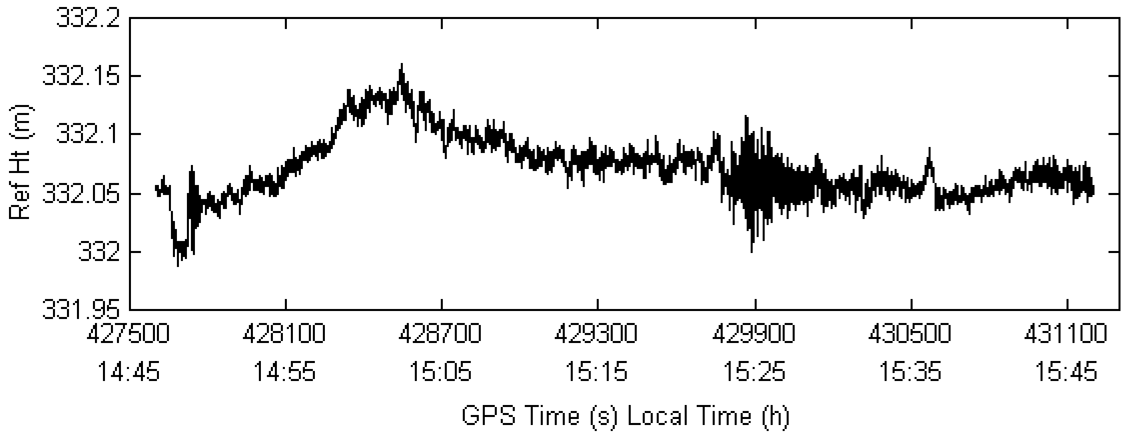

Figure 6.10 Lake Okanagan (P.M.) Fixed Ambiguity Height Solution.

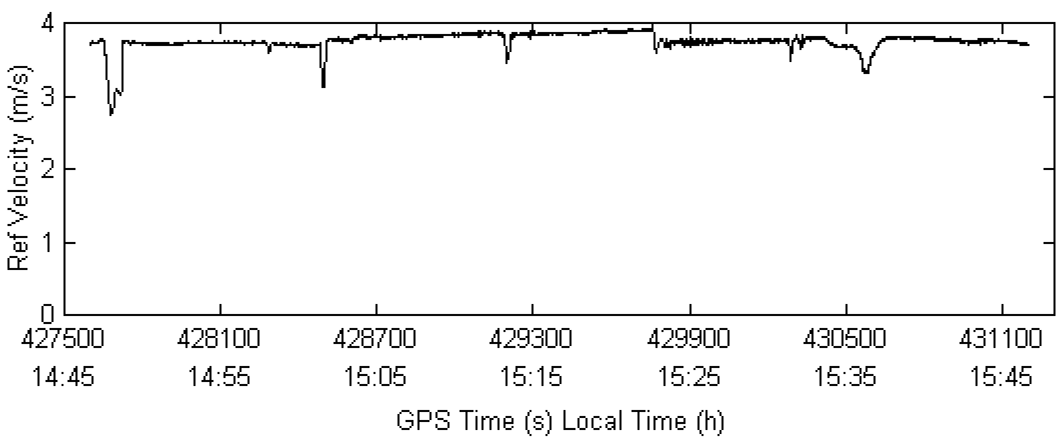

Figure 6.11 Lake Okanagan (P.M.) Fixed Ambiguity Horizontal Velocity.

The plot of the separation between the remote and the reference stations and the plot of the separation between the remote and the PL for the afternoon session are shown in Figures 6.12 and 6.13. The elevation of the PL, as observed by the remote receiver is shown in Figure 6.14. Periods where the remote receiver did not have lock on the PL signal are indicated by a PL elevation of 0°. The PL signal to noise ratios, as measured by the reference station and the remote station is shown in Figure 6.15. Note that the signal level at the reference is relatively constant (averaging 45.8 dB-Hz), whereas the signal level at the remote shows significant variation, which is highly correlated to the remote-PL separation. The average signal to noise ratio for the PL at the remote was only 37.4 dB-Hz. The remote receiver tended to lose the PL signal at around 32 dB-Hz, and regain the signal at approximately 35 dB-Hz.

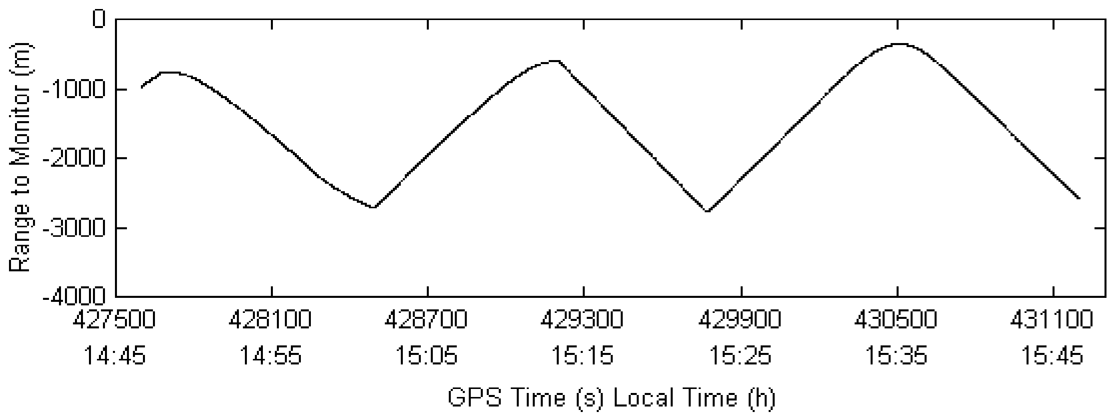

Figure 6.12 Lake Okanagan (P.M.) Slant Range Between Reference and Remote.

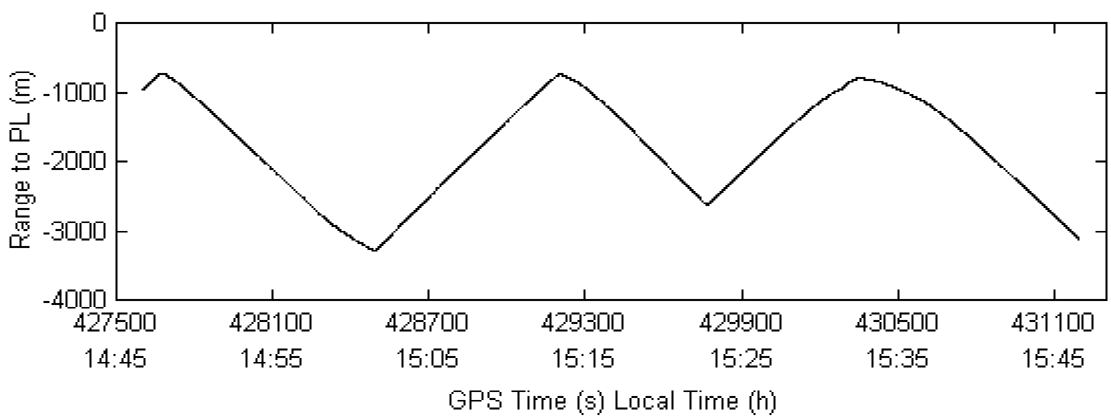

Figure 6.13 Lake Okanagan (P.M.) Slant Range Between PL and Remote.

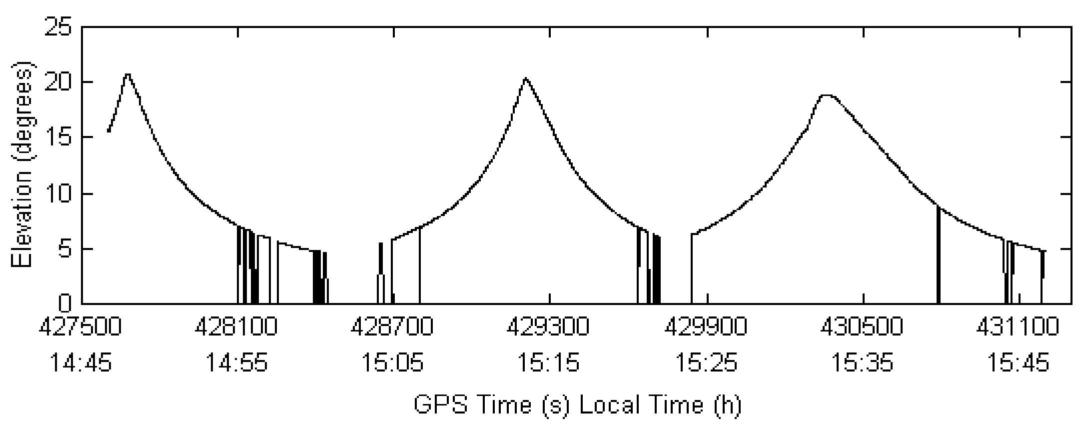

Figure 6.14 Lake Okanagan (P.M.) Elevation of PL as Observed by the Remote.

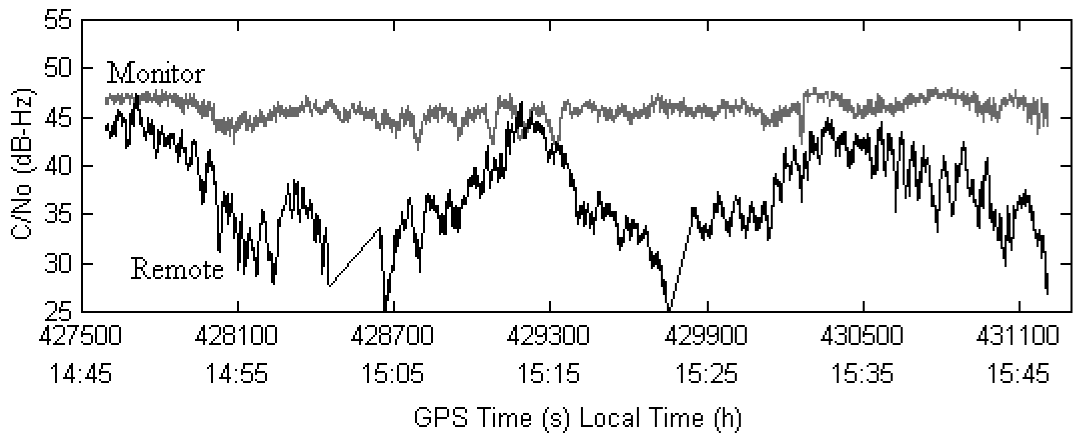

Figure 6.15 Lake Okanagan (P.M.) PL C/N_0 as Measured By Reference and Remote.

The integer ambiguity analysis proceeded much as in the previous section, except that the data sets were offset by only 50 seconds. Only data points for which lock was maintained on the PL for the entire ambiguity search are included in Figure 6.16. Continuous phase lock was maintained on the pseudolite signal when the boat/PL separation was less than approximately 2 km. Intermittent phase lock was achieved at separations between approximately 2 km and 3.25 km. The PL signal was not tracked successfully at ranges greater than approximately 3.25 km. For both the unaugmented and pseudolite augmented configurations, all initial ambiguity solutions were the correct ambiguity set. Again, the same trend is apparent: the pseudolite augmented case shows a consistent improvement in the time to resolve the integer ambiguities. Also note the distinct correlation between the separation between the remote and the reference stations (Figure 6.12) and the integer ambiguity resolution times.

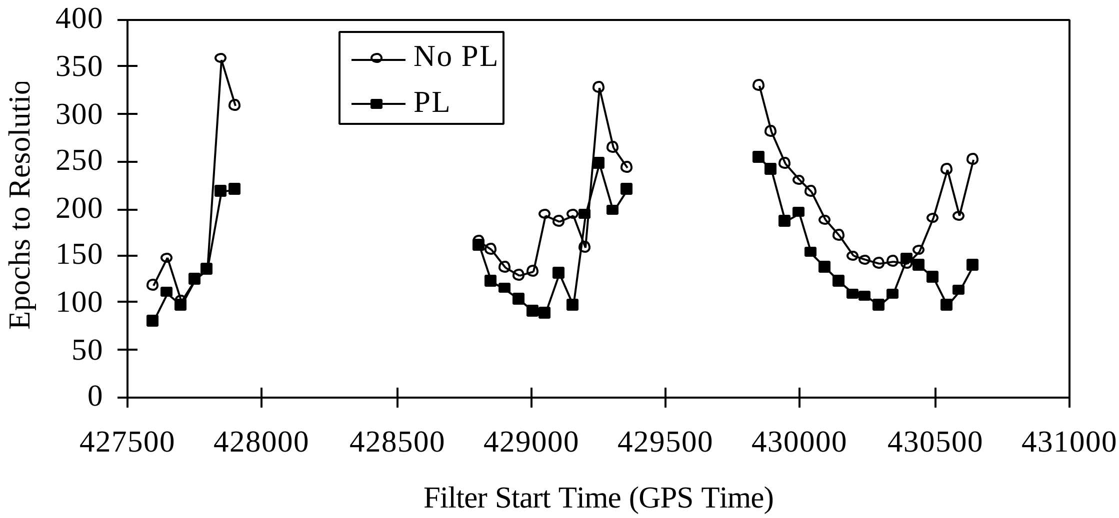

Figure 6.16 Lake Okanagan (P.M.) Comparison of SFLYPL Integer Ambiguity Resolution Times for the Unaugmented and PL Augmented GPS Constellations. PL Phase Noise 1.0 cm^2. All Epochs Affected By Loss of Lock on PL Removed.

A comparison of the average and RMS times for ambiguity resolution are summarized in Figure 6.17. The PL augmented configuration showed an improvement in the average ambiguity resolution time of 25.3 % over the unaugmented configuration.

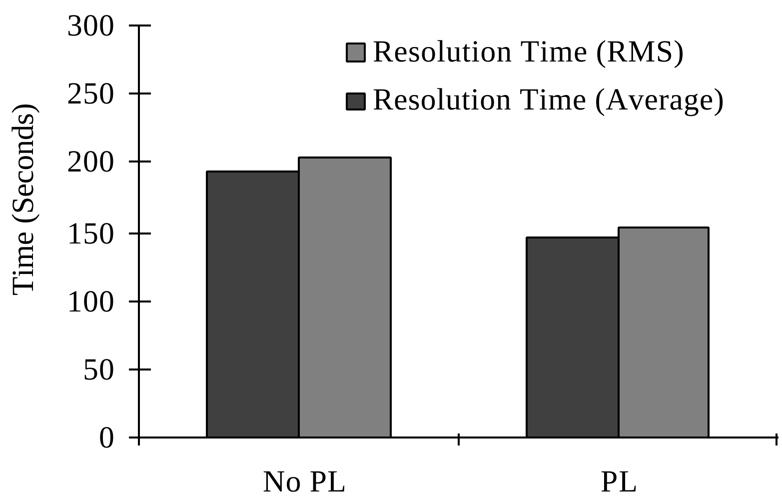

Figure 6.17 Lake Okanagan (P.M.) Average and RMS Integer Ambiguity Resolution Times for the Unaugmented and PL Augmented GPS Constellations.

6.3 Effect of Relative Coordinate Error Between the PL and the Reference Receiver

As described in section 2.2.1, a satellite coordinate (orbital) error tends to be of little concern as this error will be highly correlated between two terrestrial GPS receivers. As a result, the error will cancel in the differential GPS process. This is not necessarily true for a PL. To illustrate this phenomenon, an error was induced in the PL coordinates. For the first case, the PL coordinates were adjusted 5 cm to the North, and for the second case, they were adjusted 19 cm to the East.

Figure 6.18 shows the difference between the latitude, longitude and height solutions for the reference trajectory and the PL augmented constellation with the PL coordinates in error 5 cm to the North. The ambiguities were not maintained for the entire data set, as was the case with correct PL coordinates. For this example, the FASF algorithm fixed ambiguities a total of 13 times throughout the data set. Each ambiguity set chosen was correct. Filter resets were initiated whenever the magnitude of the residuals exceeded a pre-defined threshold, or when the fixed ambiguity solution was more than 4 sigma away from the float solution [Weisenburger, 1997]. The four longest duration periods where the ambiguities were maintained are indicated by grey shading. Numerous short duration (typically 5 second) periods where the ambiguities were solved are evident, especially in the second half of the data set. A float solution was maintained during the remainder of the data set. When the ambiguities were not fixed, the intentional error in the PL coordinates was to be absorbed into the parameters. Biases in the latitude, longitude and height errors are evident. When the ambiguities were fixed, the PL coordinate error was evident in the PL residuals, as shown in Figure 6.19. The degree to which the PL coordinate error affected the solution was dependent on the relative geometry between the GPS receivers and the PL, as described in Section 3.3.

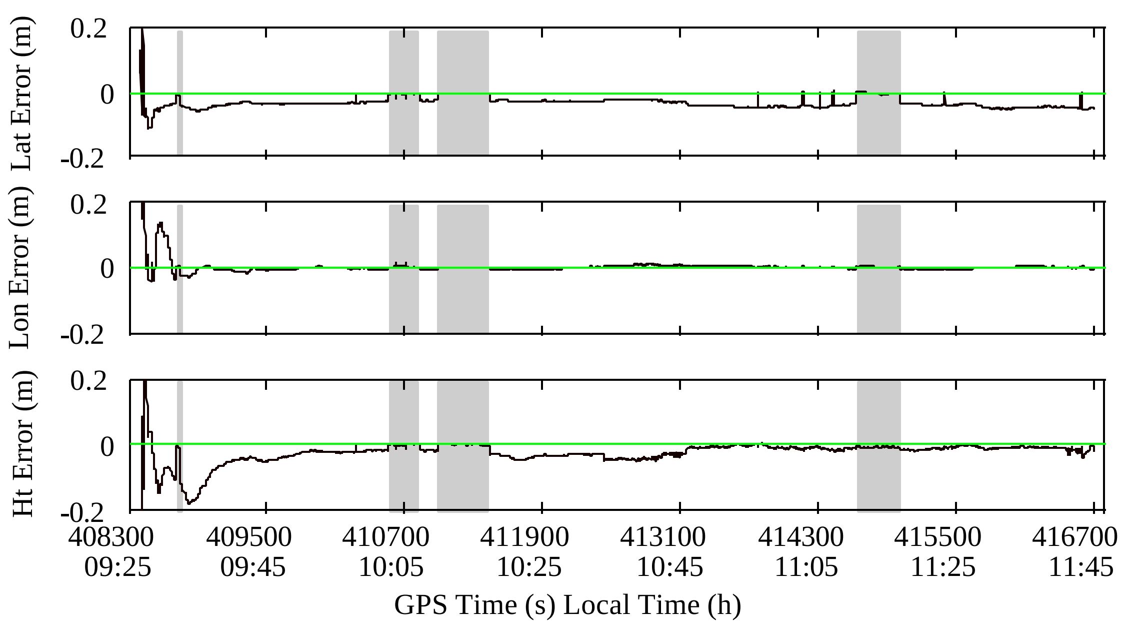

Figure 6.18 Lake Okanagan. SFLYPL Comparison Between Reference Trajectory and PL Augmented (5 cm PL Coordinate Error to the North) GPS Constellations.

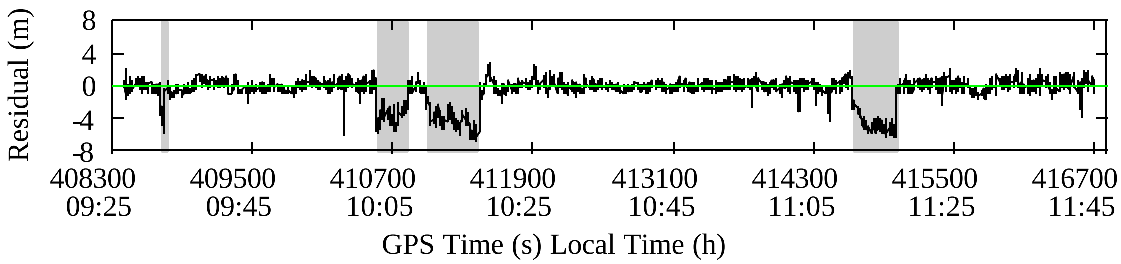

Figure 6.19 Effect of PL Relative Coordinate Error (5 cm to the North) on PL Carrier Phase Residuals.

The above analysis was repeated, except with the PL coordinates adjusted 19 cm (one L1 wavelength) to the East. Figure 6.20 shows the resulting differences in latitude, longitude and height between the reference trajectory and the PL augmented constellation. The ambiguities were solved correctly after only 94 seconds, and they were maintained for three minutes, when the FASF algorithm was reset. A float solution was maintained for the remainder of this analysis. The PL residuals are shown in Figure 6.21. The three minute period where the ambiguities were solved is indicated by grey shading. Even with a 19 cm error in the PL coordinates, the ambiguities were solved correctly once. A closer inspection of Figure 5.25 shows that at the beginning of the data set, the reference and remote receivers observe approximately the same error in the PL coordinates. Thus, in the double difference process, most of the induced 19 cm error will be removed. As the boat moves, however, the amount of error observed by the remote changes. A float solution was maintained for the majority of the data set, resulting in the PL coordinate error being absorbed into the parameters.

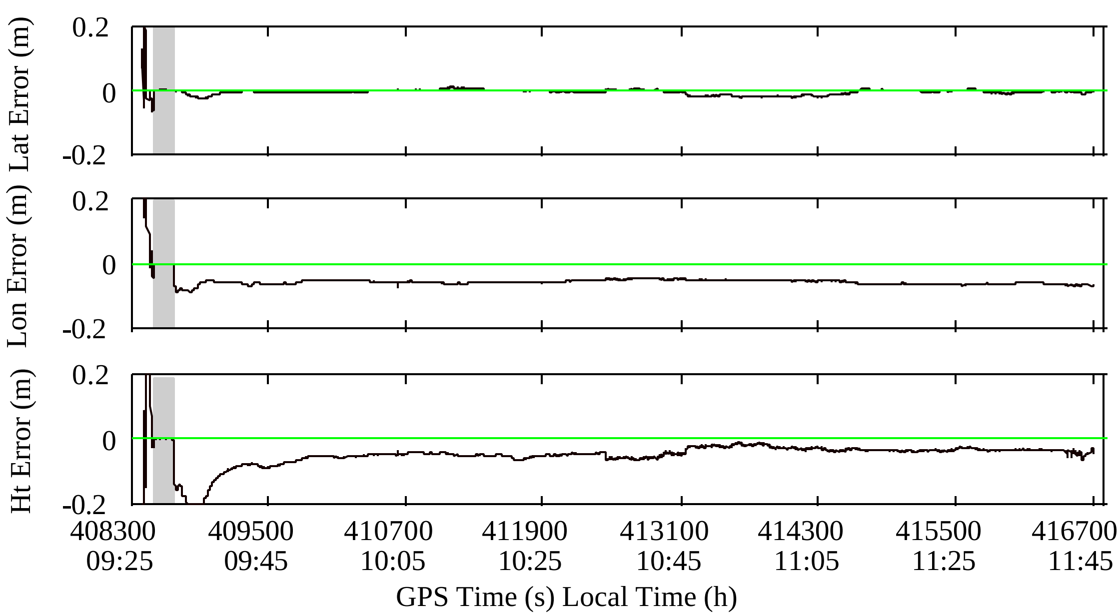

Figure 6.20 Lake Okanagan. SFLYPL Comparison Between Reference Trajectory and PL Augmented (19 cm PL Coordinate Error to the East) GPS Constellations.

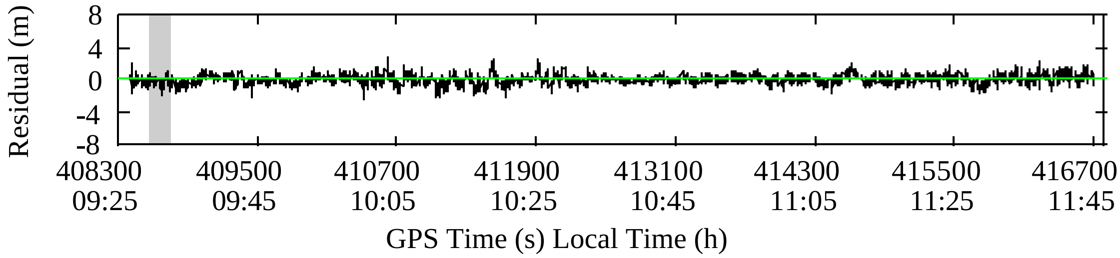

Figure 6.21 Effect of PL Relative Coordinate Error (19 cm to the East) on PL Carrier Phase Residuals.

CHAPTER 7

CONCLUSIONS AND RECOMMENDATIONS

7.1 Conclusions

Based on the results reported in this thesis, the following conclusions regarding the augmentation of GPS with PLs in a marine environment are presented:

1) The use of a PL will increase the number of observations at a given epoch, improving the overall availability of GPS. The relative geometry between the pseudolite, the GPS satellite constellation and the GPS user will determine the magnitude of the improvement to the accuracy (HDOP) and the internal (Marginally Detectable Blunder, or MDB) and external (Maximum Horizontal Error, or MHE) reliability measures. The HDOP measure alone is not a reliable indicator of the sensitivity of the DGPS solution to horizontal error. Periods can occur where the HDOP measure is acceptable and the MHE measure is excessive (50 metres or more). A simulation analysis at Calgary indicated that the use of one PL reduced the percent of epochs that the MHE exceeded 100 m from 9.2 to 1.3, and the percent of epochs that the MHE exceeded 20 m from 27.5 to 9.4. During the Glenmore Reservoir and Lake Okanagan field tests (mask angle 10°, all available satellites), the use of one PL reduced the average HDOP of an unaugmented GPS constellation by an average of 12 %. The MHE was reduced by an average of 35 %.

2) DGPS Absolute horizontal positioning accuracy with a PL was slightly worse than for the unaugmented GPS constellation. A constant multipath environment between the PL and the reference station causes a time invariant error, or bias, in the PL pseudorange measurement made by the reference receiver. This, in turn, causes a bias in the differential corrections calculated for the PL. When applied by the remote receiver, the biased differential corrections for the PL propagate into the least squares adjustment and result in biased values for the latitude, longitude and height errors, and residuals. It is possible to estimate the systematic multipath error of the reference receiver's PL pseudorange measurement, and "correct" the PL's differential correction. For the Lake Okanagan field test, the multipath component was estimated at 1.25 metres. With reference receiver multipath corrected PL pseudorange measurements, the positioning accuracy of a PL augmented configuration was virtually identical to that of an unaugmented GPS constellation, with respect to 50^{th} and 95^{th} percentile horizontal errors and 2DRMS horizontal accuracy (mask angle 10°, all available satellites). With one satellite rejected, the PL augmented configuration had an improvement in 50^{th} and 95^{th} percentile horizontal errors and 2DRMS horizontal accuracy of 8.8 %, 10.9 % and 8.8 % respectively.

3) PLs can improve the performance of Fault Detection and Exclusion algorithms. By reducing the magnitude of the Marginally Detectable Blunder, errors can more easily be detected by statistical testing of the residuals. Also, by increasing the redundancy of a solution, the rate at which an error is absorbed by the residual for that observation is increased.

4) PL augmentation improves integer ambiguity resolution performance by decreasing the average time required to solve for the correct integer ambiguity set, and increasing the reliability of the ambiguity solution. For the Lake Okanagan field tests, (mask angle 10º, all available satellites) all the PL augmented constellation showed an improvement in the average integer ambiguity resolution times of 37.5 % (morning session) and 25.3 % (afternoon session). For the morning session, the number of correct initial ambiguity solutions improved from 95 % (unaugmented configuration) to 100 % (PL augmented configuration). With one satellite rejected, the improvement in integer ambiguity resolution time for the PL augmented configuration was 62 %. The percentage of correct initial ambiguity solutions increased from 78.9 % (unaugmented configuration) to 93.4 % (PL augmented configuration). For the case of an incorrect ambiguity solution, the use of a PL resulted in a much faster filter reset time (i.e. recognition that the ambiguity solution was incorrect) and a faster time to recompute the correct ambiguity set. The average filter reset time was reduced by 74 %, and the average time to recompute the correct integer ambiguity set was reduced by 54 %.

7.2 Recommendations

The following recommendations are presented for consideration:

1) Analysis of PL augmented DGPS data should be conducted with larger separations (greater than 10 km) between the remote platform and the monitor/pseudolite stations. If the relative distance between the PL/reference receiver and the PL/ remote receiver is increased, or if the effect of the troposphere is sufficiently great over the two propagation paths, errors due to the spatial decorrelation of the tropospheric delay may become significant. At greater distances, adaptive tropospheric modelling of each transmission path (PL to reference and PL to remote receiver) may be required to successfully solve for and maintain the integer ambiguities;

2) Further investigation into the causes, quantification and mitigation of PL multipath as observed by the reference receiver are necessary. Determination of the effect of groundplanes, directional or polarized antennas and local topography on the PL signal should be pursued;

3) Further investigation into the effect of remote receiver dynamics on integer ambiguity resolution is required. The remote platform should transit toward (or away from) the PL so that there is very little change in the relative geometry. Under an identical constellation (24 hours later), the remote platform should transit past the PL so that there is a relatively large change in the relative geometry. Ideally, this test should be done with two remote platforms so that all atmospheric conditions are consistent;

4) PL capable real-time C^3NAV and SFLY programs could be developed, incorporating dynamic tropospheric modelling for the PL tropospheric delay correction;

5) A real-time monitoring system of the transmitted DGPS corrections using the PL signal as a data link could be developed to ensure the integrity of the broadcast signal;

6) Investigations of the effect of latency of PL differential corrections on DGPS accuracy should be completed. A comparison between the internal PL oscillator, a 5 MHz OCXO and a stable 10 MHz (ex. rubidium) external oscillator should be made;

7) Field testing should be conducted using multiple PLs at various geometries (including variations in azimuth and elevation). Additionally, field testing should include a collocated PL/reference antenna, and a non-collocated PL antenna but with the PL oscillator synchronized to GPS time;

8) Field testing of both a pulsed PL and the new Stanford Telecom P-Code PL, using the STel SYNCHRONICITY interface software. The use of a pulsed PL will effectively mitigate the "near/far" problem. The higher bandwidth of the P-Code PL should result in more precise code and carrier measurements, and a signal that is more resistant to the deleterious effect of multipath and signal jamming.

The use of the SYNCHRONICITY software will allow easier configuration of the PL to broadcast at specific PRNs and at a frequency offset from L1.

REFERENCES

Baarda, W. (1967) "Statistical Concepts in Geodesy", Netherlands Geodetic Commission, Publications on Geodesy, New Series, Volume 2, Number 4.

Baarda, W. (1968) "A Testing Procedure for Use in Geodetic Networks", Netherlands Geodetic Commission, Publications on Geodesy, New Series, Volume 2, Number 5.

Barltrop, K.J., Stafford, J.F. and Elrod, B.D. (1996) "Local DGPS With Pseudolite Augmentation and Implementation Considerations for LAAS", *Proceedings of the Institute of Navigation GPS-96,* Kansas City, Kansas, September 17-20, 1996. pp. 449-459.

Braasch, M.S. (1995) "Multipath Effects", *Global Positioning System: Theory and Applications, Volume I*, Volume 164, Progress in Astronautics and Aeronautics, The American Institute of Astronautics and Aeronautics, Washington, 1996. pp. 547-568.

Cannon. M.E and Lachapelle, G. (1992) "Analysis of a High Performance C/A Code GPS Receiver in Kinematic Mode" *Proceedings of the Institute of Navigation National Technical Meeting 1992*. pp. 379-390.

Chen, D. (1994) "Development of a Fast Ambiguity Search Filter (FASF) Method for GPS Carrier Phase Ambiguity Resolution", Ph.D. Dissertation. UCGE Reports Number 20071, The Department of Geomatics Engineering, The University of Calgary. December, 1994.

Denaro, R., Harvester, V.G. and Harrington, R.L. (1980) "GPS Phase I User Equipment Field Tests", *Global Positioning System*, Vol I, Institute of Navigation, 1980, pp. 125-131.

Elrod, B.D. and Van Dierendonck, A.J. (1995) "Pseudolites", *Global Positioning System: Theory and Applications, Volume II*, Volume 164, Progress in Astronautics and Aeronautics, The American Institute of Astronautics and Aeronautics, Washington, 1996. pp. 51-79.

Elrod, B., Barltrop, K. and Van Dierendonck, A.J. (1994) "Testing of GPS Augmented with Pseudolites for Precision Approach Applications", *Proceedings of the Institute of Navigation GPS-94,* Salt lake City, Utah, September 20-23, 1996. pp. 1269-1278.

Federal Radionavigation Plan (1994) U.S. Department of Transportation. Report Number DOT-VNTSC-RSPA-95-1, pp. 2-21 to 2-29.

Fenton, P. C., Falkenberg, W. H., Ford, T., Ng, K. K. and Van Dierendonck, A. J. (1991) "NovAtel's GPS Receiver - the High Performance OEM Sensor of the Future", *Proceedings of the Institute of Navigation GPS-91,* Albuquerque, New Mexico, September 11-13, 1991. pp. 49-58.

Ford, T., Neumann, J., Toso, N., Petersen, W., Andersen, C., Fenton, P., Holden, T. and Barltrop, K. (1996) "HAPPI - A High Accuracy Pseudolite/GPS Positioning Integration", *Proceedings of the Institute of Navigation GPS-96,* Kansas City, Kansas, September 17-20, 1996. pp. 1719-1728.

Frodge, S., Labrecque, V. and Barker, R. (1995) "Performance of the Real-Time On-The-Fly GPS Positioning System on Board a Dredge", *Proceedings of the Institute of Navigation 1995 National Technical Meeting,* Anaheim, California, January 18-20, 1995. pp. 505-513.

Henriksen, J., Lachapelle, G., Raquet, J. and Stephen, J. (1996) "Analysis of Stand-Alone GPS Positioning Using Post-Mission Information", *Proceedings of the Institute of Navigation GPS-96,* Kansas City, Kansas, September 17-20, 1996. pp. 251-259.

Hofmann-Wellenhof, B., Lichtenegger, H. and Collins, J. (1994) *GPS Theory and Practice (3rd Edition)*, Springer-Verlag, Wien.

Hopfield, H.S. (1969) "Two Quartic Tropospheric Refractivity Profile for Correcting Satellite Data", *Journal of Geophysical Research*, April, 1969.

Klein, D. and Parkinson, B.W. (1984) "The Use of Pseudo-Satellites for Improving GPS Performance", *Global Positioning System*, Vol III, Institute of Navigation, 1986, pp. 135-146.

Lachapelle, G., Kielland, P. and Casey, M. (1991) "GPS for Marine Navigation and Hydrography", *International Hydrographic Review,* Monaco LXIX(1), March, 1992.

Lachapelle, G., Cannon, M.E. and Lu, G. (1992) "High Precision GPS Navigation With Emphasis on Carrier Phase Ambiguity Resolution", *Marine Geodesy*, Volume 15, Number 4, pp. 253-269.

Lachapelle, G. (1995) "GPS Theory and Applications", ENGO 625 Course Notes. The Department of Geomatics Engineering, The University of Calgary, 1995.

Leick, A. (1995) *GPS Satellite Surveying*, 2nd Edition. John Wiley & Sons, Inc. 1995.

Morley, T. and Lachapelle, G. (1997) "GPS Augmentation With Pseudolites for Navigation in Constricted Waterways", *Proceedings of the Institute of Navigation 1997 National Technical Meeting,* Santa Monica, California, January 14-16, 1997. pp. 595-605.

Ndili, A. (1994) "GPS Pseudolite Signal Design", *Proceedings of the Institute of Navigation GPS-94.* pp. 1375-1382.

Parkinson, B.W. and Enge, P.K. (1995) "Differential GPS", *Global Positioning System: Theory and Applications, Volume II*, Volume 164, Progress in Astronautics and Aeronautics, The American Institute of Astronautics and Aeronautics, Washington, 1996. pp. 3-50.

Pathak, M.C., Kotnala, K.L., Prabaharan, N. and Ganesan, P. (1990) "Positioning and Surveying Requirements for Exploration and Exploitation of Ocean Wealth", *International Hydrographic Review*, LXVII(1), January 1990. pp. 93-101.

Raquet, Capt. J., Lachapelle, G., Qiu, W., Pelletier, C., Nash, Capt. T., Snodgrass, Capt. F.B., Fenton, P and Holden, T. (1996) "Development and Testing of a Mobile Pseudolite Concept for Precise Positioning", *NAVIGATION: Journal of the Institute of Navigation*, Vol. 43, No. 2, Summer 1996. pp. 149-165.

Seeber, G. (1993) *Satellite Geodesy. Foundations, Methods, and Applications*. Walter de Gruyter & Company, Berlin.

Shively, C. and Faunce, K. (1996) "Preliminary Experimental Evaluation of LAAS Integrity Methods", *Proceedings of the Institute of Navigation 1996 National Technical Meeting*, Santa Monica, California, January 22-24, 1996. pp. 811-823.

Spilker, J.J. (1980) "GPS Signal Structure and Performance Characteristics", *Global Positioning System*, Vol I, Institute of Navigation, 1980, pp. 29-54.

Spilker, J.J. (1994) "GPS Navigation Data", *Global Positioning System: Theory and Applications, Volume I*, Volume 164, Progress in Astronautics and Aeronautics, The American Institute of Astronautics and Aeronautics, Washington, 1996. pp. 121-176.

Steeves, R. R. and Fraser, C.S. (1987) "Statistical Post-Analysis of Least Squares Adjustment Results", *Papers For The CISM Adjustment and Analysis Seminars*, Canadian Institute of Geomatics, Krakiwsky, E.J., editor (1987), pp. 182 - 210.

Tang, C. (1996) "Accuracy and Reliability of Various DGPS Approaches", M.Sc. Thesis, UCGE Report Number 20095. Department of Geomatics Engineering, The University of Calgary.

Van Dierendonck, A.J. (1990) "The Role of Pseudolites in the Implementation of Differential GPS", *IEEE PLANS 1990*, pp. 370-377.

van Graas, F. (1996) "Signals Integrity", *System Implications and Innovative Applications of Satellite Navigation*. AGARD-LS-207, June, 1996, pp. 7-1 to 7-12.

Vanicek, P. and Krakiwsky, E. J. (1981) *Geodesy: The Concepts*, North-Holland, Amsterdam, The Netherlands.

Weisenburger, S. (1997) "Effect of Constraints and Multiple Receivers for On-The-Fly Ambiguity Resolution", M.Sc. Thesis, UCGE Report Number 20109. Department of Geomatics Engineering, The University of Calgary.

Weisenburger, S. and Cannon, M.E. (1997) "Performance Improvements Using Constraints in Marine OTF Ambiguity Resolution", *Proceedings of the Institute of Navigation 1997 National Technical Meeting*, Santa Monica, California, January 14-16, 1997. pp. 585-594.

Zumberge, J.F. and Bertiger, W.I. (1994) "Ephemeris and Clock Navigation Message Accuracy", *Global Positioning System: Theory and Applications, Volume I*, Volume 164, Progress in Astronautics and Aeronautics, The American Institute of Astronautics and Aeronautics, Washington, 1996. pp. 585-600.